Tesis Doctoral

Control coherente de sistemas cuánticos

Poggi, Pablo Matías

2017-12-07

UNIVERSIDAD DE BUENOS AIRES

Facultad de Ciencias Exactas y Naturales

Departamento de Física

Control coherente de sistemas cuánticos

Tesis presentada para optar al título de Doctor de la Universidad de Buenos Aires en el área de Física

Lic. Pablo Matías Poggi

Director de Tesis: Diego Wisniacki

Director de Tesis: Fernando Lombardo

Consejero de Estudios: Cristina Caputo

Lugar de trabajo: Departamento de Física "Juan José Giambiagi" - FCEyN - UBA.

Ciudad Autónoma de Buenos Aires

Fecha de defensa: 7 de diciembre de 2017

Control coherente de sistemas cuánticos

Resumen

Durante las últimas décadas se han logrado grandes avances en la manipulación de sistemas físicos en la escala nano y subnanoscópica, donde la coherencia cuántica juega un papel dominante. Algunos hitos registrados en los últimos años son la manipulación óptica de partículas individuales en trampas de iones, la interacción controlada de un solo electrón con fotones individuales en puntos cuánticos de silicio y la realización de bits cuánticos (qubits) con largos tiempos de coherencia en circuitos superconductores. Actualmente, la habilidad de diseñar la evolución de sistemas cuánticos con gran precisión está allanando el camino para una nueva revolución en las tecnologías cuánticas.

En esta Tesis estudiamos desde el punto de vista teórico el problema de control en sistemas cuánticos. Un aspecto central de este problema es que la presencia de disipación y decoherencia por lo general impide que el sistema sea manipulado arbitrariamente. Cuando estos efectos no pueden ser eludidos, es esencial efectuar los protocolos de control de la manera mas rápida posible. En este contexto, realizamos un estudio de los límites fundamentales que existen para la velocidad de evolución en sistemas cuánticos. Estos límites surgen de generalizaciones de la relación de incerteza entre tiempo y energía, que impone cotas inferiores a los tiempos de evolución. Estudiando el escenario general de un problema de control, donde los operadores Hamiltonianos dependen explícitamente del tiempo, mostramos que en general estas relaciones no proveen información útil que permita acotar tiempos mínimos en estos problemas. A la luz de estos resultados, proponemos nuevos métodos que efectivamente pueden ser aplicados a cualquier sistema cuántico controlado y que permiten estimar cotas para dichos tiempos.

Un ingrediente esencial de las aplicaciones modernas de la teoría de control son los métodos de optimización. En esta Tesis estudiamos e implementamos numéricamente métodos de control óptimo para sistemas cuánticos en diversos modelos de interés. En particular, utilizamos dichas herramientas para buscar los tiempos mínimos de evolución en sistemas cuánticos que presentan múltiples cruces evitados en su espectro de energías. Para este tipo de modelos, en primer lugar proponemos y caracterizamos un método general para realizar tareas de control, que genera evoluciones con velocidad óptima en cada cruce. Luego, usando métodos de optimización mostramos que el tiempo de evolución puede disminuirse a medida que el número de niveles del sistema aumenta. Finalmente, a partir de estudiar el efecto de campos periódicos en estos sistemas, logramos identificar los mecanismos físicos

que generan este fenómeno y proponer una solución analítica para el campo de control.

Adicionalmente, estudiamos la relación entre la controlabilidad de un sistema cuántico y su complejidad. Usando control óptimo, obtuvimos los campos necesarios para generar distintos procesos en una cadena de spines y estudiamos sistemáticamente las propiedades de dichos campos como función de distintos aspectos que hacen a la complejidad del sistema. Encontramos que el ancho de banda de los campos es, por lo general, independiente de la dimensión del sistema. Asimismo, la complejidad del espectro de Fourier del campo efectivamente aumenta a medida que se incrementa el número de excitaciones en el sistema. Sin embargo, también concluimos que la naturaleza regular o caótica del sistema no afecta significativamente su controlabilidad.

Finalmente, estudiamos sistemas cuánticos abiertos en presencia de campos externos. En ese contexto, actualmente se debate si los entornos no Markovianos pueden ser usados como un recurso para mejorar la controlabilidad de dichos sistemas. Una de las características más atractivas de estos sistemas es que describen escenarios en los que la pérdida de información y de coherencia son reversibles y, por lo tanto, es posible flujo temporario de información desde el entorno hacia el sistema. Estudiamos la relación entre el grado de no-Markovianidad y la acción de campos de control dependientes del tiempo en un sistema de dos niveles interactuando con un entorno estructurado a baja temperatura. Para este sistema, hallamos que aplicando campos periódicos sobre el sistema es posible aumentar considerablemente el grado de no-Markovianidad con respecto al caso estático. Asimismo exploramos la relación entre los efectos no Markovianos y el control, y argumentamos que dichos efectos no pueden considerarse como un recurso para realizar protocolos de control.

Palabras claves: Control cuántico, Modelo de Landau-Zener, Control óptimo, Sistemas cuánticos abiertos, Sistemas cuánticos complejos

Coherent control of quantum systems

Abstract

During the past decades, major technological advances have made it possible to accurately manipulate in the laboratory physical systems in the nano- and subnanoscale, where quantum coherence plays a dominant role. Examples range from single site optical manipulation in ion traps, to coupling single electron to photons in silicon quantum dots and the realization of long-lived coherent qubits in superconducting circuits, all of which have been realized over the past few years. In this context, the increasing ability to precisely engineer the evolution of quantum systems is paving the way for a new revolution in quantum technologies.

In this Thesis we study from a theoretical point of view the problem of control in quantum systems. One key aspect of this problem is that the presence of decoherence and dissipation often prevents full control over a system. When such effects are unavoidable, it is essential to drive the system in the fastest possible way. To this end, we studied the fundamental limitations which exist to the speed of evolution in quantum systems. These limitations arise from generalizations of time-energy uncertainty relation which imposes bounds on the minimal evolution time. By studying these relations in the general control scenario where quantum Hamiltonians are time-dependent, we show that they give no meaningful information about the minimal evolution time. In light of these results, we propose new expressions which can be applied to any driven system, and that allow us to obtain estimates for such bounds.

An essential ingredient of modern control applications is the use of optimization methods. In this Thesis we studied and implemented numerically quantum optimal control methods in numerous physical systems. In particular, we used them as a tool for exploring the minimal evolution time in quantum systems with multiple avoided crossings in their energy spectrum. For this type of models, we first propose and characterize a general method for performing control tasks which is time-optimal at each avoided crossing. Then, using optimization methods, we found that the evolution time can be further minimized as the number of levels increases. Furthermore, we present a detailed study of the effects of time-periodic fields in these systems, which allowed us to identify the physical mechanisms of the optimal speed up, and propose an analytical closed form for the required control fields.

We also studied the connection between the complexity of a quantum system and its controllability. By using optimal control theory, we derived the control fields necessary to drive various physical processes in a spin chain. Then, we study the spectral properties of such fields and how they relate to different aspects of the system complexity. We find that the spectral bandwidth of the fields is, quite generally, independent of the system dimension. Conversely, the spectral complexity of such fields does increase with the number of particles. Nevertheless, we find that the regular or chaotic nature of the system does not affect significantly its controllability.

Finally, we studied control and the effects of driving in open quantum systems. There, it its currently debated whether non-Markovian effects could be used as a resource which improves controllability. One of the most appealing features of non-Markovianity is that it captures scenarios where loss of information and coherence are reversible, and thus a temporary backflow of information from the environment to the system is possible. We studied the interplay between the degree of non-Markovianity and the action of time-dependent control fields in an open two-level quantum system. We find that periodical modulation of a field acting solely on the system can greatly enhance the degree of non-Markovianity with respect to the undriven case. We also explore the interplay between non-Markovian effects and control, and conclude that those effects cannot be regarded as a resource for performing controlled operations in quantum systems.

Keywords: Quantum control, Landau-Zener, Optimal control, Open quantum systems, Complex quantum systems

Agradecimientos

En este espacio quiero agradecer a todas aquellas personas que me ayudaron en esta etapa de casi cinco años que culmina con la realización de esta Tesis.

Primero que nada, le agradezco profundamente a mi equipo de Directores, Fernando y Diego, por haberme guiado, ayudado y apoyado en el camino de la investigación durante todo este tiempo. Me alegra ver que hemos llegado a este punto y seguimos super motivados trabajando juntos todos los dias. Les quiero sobre todo reconocer y agradecer profundamente la posibilidad que me dieron de poder viajar para ir a conferencias todos los años, sin lo cual este trabajo no hubiese sido lo que es. Mil gracias, muchachos.

Quiero tambien extender ese agradecimiento al CONICET, a la Universidad (libre, pública y gratuita) de Buenos Aires por haberme brindado el apoyo para realizar este trabajo. Ese apoyo no fue destinado a mi particularmente, sino a toda una generación que atravesó la primera etapa de su vida universitaria con la idea de que el desarrollo científico de un país es un factor esencial para su desarrollo y el bienestar de su población. Ese apoyo y, sobre todo, esa idea puede correr riesgo circunstancialmente, pero nunca, nunca debe perderse.

Quiero agradecer a toda la comunidad del Departamento de Física junto a la cual trabajé durante estos años, en especial a toda la gente de Qufiba, con quienes compartí conferencias y charlas en las cuales aprendí muchísimo. Quiero tambien agradecer a todos aquellos con quienes compartí cursos como docente aquí y en el CBC, y particularmente le agradezco a Cristina, por la pasión que transmite y por siempre tener palabras de apoyo y consejo para mi.

Les agradezco a Rosa, a Tino y a todo el grupo de sistemas complejos de UPM e ICMAT por la hospitalidad y predisposición durante mis seis meses de trabajo en España, que fueron muy productivos, y donde la pasé *de película*.

Muchísimas gracias a Mechi, Fernando, Adrián, a todo es-importante y a mis amigos del colegio y la vida, por la amistad, nada mas y nada menos.

A mi mamá y a mis hermanos Martín y Maria Clara me gustaría reconocerlos apropiadamente, pero la realidad es que no hay nada que pueda escribir que haga justicia a lo infinito que les agradezco su compañerismo, ayuda incondicional y apoyo total en el camino que elegí para mi vida profesional.

Y finalmente quiero agradecerle con todo mi corazón a Mariana, mi compañera de siempre, con quien nos embarcamos juntos hace años en un camino que, sin saberlo, nos ha llevado y nos sigue llevando por caminos increíbles. Y es que son increíbles, gracias a vos. Gracias.

Pablo Matías Poggi

Ciudad Autónoma de Buenos Aires, Octubre 2017.

A mis viejos
A mis hermanos
A Mariana

Contents

Contents **viii**

1 Introduction **1**

2 General aspects of control in quantum systems **13**

2.1 Controllability 13

2.2 Bounds on the minimal evolution time: the quantum speed limit . . 15

2.2.1 Quantum speed limit: overview 16

2.2.2 Geometrical interpretation 17

2.2.3 Connection with quantum control 19

2.3 Optimal control theory 25

2.3.1 Krotov method of optimization 25

2.3.2 Quantum control landscapes 28

2.3.3 Connection with the quantum speed limit 29

3 Quantum control via navigation of the energy spectrum **33**

3.1 Avoided level crossings and the Landau-Zener model 33

3.1.1 Example: two-photon generation in the Jaynes - Cummings model 37

3.2 Time-periodic driving at avoided crossings 39

3.2.1 Application to a multilevel system 44

4 Optimal control of quantum systems **49**

4.1 Optimal evolution time in a two-level system 49

4.2 Analysis of the quantum speed limit bounds 52

4.3 Optimal evolution time for systems with many avoided crossings . . 58

4.3.1 Multilevel model 58

4.3.2 Exploring the quantum speed limit with optimal control . . 61
4.4 Analysis of optimal control fields 64
4.4.1 Analytical approximate solution for the time-dependent problem 67
4.4.2 Initial guess and performance of the optimization 72

5 Complexity and control in quantum systems 75
5.1 Signatures of quantum chaos 75
5.2 Spin chain model 77
5.2.1 Symmetries and sources of complexity 78
5.2.2 Control processes 79
5.3 Optimal control fields 83
5.3.1 Frequency bandwidth 83
5.3.2 Spectral localization 86
5.3.3 Control fields and energy spectrum 88

6 Control in open quantum systems and non-Markovian effects 93
6.1 Open quantum systems and dynamical maps 93
6.1.1 Markovian quantum maps and control 94
6.1.2 Non-Markovian quantum maps 97
6.2 Driven open quantum systems: an exactly solvable model 101
6.3 Non-Markovian effects in periodically driven systems 106
6.4 Optimal control and non-Markovianity 113

7 Conclusions 121

A Quantum speed limit calculations 131
A.1 Derivation of Pfeifer's theorem 131
A.2 QSL for a constrained two-level problem 132
A.3 Minimum time bounds for the many-level problem 133

B The LiCN/LiNC isomerizing system 135

C Spin chain model 137
C.1 Symmetries 137
C.2 Split-operator technique 138

D Driven open two-level system **141**

D.1 Time-local equation of motion under the RWA 141

D.2 Hierarchy equations of motion 142

D.3 Weak coupling solution 143

Chapter 1

Introduction

During the past decades, major advances have been made in accurately controlling in the laboratory physical systems in the nano- and subnano-scale, where quantum coherence plays a dominant role. Examples range from single site optical manipulation in ion traps [1, 2], to coupling single electron to photons in silicon quantum dots [3] and the realization of long-lived coherent qubits in superconducting circuits [4], all of which have been realized over the past few years.

This ability to engineer the evolution of quantum systems is paving the way for a new revolution in quantum technologies [5, 6]. The power of these is typically based on the *beautifully strange* features of quantum mechanics, namely state superposition and entanglement. For example, superposition allows for quantum systems to exist in a combination of classically distinct states, where components can evolve in time and interfere between each other. This extraordinary feature gives rise to what is usually called quantum parallelism [7], which refers to the ability of quantum systems to act as computer registers (such as qubits) which take multiple values simultaneously. In virtue of this feature, in a computation functions have to be called only once but are evaluated in all states in the superposition. This feature allows to perform computational operations in much less steps as opposed to classical registers, as illustrated by the famous Deutsch-Joza algorithm [8].

In order to fully harness the useful properties of quantum systems, active control has to be performed over them, and this represents a formidable technological and theoretical challenge: one should be able to prepare a system in a chosen initial state, perform the desired evolution, and finally measure the state in a very precise way [9]. Moreover, interactions between the system and the external controller

inevitably brings around noise. This, in addition to the intrinsic environmental noise, poses a threat to the quantum features of the system.

In this Thesis we study from a theoretical point of view several aspects related to the control of quantum systems. For that, let us begin by posing a typical quantum control problem in the following way. Consider a quantum system $\mathcal{S}$ described by a free (also called "drift") Hamiltonian H_0. Suppose we can initialize the system in some pure state $|\psi_0\rangle$, which could for example be the ground state of H_0. We now wish the system to evolve into some target state $|\psi_g\rangle$ in some time T. The free, uncontrolled dynamics of the system, given by

$$|\psi(t)\rangle = \mathrm{e}^{-\frac{i}{\hbar}H_0 t}\,|\psi_0\rangle \tag{1.1}$$

will not, in general, take the system to the desired state; in other words, the fidelity of the process at time T,

$$\mathcal{F}(T) = |\langle\psi_g|\psi(T)\rangle|^2 \tag{1.2}$$

will be far from one. In order to steer the dynamics to the target state, we need to introduce a new term in the system Hamiltonian, $V(t)$ which models the interaction between the system and some external control agent

$$H_0 \to H(t) = H_0 + V(t). \tag{1.3}$$

The control Hamiltonian $V(t)$ is a function of one or more generally time-dependent control parameters, or *control fields*

$$V(t) = V\left(\{(u_1(t), u_2(t), \ldots, u_k(t)\}\right). \tag{1.4}$$

The functions $\{u_i(t)\}$ typically represent electromagnetic fields or forces (note that in this picture the control fields are described classically). The goal is then to engineer the time-dependence of these fields in such a way that the controlled evolution of the system, now described via the equation

$$i\hbar\frac{d}{dt}\,|\psi(t)\rangle = \left(H_0 + V(t)\right)|\psi(t)\rangle\,, \tag{1.5}$$

maximizes the fidelity $\mathcal{F}$ of the desired process, i.e. reaches $|\psi_g\rangle$ at time $t = T$ with probability as close to 1 as possible. Note that this formulation admits alternative definitions of fidelity other than (1.2), which correspond to different objectives of the control problem. For instance, we may be interested in reaching a definite expectation value of an observable A or performing some unitary gate U_G, for which we will have other measures of success

$$\mathcal{F}_2 = \langle\psi(T)|\,A\,|\psi(T)\rangle \tag{1.6}$$

$$\mathcal{F}_3 = \mathrm{tr}\left[U_G^\dagger U(T)\right], \tag{1.7}$$

respectively, where in the latter the process is independent of $|\psi_0\rangle$. These variations are often referred to as state-to-state control, observable control and unitary control, respectively.

There are two main paradigms for solving quantum control problems: open-loop and closed-loop control [10]. The main characteristic of open-loop methods is that complete knowledge of the system is assumed to be contained in the Hamiltonian and so uncertainty about the parameters and about couplings between the system and noise sources is taken to be negligible. This is the type of methods we will study in this Thesis. Closed-loop procedures, on the other hand, require feedback between the system and the control. In this way, information about the state variables obtained from direct measurements is fed back to the system through a controller to achieve the desired objective.

The quantum control problem stated above has an obvious practical appeal. As already mentioned, the ability to precisely manipulate physical systems in the atomic scale is bound to generate technologies which can improve substantially communication, computation and measurement devices. From a fundamental point of view, numerous questions arise naturally. The most important one is how can we, in practice, engineer the required control fields in each situation of interest. Interestingly, the first systematic studies about this were not done in the context of quantum information processing, but in the field of quantum chemistry. There, the advent of laser sources in the 1960s had encouraged scientists to try to control chemical reactions not by changing the temperature or pressure of a sample, but by shining it with monochromatic light which could selectively break a specific bond in a polyatomic molecule, in a process called photodissociation [11, 12]. However, the first attempts to do that, which consisted in continuously exciting a vibrational mode of the molecule with laser radiation, proved to be unsuccessful [13]. More sophisticated methods were needed, and the first proposals and quantum-mechanical calculations were done by Tannor and Rice [14, 15], who showed that the selectivity[1] of a chemical reaction could be controlled by properly tuning the time-delay between two laser pulses. Almost simultaneously, Brumer and Shapiro [16] showed that tuning the phases of the different components on a laser pulse acting on a coherent superposition of energetically degenerate states allowed to control the interference between such states and thus to steer the product ratio of a chemical reaction to a preferred value. Both ideas proved to be successful, leading to experimental realizations of controlled ionization of Na_2 [17]

[1] The selectivity of a reaction refers to choosing whether one product of a reaction is preferred over another, e.g. $ABC \rightarrow AB + C$ with respect to $ABC \rightarrow A + BC$.

and dissociation of HI [18] molecules.

By the mid-1980s, technological advances had made it possible to shape femtosecond laser pulses using spatial light modulators thus opening new pathways to control chemical reactions. These advances naturally led to the issue of finding the optimized pulse shape for different control problems [11]. Optimization methods have a long history of success in various branches of science and engineering. The most famous example is given by the optimal lunar landing problem studied during the times of the Apollo Program, where Meditch [19] analytically figured out how to minimize fuel consumption and landing time using Pontryagin maximum principle [20]. The works of Rabitz and Tannor [21, 22, 23] were the first to adapt tools of mathematical optimal control theory to quantum systems. The structure of an optimization problem is simple: we first need to establish quantitative objectives, such as the fidelity measures of eqns. (1.2), (1.6) or (1.7), and penalties, for example restrictions on the control field amplitude or bandwidth. These are then casted as functionals of the control field [13],

$$J[u] = J_o + J_p, \tag{1.8}$$

where J_o contain the objectives and J_p the penalties defined for the control problem. The goal is then to minimize the functional $J[u]$ with respect to $u(t)$, while at the same time allowing $u(t)$ and the system state vector $|\psi(t)\rangle$ to solve the corresponding Schrödinger equation (1.5). We will analyze in detail how to approach this problem using Krotov's method [24] in Chap. 2.

In the past three decades optimal control of quantum systems (or quantum optimal control, QOC) has been a subject of intense investigation [25]. Many numerical approaches have been put forward, including the already mentioned by Krotov and extensions of it [24, 23] and gradient ascent algorithms such as GRAPE [26, 27]. The difference between these is given by the way the optimal field is obtained in an iterative algorithm, which has an impact on convergence properties. Also, extensions have been made to optimal control of open quantum system dynamics [28, 29, 30]. Numerous works have also been devoted to studying the quantum control landscape [31], which represents the functional dependence of objective (1.8) on the control variables. Rigorous calculations and extensive numerical evidence [32, 33, 34, 35, 36] show that the landscape has a benign topology if no constraints are placed on the control problem [37], thus preventing local search algorithms to fall into *traps* or local maxima during the optimization procedure.

The scope of quantum optimal control was quickly extended from the control

of chemical reactions to problems in quantum information science. For instance, theoretical state preparation protocols were proposed for squeezed states [38], non-classical states in a cavity [39], as well for transport of ions and atoms [40]. Optimization of quantum gates has also been thoroughly studied in many setups, such as cold ions [41], cold atoms [42], nitrogen vacancy centers [43] and superconducting qubits [44]. Experimental realizations of these sort of protocols have flourished over the past decade, and optimal control is nowadays routinely used as a tool for emerging quantum technologies, with applications to the transport of ions in segmented traps [45], precision magnetometry [46], atom interferometry [47] and gate generation in quantum circuits [48].

Besides the main question about how to design the shape of control fields, there are many other theoretical aspects of quantum control which are of fundamental interest. One of them is the existence of a quantum speed limit [49], that is, a fundamental limitation on the speed of evolution of a quantum system. The connection with quantum control is straightforward: if such a limitation exists, then it is essential to take it into account in order to (i) do not attempt to perform control operations below the minimum evolution time, (ii) try to control the system of interest as fast as possible in order to minimize detrimental decoherence and dissipation effects. The idea that the speed of evolution is bounded originates from Heisenberg uncertainty relation between time and energy

$$\Delta E \Delta t \geq \frac{\hbar}{2}. \tag{1.9}$$

This inequality is actually derived from wave mechanics, but it was put into firm grounds for general quantum systems by Mandelstam and Tamm [50] and Bhattacharyya [51], who derived an analogous inequality relating the evolution time of a quantum state and its energy dispersion ΔE, for time-independent unitary evolution. Investigation about the quantum speed limit gained much attention with the early proposals of quantum information processing schemes, since the former could imply limitations to the latter. Since then, a vast number of works have been devoted to characterize bounds on the evolution time for pure and mixed states, open quantum systems and time-dependent Hamiltonians [52, 53]. The connection with quantum control received much attention since the work of Caneva *et al.* [54], who showed that optimal control methods could be used to explore what is the minimal time needed to control a quantum system, and provided a link with the quantum speed limit bounds for some specific systems. Later, results by Sorensen *et al.* [55] showed that quantum control landscapes become increasingly complicated when the evolution time is a limited resource, specially for complex systems, and so the performance of optimization techniques could be dramatically

affected. Both the question of how to perform optimization near the quantum speed limit, and how to obtain bounds on the minimum time for time-dependent closed and open systems still represent open challenges.

An important aspect of quantum control which is attracting increasing attention is its relation with complexity in quantum systems. Optimal control protocols have been studied for a variety of scenarios in quantum systems with large state space dimension, such as generation of entangled states in many-body systems [56], minimizing defects when crossing phase transitions [57] and optimization of unitary gates for qudits [58]. Recently, a new method was developed in order to enhance the performance of optimization in a many-body scenario, where the computational cost of usual methods such as Krotov becomes prohibitively big [59]. This work paved the way for a few systematic numerical [60] and analytical [61] studies about the interplay between the dimension of the system under control and the complexity of the control fields. A lot of attention is still drawn to these topics, and deeper understanding is needed about how to quantify the resources needed for controlling complex quantum systems, and specially about what aspects of complexity affect controllability.

Another fundamental aspect of interest in quantum control is its application to open quantum systems. In these cases, the goal is to control the reduced dynamics of a central system which is coupled to a larger system with many unaccessible degrees of freedom, i.e., the environment [62]. Typically, the effects of large, unstructured and/or high temperature environments are well described by completely positive divisible maps [63], which are usually called Markovian [64, 65]. These maps can always be casted in the form of a Lindblad equation, i.e. a time-local master equation. Thanks to this, optimal control problems can be properly formulated in this scenario, in a similar fashion as it is done with Schrödinger equation [66]. However, this approach has obvious limitations, since the environmental effects are hard-wired in the Lindblandian, and the control has a limited capability of counteracting decoherence and dissipation. Note that there are cases where this can be beneficial; as noted by Verstraete and Cirac [67], if we can design the environment in such a way that it drives the system to some fixed point in state space, then this would result in a robust strategy for state preparation. If there is no room for environment engineering, then the best route for control in Markovian maps is usually to perform operations in the minimum possible time, and we will address this case in Chap. 3.

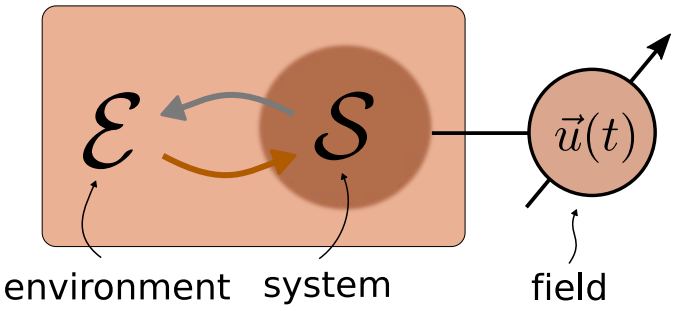

FIGURE 1.1: Schematic picture of the object of study of this Thesis, in which we investigate control of quantum systems $\mathcal{S}$ by means of external driving fields $\vec{u}(t)$ while, in general, interacting with an environment $\mathcal{E}$

There is, however, another scenario for control in open quantum systems. The effects of small, structured and/or low temperature environments give rise to non-Markovian maps, which are more intriguing and challenging to explore. Without a doubt, one of the most appealing features of non-Markovian dynamics, is that it captures scenarios where loss of information and coherence are reversible, and thus a temporary backflow of information from the environment to the system is possible [64, 65]. The lack of an unified mathematical framework to study these systems determines that control problems in non-Markovian dynamics form part of a still largely uncharted territory [66]. There have been interesting studies that show that non-Markovianity may be beneficial to controllability [68, 69], but still a more complete assessment about how these effects influence control in quantum systems has to be developed.

In this Thesis we investigate various aspects related to control of quantum systems in a general setting, which is schematically depicted in Fig. 1.1. There we have three interacting parts: the system $\mathcal{S}$, the environment $\mathcal{E}$ and the control $\vec{u}(t)$. Our goal is to explore how the features of each agent affect our overall ability to control the system. We do so by taking a constructive approach, by means of which we study in detail simple physical models, to later build on their complexity in order to develop a more general understanding of the physical and mathematical aspects of the general control problem. As we will see throughout this Thesis, basic but non-trivial phenomena found in the simplest cases will appear intertwined in more complex scenarios. For instance, we will exhaustively analyze a driven two-level quantum system described by the Landau-Zener Hamiltonian [70, 71], using both fixed (oscillating, linear, piecewise constant) fields and also optimal control techniques. This will allow us to construct a method for controlling multilevel systems, which is suitable for application in open quantum systems where the environmental influence is adverse to the control. We also propose variations

of this technique to perform time-optimal control. We will show that we are able to derive a simple physical interpretation of the time-optimal fields derived numerically for this multilevel systems based on an analytical study of the periodically driven two-level model. This model, in turn, will also give us an important insight about the interplay between driving in open quantum systems and the emergence of non-Markovian effects. For those cases, we will also explore situations in which the environment is essential for controlling a quantum system.

Relating the features of optimal control fields to the underlying physical mechanisms they produce also bridges a gap in the literature concerning optimal and coherent control as seemingly disconnected subjects [16]. We will also analyze how systematic quantitative analysis of the shape of these fields can also be used as a tool to assess the complexity of controlling a many-body quantum system, where the system dimension is too large to be able to construct a control method from physical intuition.

We will also use the two-level Landau-Zener model to test the quantum speed limit bounds which we mentioned earlier. Analyzing this simple model in the context of quantum control will already make us note that, in order to obtain useful information about the minimum evolution times in control problems, a different approach is needed. We will then propose a general framework for such an approach and derive a new set of bounds that can be applied to any driven quantum system.

The outline of this Thesis is as follows. In Chap. 2 we introduce and discuss some general topics related to quantum control. We review the notion of controllability of quantum systems, and discuss the quantum speed limit, that is, the existence of limitations to the speed of evolution in quantum mechanics. We link this topic with quantum control, and propose a new methods to obtain bounds on the minimum evolution time. We also give an overview of Krotov's method for quantum optimal control, and discuss some of its salient features.

In Chap. 3 we study a method for performing state control in quantum systems. The original proposal for the method [72] made use of adiabatic transitions at the avoided crossings of the eigenenergy spectrum. We show that the we can enhance the speed of the control protocol without using optimization by using sudden variations of the control field, and study its performance in closed and open quantum systems. We also study the dynamics of a two-level system under the influence of a time-periodic field. By analyzing the Floquet spectrum of quasienergies we

identify the optimal working point for population transfer, and discuss the applicability of these results in many-level models.

In Chap. 4 we study optimal control of quantum systems with many avoided crossings in their energy spectrum. We begin by studying the solution for time-optimal control in a two-level system, and relate the minimum evolution time with the quantum speed limit formulation. We also make use of the methods derived in Chap. 2 for bounding evolution times and assess their usefulness. We then apply optimization techniques to improve the control method introduced in Chap. 3. We find that we can enhance the total control time in those systems, and we investigate the physical mechanisms for such speed up by studying the shape of the optimal control fields. From these results, we also propose a closed form for the optimized fields, and derive an analytical approximate solution for the time-evolution of the state of the system.

In Chap. 5 we investigate the connection between the complexity of a quantum system and its controllability. For that we study optimal control on a chain of spin-1/2 particles, both in the few- and many-body regimes and systematically study the features of the control fields as a function of the complexity of the system. Then, in Chap. 6 we turn our attention to driven open quantum systems. By studying an exactly solvable model, we investigate how the non-Markovian features of the dynamics are affected by the presence of time-dependent driving fields. We also adapt the optimal control methods used in previous chapters to non-unitary evolution and assess the role of non-Markovianity in the controllability of the system. Finally, in Chap. 7 we summarize the conclusions of this thesis and point out potential directions for future research.

List of publications

(i) P. M. Poggi, F. C. Lombardo, D. A. Wisniacki, Controlling open quantum systems using fast transitions. Phys. Rev. A 87, 022315 (2013).

(ii) P. M. Poggi, F. C. Lombardo, D. A. Wisniacki, Quantum Speed Limit and optimal evolution time in a two-level system, Europhys. Lett. 104, 40005 (2013).

(iii) P. M. Poggi, F. J. Arranz, R. M. Benito, F. Borondo, D. A. Wisniacki, Maximum Population Transfer in a Periodically Driven Two-Level System. Phys. Rev. A 90, 062108 (2014).

(iv) P. M. Poggi, F. C. Lombardo, D. A. Wisniacki, Enhancement of quantum speed limit time due to cooperative effects in multilevel systems. J. Phys. Math. and Theo. 48, 35FT02 (2015).

(v) P. M. Poggi, F. C. Lombardo, D. A. Wisniacki, Time-optimal control fields for quantum systems with multiple avoided-crossings. Phys. Rev. A 92, 053411 (2015).

(vi) P. M. Poggi, D. A. Wisniacki, Optimal control of quantum many-body systems: chaos and complexity. Phys. Rev. A 94 033406 (2016).

(vii) P. M. Poggi, F. C. Lombardo, D. A. Wisniacki, Driving-induced amplification of non-Markovianity in open quantum systems evolution, Europhys. Lett. 118, 20005 (2017).

Chapter 3 is based on publications (i) and (iii). Chapter 4 is based on publications (ii), (iv) and (v). Chapter 5 is based on publication (vi) and Chapter 6 is based on publication (vii).

Introducción

Durante las últimas décadas, se han logrado grandes avances en el grado de manipulación de sistemas físicos en la escala nano y subnanoscópica, donde la coherencia cuántica juega un papel dominante. Algunos hitos registrados en los últimos años son: la manipulación óptica de partículas individuales en trampas de iones, la interacción controlada a través de fotones de electrones individuales en puntos cuánticos de silicio y la realización de bits cuánticos (qubits) con largos tiempos de coherencia en circuitos superconductores. Actualmente, la habilidad de diseñar la evolución de sistemas cuánticos con gran precisión está allanando el camino para una nueva revolución en las tecnologías cuánticas.

Con el fin de aprovechar plenamente las propiedades útiles de los sistemas cuánticos, se debe realizar un control activo sobre ellos. Esto representa un desafío tecnológico y teórico formidable: uno debe ser capaz de preparar un sistema en un estado inicial determinado, realizar la evolución deseada, y finalmente medir el estado de una manera muy precisa. Además, las interacciones entre el sistema y el control externo inevitablemente provocan ruido. Esto, además del ruido ambiental intrínseco, representa una amenaza para las características cuánticas del sistema.

En esta Tesis investigamos varios aspectos relacionados con el control de los sistemas cuánticos en un contexto general, que se representa esquemáticamente en la Figura 1.1, donde observamos tres partes que interactúan: el sistema $\mathcal{S}$, el entorno $\mathcal{E}$ y el control $\vec{u}(t)$. Nuestro objetivo es explorar cómo las características de cada agente afectan nuestra capacidad de controlar el sistema. Para ello utilizamos un enfoque constructivo, mediante el cual estudiamos en detalle modelos físicos simples, para luego incrementar su complejidad y desarrollar una comprensión más general de los aspectos físicos y matemáticos del problema general de control. Como veremos a lo largo de esta Tesis, los fenómenos básicos pero no triviales encontrados en los casos más simples aparecerán entrelazados en escenarios más complejos. Por ejemplo, analizaremos de forma exhaustiva un sistema cuántico de dos niveles que se describe por medio de campos fijos (oscilantes, lineales,

constantes por partes) y también técnicas de control óptimo. Esto nos permitirá construir un método para controlar sistemas de muchos niveles, el cual es adecuado para su aplicación en sistemas cuánticos abiertos donde la influencia ambiental es adversa al control. También proponemos variaciones de esta técnica para realizar un control en un tiempo óptimo. Vamos a demostrar que somos capaces de derivar una interpretación física simple de los campos óptimos derivados numéricamente para estos sistemas, basándonos en un estudio analítico del modelo de dos niveles forzado periódicamente. Este modelo, a su vez, también nos dará una visión importante sobre la interacción entre la conducción en sistemas cuánticos abiertos y la aparición de efectos no-Markovianos. Para esos casos, también exploraremos situaciones en las que el entorno es esencial para controlar un sistema cuántico.

En este Capítulo presentamos una introducción general a los diversos tópicos mencionados anteriormente, incluyendo un resumen histórico de la aplicación de métodos de control óptimo en sistemas cuánticos y una visión general de los avances sobre el estudio del límite de velocidades cuántico en los últimos años. Asimismo mencionamos los antecedentes mas inmediatos relacionados al estudio de complejidad y control en sistemas cuánticos, y al estudio de efectos no Markovianos en sistemas cuánticos abiertos. Finalmente exponemos el esquema de esta Tesis capítulo por capítulo, y enumeramos el listado de publicaciones desarrolladas en base a este trabajo.

Chapter 2

General aspects of control in quantum systems

In this chapter we present an overview of general aspects about control in quantum systems. We do this before turning our attention to specific models and physical setups, in order to gain insight about the global properties and potential limitations which can be encountered when dealing with quantum control problems. First, we will study the concept of controllability, which allows us to precisely determine, given a certain control process and the structure of the system Hamiltonian, whether it is possible to find a control field which solves the problem or not. Next, we discuss the existence of minimal evolution times for controlling quantum systems, and introduce the concept of quantum speed limit. We will then propose novel methods for obtaining lower bounds on such minimal times, which represent one of the main novel contributions of this Thesis. Finally, we will present the general theoretical framework of optimal control applied to quantum systems, and give an overview of its more important features.

2.1 Controllability

Given a physical system in an experimental situation in which one or more externally controllable parameters are available, the question arises about what type of (or how many different) transformations can be performed by properly tuning those parameters in time. In other words, we can ask ourselves what is the degree of *controllability* of the system in those conditions. Here, we will address this question following the methods of the book by D'Alessandro [73].

We begin by considering Schrödinger equation for quantum unitary evolution,

$$\frac{d}{dt}\left|\psi(t)\right\rangle = -i\, H(\vec{u}(t))\left|\psi(t)\right\rangle, \tag{2.1}$$

where $H(\vec{u})$ represents the system Hamiltonian, which contains one or several of the control parameters in $\vec{u}(t) = (u_1(t), u_2(t), \ldots, u_k(t))$ and we set $\hbar = 1$. The system in (2.1) is said to be (pure state) controllable if, for all $\left|\psi_0\right\rangle$, $\left|\psi_1\right\rangle$, there exists a control function $\vec{u}(t)$ and a final time $T > 0$ such that there is a solution $\left|\psi(t)\right\rangle$ that satisfies $\left|\psi(0)\right\rangle = \left|\psi_0\right\rangle$ and $\left|\psi(T)\right\rangle = \left|\psi_1\right\rangle$.

We will now see that a test can be performed in order to check whether a system is controllable. To do this, we rewrite the time evolution equation (2.1) into its operator form,

$$\frac{d}{dt}U(t) = H(\vec{u}(t))U(t),\ U(0) = \mathbb{I}, \tag{2.2}$$

and define the reachable set $\mathcal{R}$ at time $T > 0$ of this system as the set of all unitary matrices $\bar{U}$ such that there exists a function $\vec{u}(t)$ that gives a solution with $U(t) = \bar{U}$. The reachable set of the system thus characterizes the transformations that can be performed by the system (2.2) by properly choosing the control fields. From this definition, it is clear that a system is controllable if its reachable set equals the set of all special unitary operators, $\mathcal{R} = SU(n)$, where n is the dimension of Hilbert space.

In order to characterize the reachable set $\mathcal{R}$, we need to analyze the system Hamiltonian. Since H is a function of the time-dependent control fields $\vec{u}(t)$, there is a whole set of different operators which can be obtained by changing these fields. We call this set the dynamical Lie algebra $\mathcal{L}$ of the system,

$$\mathcal{L} = \mathrm{span}_{\vec{u}(t)}\left\{-i\, H(\vec{u}(t))\right\} \tag{2.3}$$

This Lie algebra, in turn, determines a Lie group via an exponential map $\mathrm{e}^{\mathcal{L}}$. Given the hermitian property of the Hamiltonian, $\mathcal{L}$ is a subalgebra of $u(n)$, and thus $\mathrm{e}^{\mathcal{L}}$ will be a subgroup of $U(n)$. This subgroup is the reachable set introduced in the previous paragraph; i.e.,

$$\mathcal{R} = \mathrm{e}^{\mathcal{L}}. \tag{2.4}$$

This connection between the reachable set and the dynamical Lie algebra allows us to test for controllability in a rather straightforward way: if we can prove that $\mathcal{L} = su(n)$, then we know that $\mathcal{R} = SU(n)$ (or $u(n)$ and $U(n)$, if that is of interest), and thus the system is controllable.

To check whether the dynamical Lie algebra covers all $su(n)$ we can compute its

dimension by constructing a basis and counting linearly independent elements in it. This basis can be constructed by means of a repeated Lie bracket (or commutator). The procedure is as follows. For simplicity, let us assume a bilineal control problem where the Hamiltonian takes the form

$$H(\vec{u}) = H_0 + \sum_{j=1}^{K} u_j H_j. \tag{2.5}$$

Now, take the operators which appear in H (which are called zero-depth elements of $\mathcal{L}$) and compute all the commutators between them. This will give a new set of operators. By keeping only the ones that are linearly independent, we obtain the set of depth 1 operators. We can continue this procedure by iteratively computing the commutators between the operators with depth k and the zero-depth set,

$$[H_1, [H_2, [\ldots, H_{p-1}, H_p]]] \tag{2.6}$$

Eventually, we will obtain no new linearly independent operators by this procedure [74]. At this point, we have constructed a basis of the dynamical Lie algebra, and we can now check for controllability: if the dimension of the constructed basis set is $n^2 - 1$, then $\mathcal{L} = su(n)$ and the system is controllable.

Note that this procedure is analogous to computing all the operators which generate the Magnus expansion of $U(t)$ in (2.2). Also, we point out that if the system is not completely controllable, then the criterion put forward in the previous paragraph will not hold. However, the system may still be controllable in some subset of physically interesting operations, as studied in [75].

2.2 Bounds on the minimal evolution time: the quantum speed limit

Given a control problem, it is usually of interest not only to derive the control field which performs the desired process, but also to do so in the shortest possible evolution time. This is typically the case in quantum computation, for example, where a vast number of operations have to performed sequentially, and thus it is essential for each of them to be realized as fast as possible, in order to avoid undesirable environmental effects which can destroy the coherence properties of the system.

In this context, during the past decade there has been a renewed interest on obtaining fundamental limitations on the speed of evolution for quantum systems.

These limitations were originally formulated via Heisenberg-like uncertainty relations by Mandelstam and Tamm in the mid 20th century, and have since then been generalized to a variety of scenarios, such as open quantum system dynamics, evolution of mixed states and time-dependent Hamiltonians. In the following section we will give an overview of this quantum speed limit (QSL) problem, with special emphasis in those results which are relevant to our work. We will then discuss the relation between QSL and quantum control.

2.2.1 Quantum speed limit: overview

In 1945, Mandelstamm and Tamm [50] derived a generalization of Heisenberg uncertainty relation between time and energy, that could be applied to any quantum system. We re-derive it here, starting from Robertson's inequality [76]

$$\langle(\delta A)^2\rangle\langle(\delta B)^2\rangle \geq \frac{1}{4}\left|\langle[A,B]\rangle\right|^2, \tag{2.7}$$

where $\delta A = A - \langle A\rangle$. For any operator A we can write Heisenberg's equation

$$\frac{dA}{dt} = -\frac{i}{\hbar}[A,H] \tag{2.8}$$

By taking the expectation value in the last expression we obtain Ehrenfest equation,

$$\langle\frac{dA}{dT}\rangle = -\frac{i}{\hbar}\langle[A,H]\rangle. \tag{2.9}$$

We now identify operator B in eqn. (2.7) with the system Hamiltonian H and combine with eqn. (2.9) to obtain

$$\Delta E\Delta A \geq \frac{\hbar}{2}\left|\frac{d\langle A\rangle}{dt}\right|, \tag{2.10}$$

where $\Delta A = \sqrt{\langle A - \langle A\rangle\rangle^2}$, and $\Delta E \equiv \Delta H$. We can further define

$$\Delta t_A = \frac{\Delta A}{\left|\frac{d\langle A\rangle}{dt}\right|}, \tag{2.11}$$

which has units of time. We then arrive at the Mandelstam-Tamm relation

$$\Delta t_A \Delta E \geq \frac{\hbar}{2}. \tag{2.12}$$

In this formulation, Δt_A is interpreted as *some* characteristic time related to the time evolution of observable A. The link between this quantity and the physical evolution time was studied first by Fleming [77] and then by Bhattacharyya [51], in the following way. Consider expression (2.12) under the specific choice of $A = |\phi_0\rangle\langle\phi_0|$, with $|\phi_0\rangle$ some arbitrary pure state. If we take the expectation values in (2.12) with respect to the evolved state $|\phi_t\rangle = U(t)\,|\phi_0\rangle$, it is easy to observe that

$$\langle A\rangle = |\langle\phi_t|\phi_0\rangle|^2 = P_t \tag{2.13}$$

where we have introduced the short-hand notation for P_t, the time-dependent non-decay probability. Eqn. (2.12) can now be expressed as

$$\frac{\left|\frac{dP_t}{dt}\right|}{\sqrt{P_t(1-P_t)}} \leq 2\frac{\Delta E}{\hbar} \tag{2.14}$$

We can use the relation $\arccos'(x) = -(1-x^2)^{-1/2}$ to write (2.14) in a more compact form

$$\frac{d}{dt}\arccos(\sqrt{P_t}) \leq \frac{\Delta E(t)}{\hbar}, \tag{2.15}$$

This is the main result by Bhattacharyya. If the initial state $|\phi_0\rangle$ evolves subject to a time-independent Hamiltonian, then the inequality above can be readily integrated from $t = 0$ to $t = T$, obtaining

$$\Delta t \Delta E \geq \hbar \arccos(\sqrt{P_t}) \;\Rightarrow\; t \geq \frac{\hbar}{\Delta E}\arccos\left(|\langle\phi_0|\phi_t\rangle|\right) \equiv t_{QSL}^{MT} \tag{2.16}$$

The last expression in (2.16) is usually referred to Mandelstam-Tamm bound. In the particular case where $|\phi_t\rangle$ is orthogonal to $|\psi_0\rangle$, we obtain $t_{QSL} = \frac{\pi\hbar}{2\Delta E}$. This expression sets a bound on the minimum time required for a system to evolve from $|\phi_0\rangle$ to an orthogonal state. For this case, Margolus and Levitin [78] also derived a similar bound, but in terms of the mean energy of the state,

$$t \geq \frac{\pi\hbar}{2\,E} \equiv t_{QSL}^{ML} \tag{2.17}$$

where $E \equiv \langle H - \varepsilon_0 \mathbb{I}\rangle$, i.e. the expectation value of the Hamiltonian with respect to the ground state. Giovannetti *et al.* [49] later generalized this result to non-orthogonal states, and coined the term "quantum speed limit tim" for t_{QSL}. Finally, Levitin and Toffoli [79] showed that the unified bound

$$t \geq \min\left\{\frac{\pi\hbar}{2\,\Delta E}, \frac{\pi\hbar}{2\,E}\right\}, \tag{2.18}$$

is tight, meaning that for every time-independent Hamiltonian there is a choice of initial state for which the equality in (2.18) holds.

2.2.2 Geometrical interpretation

Bhattacharyya's result (2.15) has an insightful geometrical interpretation, which was first noted by Anandan and Aharonov [80] in the following way. Let us define the Fubini-Study distance between two pure states,

$$s(\phi, \psi) = 2\arccos(|\langle\phi|\psi\rangle|). \tag{2.19}$$

It can be easily seen that this definition has the usual properties required for a distance,

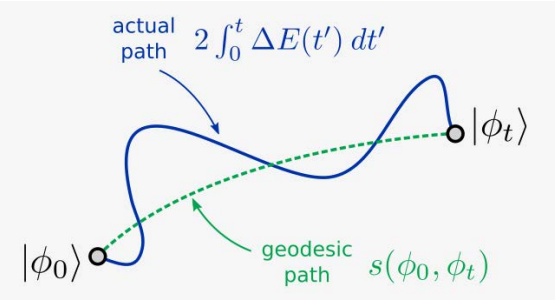

FIGURE 2.1: Schematic drawing of the time evolution of quantum states. Anandan-Aharonov relation (2.20) expresses the fact that the length of the actual path of the evolution is necessarily larger or equal than the length of the geodesic path between the initial and evolved state.

1. $s(\phi,\psi) \geq 0$
2. $s(\phi,\phi) = 0 \Leftrightarrow |\phi\rangle = |\psi\rangle$ (up to a global phase)
3. $s(\phi,\psi) = s(\psi,\phi)$
4. $s(\phi,\psi) \leq s(\phi,\chi) + s(\chi,\psi)$

With this definition, we can rewrite expression (2.15) in differential form

$$ds(\phi_0,\phi_{dt}) \leq 2\Delta E(t)\,dt \;\Rightarrow s(\phi_0,\phi_t) \leq \int_0^t \Delta E(t')\,dt', \tag{2.20}$$

where we have set $\hbar = 1$. The last inequality in (2.20) is the Anandan-Aharonov relation, and expresses a simple geometrical statement: the distance traversed in state space by the quantum system going from $|\phi_0\rangle$ to $|\phi_t\rangle$ is always larger than or equal to the length of the geodesic path joining both states, as can be appreciated in the schematic drawing of Fig. 2.1.

Note that expression (2.20) also tells us that energy variance $\Delta E(t)$ can be seen as a measure of the Hilbert space velocity of the state $|\phi_t\rangle$. In particular, ΔE measures the component of $|\dot{\phi}_t\rangle$ which is perpendicular to $|\phi_t\rangle$ [81]. We can see this in the following way. If we write the time derivative of the quantum state as $|\dot{\phi}_t\rangle = |\dot{\phi}_t\rangle^{\parallel} + |\dot{\phi}_t\rangle^{\perp}$, then we have that, by definition,

$$|\dot{\phi}_t\rangle^{\parallel} = |\phi_t\rangle \left\langle \phi_t|\dot{\phi}_t \right\rangle = -i\langle E\rangle\,|\phi_t\rangle\,, \tag{2.21}$$

where we have used $|\dot{\phi}_t\rangle = -iH_t\,|\phi_t\rangle$ and noted $\langle\phi_t|\,H_t\,|\phi_t\rangle \equiv \langle E\rangle$. This result tells us that the phase of the quantum state evolves at a rate given by $\langle E\rangle$. The remaining perpendicular component of the velocity, $|\dot{\phi}_t\rangle^{\perp} = |\dot{\phi}_t\rangle - |\dot{\phi}_t\rangle^{\parallel}$, is such

that

$$\begin{aligned} \|\dot{|\phi_t\rangle}^{\perp}\|^2 &= \left\langle \dot{\phi}_t|\dot{\phi}_t \right\rangle + \left\langle \dot{\phi}_t^{\parallel}|\dot{\phi}_t^{\parallel} \right\rangle - \left\langle \dot{\phi}_t|\dot{\phi}_t^{\parallel} \right\rangle - \left\langle \dot{\phi}_t|\dot{\phi}_t^{\parallel} \right\rangle \\ &= \langle H^2 \rangle - \langle H \rangle^2 = \Delta E^2 \end{aligned} \tag{2.22}$$

As we have already seen, the Mandelstam-Tamm bound is recovered from the Anandan-Aharonov relation when the dynamics is generated by a time-independent Hamiltonian, in which ΔE is always time-independent itself. As such, the inequality (2.16) has a purely geometrical nature, and its saturated if and only if the motion of the system state is along a geodesic in Hilbert space.

Most of the extensions and generalizations of the quantum speed limit formulation have been pursued in this geometrical setting. In particular, bounds have been derived for the maximum speed of evolution under non-unitary dynamics almost simultaneously by Deffner and Lutz [82], Del Campo *et al.* [83] and Taddei *et al.* [84]. Special attention has been devoted to studying the predicted speed-up of the evolution in open systems undergoing non-Markovian dynamics [85, 86, 87, 88]. Extensive analysis of the current results on these topics have been published as reviews in Refs. [52, 53].

2.2.3 Connection with quantum control

Let us go back to the (unitary) quantum control problem described in the Introduction. We consider a quantum system initially prepared in state $|\psi_0\rangle$, evolving according to a Hamiltonian $H(u(t))$, and we wish to drive the system to some target state $|\psi_g\rangle$ at some final time T by properly choosing $u(t)$. It is natural to ask then, what does the quantum speed limit formulation tells us about the time T required to perform that process? Can it be made arbitrarily fast? Can we establish a lower bound for T?

At first glance, it is obvious that nor the Mandelstam-Tamm (2.14) nor the Margolus-Levitin (2.17) bounds can be applied to this setting, since quantum control problems deal generally with time-dependent Hamiltonians. We then go back to Anandan - Aharonov relation (2.20) to obtain a bound on the evolution time. This can be done in a number of ways: one of them was proposed by Deffner and Lutz [89], and it simply consists on rewriting eq. (2.20) as

$$t \geq \frac{\arccos\left(|\langle \psi_0|\psi(t)\rangle|\right)}{\overline{\Delta E}} \tag{2.23}$$

where we defined the time-average of the energy variance simply as

$$\overline{\Delta E} = \frac{1}{t}\int_0^t \Delta E(t')\, dt'. \tag{2.24}$$

We can now evaluate (2.23) in $\tau = T$, such that if there is a time T such that $|\psi(T)\rangle = |\psi_g\rangle$, then the following relation must hold

$$T \geq \frac{\arccos\left(|\langle\psi_0|\psi_g\rangle|\right)}{\overline{\Delta E}} \equiv T^*_{QSL} \tag{2.25}$$

However, a closer look at expression (2.25) reveals that, in order to compute the bound, we need both an actual choice of $u(t)$ and the complete time-evolved state $|\psi(t)\rangle$. This contradicts our initial purpose, which is to estimate the minimum evolution time without solving the dynamics, and moreover without knowing the actual control field which will be used to drive the system. The contradiction is also notorious when casting the expression (2.25) into the form

$$T^*_{QSL} = \frac{s(\psi_0, \psi_g)}{\int_0^T \Delta E(t')\, dt'} T = \frac{s_{\text{geod}}}{s_{\text{path}}} T. \tag{2.26}$$

In the last expression, we can see that the bound estimate T^*_{QSL} depends on two geometrical quantities: the length of the geodesic between $|\psi_0\rangle$ and $|\psi_g\rangle$ and the length of the actual path. Moreover, the quantum speed limit time could go to zero if the $s_{\text{path}} \gg s_{\text{geod}}$. It is then clear that this quantity gives us information about distances in Hilbert space, but not about the speed at which those paths are traversed.

Let us also note that other bounds on the evolution time can be extracted from the general Anandan - Aharonov relation. We will use them in Chapter 4 when analyzing the problem of time-optimal control of a two-level system in detail. This will allow us to show that, although valid, all of these bounds require complete information about the evolution of the system, and thus are not useful for obtaining an *a priori* estimate on the minimum time required for a certain control process.

2.2.3.1 Methods for obtaining bounds on minimum evolution times

In the previous paragraphs we showed that the usual quantum speed limit formulation is in general not suitable for obtaining bounds on the evolution time of a controlled quantum system *a priori* (i.e., without needing to solve Schrödinger equation). Here, we propose various methods to overcome this limitation which, together with its application to different physical models in Chapter 4, represent

one of the main results of this Thesis.

We begin by explicitly formulating the problem of interest. Consider a quantum system which evolves unitarily under the action of a parameter-dependent Hamiltonian $H(\vec{u})$, with $\vec{u} = \vec{u}(t)$ the (generally time-dependent) control fields. Although the form of the fields can be unknown, we consider that the control fields may have constraints of the form $|u_i(t)| \leq u_i^{max}$. Let us fix an initial state $|\psi_0\rangle$ and a target state $|\psi_g\rangle$. We wish to obtain a lower bound on the evolution time T, where T is such that $|\psi(0)\rangle = |\psi_0\rangle$ and $|\psi(T)\rangle = |\psi_g\rangle$. The bound should be computable with all given information, i.e., it should be of the form

$$T \geq t_{min}\left(H, \{u_i^{max}\}, |\psi_0\rangle, |\psi_g\rangle\right) \tag{2.27}$$

Our first approach to this problem is to manipulate the Anandan - Aharonov relation (2.20) in order to drop any implicit or explicit dependence on $|\psi(t)\rangle$ or $\vec{u}(t)$. This can be done by using the following inequality

$$2\Delta E(t) \leq \sqrt{2}\|H(t)\| \equiv \sqrt{2\,\mathrm{tr}(H(t)^2)}. \tag{2.28}$$

Note that a weaker version of this inequality can be easily derived by expanding the evolved state in the instantaneous eigenbasis of H, $|\psi\rangle = \sum_k c_k |k\rangle$ so that

$$\begin{aligned} 4\Delta E^2 &= 4\sum_k |c_k|^2 \varepsilon_k^2 - 4\left(\sum_k |c_k|^2 \varepsilon_k\right)^2 \\ &\leq 4\sum_k |c_k|^2 \varepsilon_k^2 \leq 4\sum_k \varepsilon_k^2 = 4\mathrm{tr}(H^2), \end{aligned} \tag{2.29}$$

where $\{\varepsilon_k\}$ are the eigenvalues of H. The derivation of the strong inequality (2.28) is a bit more involved, and can be found in a paper by Brody [90]. Combining (2.20) and (2.28) we can write

$$s(\psi_0, \psi(T)) \leq \sqrt{2}\int_0^T \|H(t')\|\, dt' \leq \sqrt{2}\|H\|_{max} T \tag{2.30}$$

In the last step, we bounded $\|H\|$ by its maximum value, which will be a function of $\{u_i^{max}\}$ in general. In this way we have successfully derived an inequality without using information about $|\psi(t)\rangle$ nor $\vec{u}(t)$. Rearranging the last expression, we obtain that if there is a time T for which $|\psi(T)\rangle = |\psi_g\rangle$, then it holds that

$$T \geq \frac{s(\psi_0, \psi_g)}{\sqrt{2}\|H\|_{max}} \equiv t_{min}^B \tag{2.31}$$

where the superscript "B" refers to Brody. The definition of t_{min}^B is clearly of the form we initially proposed, c.f. eq. (2.27). Note, however, that this expression scales unfavorably with the dimension n of the system, since its computed via

$\|H\| = \sum_k \epsilon_k^2$, i.e., a sum of n positive numbers.

Another approach to obtain a bound of the form (2.27) can be derived from a result by Pfeifer in Refs. [91, 92], in which he proposes that general time-energy uncertainty relations for time-dependent Hamiltonians should be computable without solving Schrödinger's equation. The main result reads as follows: given a quantum state $|\psi(t)\rangle$ which evolves according to $i\frac{d}{dt}|\psi(t)\rangle = H(t)|\psi(t)\rangle$ with $|\psi(0)\rangle = |\psi_0\rangle$, and an arbitrary reference state $|\varphi\rangle$, then the following relation holds

$$|\langle\varphi|\psi(t)\rangle| \lesseqgtr \sin_*(\delta \pm h(t)) \tag{2.32}$$

where $\delta = \arcsin(|\langle\varphi|\psi_0\rangle|) = \frac{\pi}{2} - \arccos(|\langle\varphi|\psi_0\rangle|)$, $\sin_*$ is the a modified sine function

$$\sin_*(x) = \begin{cases} 0 & \text{if} \quad x \leq 0 \\ \sin(x) & \text{if} \quad 0 < x \leq 1 \\ 1 & \text{if} \quad x > 1 \end{cases} \tag{2.33}$$

and we defined

$$h(t) = \min_{|\psi_0\rangle,|\varphi\rangle} \left\{ \int_0^t \Delta E_\varphi(t')\, dt', \int_0^t \Delta E_{\psi_0}(t')\, dt' \right\} \tag{2.34}$$

where we use the notation $\Delta E_\chi \equiv \langle\chi| H^2 |\chi\rangle - \langle\chi| H |\chi\rangle^2$. We show the derivation of this theorem in Appendix A.1. Pfeifer's relation (2.32) is appealing to the quantum control problem studied here, since it gives bounds for the probability of finding a *driven* system in an *arbitrary* state $|\varphi\rangle$ [91]. More interestingly, we can extract a bound on the evolution time itself, in the following way. If we consider the upper bound in (2.32) for such probability, and consider the reference state to be our target state, $|\varphi\rangle = |\psi_g\rangle$, we get that, at time $t = T$

$$|\langle\psi_g|\psi(T)\rangle| \leq \sin_*(\delta + h(T)). \tag{2.35}$$

From this expression its clear that, in order to have a successful control process, we need the upper bound to be as large as possible, i.e. 1. Looking at the definition (2.33), it is then sufficient to impose

$$\delta + h(T) \geq \frac{\pi}{2} \Rightarrow h(T) \geq \frac{\pi}{2} - \delta = \frac{1}{2} s(\psi_0, \psi_g) \tag{2.36}$$

Note that $h(T)$ depends on T via the control field $\vec{u}(T)$. In order to obtain a lower bound for the evolution time, we proceed as we did when deriving (2.30) and bound the integral in (2.34) by

$$h(T) \leq \Delta E_\chi^{max} T \text{ with } \chi = \psi_0, \psi_g, \tag{2.37}$$

where, again, we expect ΔE_χ^{max} to be an explicit function of $\{u_i^{max}\}$. Rearranging the expression above we arrive at

$$T \geq \frac{s(\psi_0, \psi_g)}{2\Delta E_\chi^{max}} \equiv t_{min}^P \text{ with } \chi = \psi_0 \text{ or } \psi_g, \tag{2.38}$$

where "P" now stands for Pfeifer. Again, t_{min}^P is also of the form (2.27) and thus allows us to obtain a lower bound on the minimum evolution time without knowing the actual shape of $\vec{u}(t)$.

We now explore an interesting property of Pfeifer's bound (2.38). Let us make the following assumptions about our general control problem. We take the Hamiltonian of the system be of the form

$$H(u(t)) = H_0 + u(t)H_c \tag{2.39}$$

where we suppose that the control field $u(t)$ has dimensionless units. We can then explicitly write down the squared variance of the Hamiltonian as

$$\Delta E^2 = \Delta H_0^2 + u^2 \Delta H_c^2 + u(\langle\{H_0, H_c\}\rangle - 2\langle H_0\rangle\langle H_c\rangle) \tag{2.40}$$

Suppose now that our control problem is such that the initial and target states $|\psi_0\rangle$, $|\psi_g\rangle$ are eigenstates of H_c. Then, we trivially obtain that $\Delta H_c = 0$, but also that the crossed term in (2.40) vanishes. Inserting this into expression (2.38) we get

$$t_{min}^P = \frac{s(\psi_0, \psi_g)}{\min\{\Delta H_0|_{\psi_0}, \Delta H_0|_{\psi_g}\}} \text{ when } \psi_0, \psi_g \text{ eigenstates of } H_c. \tag{2.41}$$

What is interesting about this result is that it is completely independent of $u(t)$; not only of its actual temporal shape, but also of its maximum possible value. This means that, even in an unconstrained control problem where $u^{max} \to \infty$, there is still a fundamental limit for the speed in which we can control the system. That limit is set only by the initial and final states, and the free Hamiltonian H_0.

Another special case is when $|\psi_0\rangle$, $|\psi_g\rangle$ are eigenstates of H_0. Then, we can proceed in an analogous way to find

$$t_{min}^P = \frac{s(\psi_0, \psi_g)}{u^{max} \min\{\Delta H_c|_{\psi_0}, \Delta H_c|_{\psi_g}\}} \text{ when } \psi_0, \psi_g \text{ eigenstates of } H_0. \tag{2.42}$$

Finally, we present a third method for obtaining a bound of the form (2.27). We begin by considering two arbitrary time-dependent Hamiltonians H_1 and H_2, and two respective states $|\psi_1(t)\rangle$ and $|\psi_2(t)\rangle$ such that $\frac{d}{dt}|\psi_k\rangle = -iH_k(t)|\psi_k(t)\rangle$ with

$k = 1, 2$ and $|\psi_1(0)\rangle = |\psi_2(0)\rangle = |\psi_0\rangle$ We can then compute

$$\begin{aligned} \frac{d}{dt}\langle\psi_1|\psi_2\rangle &= i\langle\psi_1| H_1 |\psi_2\rangle\, i\langle\psi_1| H_2 |\psi_2\rangle \\ &= i\langle\psi_1| (H_1 - H_2) |\psi_2\rangle \end{aligned} \tag{2.43}$$

We can then integrate the above expression from $t = 0$ to $t = T$, which yields

$$\begin{aligned} \langle\psi_1(T)|\psi_2(T)\rangle - 1 &= i\int_0^T \langle\psi_1(t')| (H_1(t') - H_2(t')) |\psi_2(t')\rangle\ dt' \\ \Rightarrow |\langle\psi_1(T)|\psi_2(T)\rangle - 1| &\leq \int_0^T |\langle\psi_1(t')| (H_1(t') - H_2(t')) |\psi_2(t')\rangle|\, dt' \\ &\leq \int_0^T \|H_1(t') - H_2(t')\|\, dt' \end{aligned} \tag{2.44}$$

We now take an approach proposed by Arenz [93]. We consider H_1 to be of the form (2.39), i.e. $H_1 = H_0 + u(t)H_c$, and also fix $H_2 = u(t)H_c$. For a successful control protocol, we have that $|\psi_1(T)\rangle = |\psi_g\rangle$, and we can also integrate $|\psi_2(t)\rangle$ up to $t = T$, which trivially yields $|\psi_2(T)\rangle = \exp(-i\alpha(T)H_c)|\psi_0\rangle$ where $\alpha(T) = \int_0^T u(t')dt'$. In this case, expression (2.44) can be casted as

$$|\langle\psi_g| \mathrm{e}^{-i\alpha(T)H_c} |\psi_0\rangle \leq \|H_0\|\, T \tag{2.45}$$

We can further bound this expression in order to get rid of the dependence on the unknown function $u(t)$. To do so, we use the spectral decomposition of $H_c = \sum_j \varepsilon_j^c |\phi_j^c\rangle\langle\phi_j^c|$ and the inequality $|\sum_j z_j - 1| \geq 1 - \sum_j |z_j|$ (with $|z_j| \leq 1$) to obtain

$$1 - \sum_j^n |\langle\psi_g|\phi_j^c\rangle \langle\phi_j^c|\psi_0\rangle \leq \|H_0\| T, \tag{2.46}$$

which then gives us a new bound of the desired form (2.27)

$$T \geq \frac{1 - \sum_j^n |\langle\psi_g|\phi_j^c\rangle \langle\phi_j^c|\psi_0\rangle|}{\|H_0\|} \equiv t_{min}^{R1} \tag{2.47}$$

A similar expression can be derived in an analogous fashion by choosing $H_2 = H_0$. In that case we obtain

$$T \geq \frac{1 - \sum_j^n |\langle\psi_g|\phi_j^0\rangle \langle\phi_j^0|\psi_0\rangle|}{u^{max}\|H_c\|} \equiv t_{min}^{R2} \tag{2.48}$$

where now $\{|\phi_j^0\rangle\}$ are eigenstates of the free Hamiltonian H_0. Expressions (2.47) and (2.48) provide different ways to bound evolution times in quantum control problems. An interesting feature of these is that they are *explicit* functions of ψ_0, ψ_g, H and u^{max}, as opposed to the two previous results (2.31) and (2.38), where the actual dependence on H and u^{max} has to be worked out on each particular problem. This means that, for example, t_{min}^{R1} will always give a result independent

of u^{max} regardless the initial and target states.

In summary, in this subsection we proposed a new approach for bounding evolution times in driven quantum systems, with the goal of obtaining information without needing to solve the dynamics of the system. In Chapter 4 we will apply the results derived here to different specific problems, and asses their utility in each case.

2.3 Optimal control theory

In the previous sections of this Chapter, we have mentioned theoretical tools that allows us to decide whether a control problem has a solution or not. Controllability considerations (Sec. 2.1) can tell us whether certain states can be connected or not, and bounds on the evolution times (Sec. 2.2) can help us estimate how long the evolution should be for the control problem to be solvable. In this section we will address the core problem of quantum control: how do we find a control field $u(t)$ that drives a quantum system in a predefined way?. In some situations we can do so by exploiting our knowledge about the physics of the undriven system, as we will do in the Chapter 3. But, in general, a more systematic approach is needed. Such an approach is given by optimal control theory.

2.3.1 Krotov method of optimization

Here we describe an approach to optimization developed by Krotov [24] and used by Tannor *et al.* for the first time in a quantum control problem [23, 94]. Other methods for optimization have been developed since then, such as GRAPE (gradient ascent pulse engineering) [26] or CRAB (chopped random-basis optimization) [59]. Krotov's approach has the advantage to have a general analytical treatment of the control problem, and a certified monotonic convergence of the objective, as well as a nice geometrical interpretation.

Consider a state of a system defined through a vector $x(t)$, which is controlled by a set of variables $u(t)$ evolving via the equation of motion

$$\dot{x} = f(x, u),\ x(0) = x_0 \tag{2.49}$$

We define a process w as a pair $w = (x(t), u(t))$ which satisfies (2.49). We can then define a functional of the process $J[w]$ which we call the objective

$$J[w] = F(x(T)) + \int_0^T f^0(t, x(t), u(t))dt, \tag{2.50}$$

where F and f^0 are functions that contain information about what aspects of the dynamics we wish to optimize. The goal is then to find a process w such that $J[w]$ takes its minimum possible value. The approach by Krotov consists in introducing an scalar function $\phi(t, x)$ and write down a new functional

$$L[w, \phi] = G(x(T)) - \int_0^T R(t, x(t), u(t))dt - \phi(0, x_0), \tag{2.51}$$

with

$$G(x(T)) = F(x(T)) + \phi(T, x(T)) \tag{2.52}$$

$$R(t, x, u) = \frac{\partial \phi}{\partial x} f(t, x, u) - f^0(t, x, u) + \frac{\partial \phi}{\partial t}. \tag{2.53}$$

Is straightforward to see that for all processes w and for every choice of $\phi(t, x)$ we have $L[w, \phi] = J[w]$. Thus, minimizing the original objective J is equivalent to minimizing the new functional L, which in turn can be done by separately minimizing $G(x(T))$ and maximizing $R(t, x, u)$. The main idea of this approach is that we now have complete freedom to choose the function $\phi(t, x)$, and we can then proceed in the following way:

1. We choose an initial trial process w^0, given by $u_0(t)$ and the corresponding solution to (2.49), $x^0(t)$.

2. We construct $\phi(t, x)$ such that $L[w, \phi]$ is a maximum with respect to $x(t)$ in w^0. By doing this, we are sure that our current state $x^0(t)$ is the worst possible choice when it comes to minimize the objective; as a result, any change in x brought by a new choice of $u(t)$ can only improve the minimization of $J[w]$.

3. Once we find $\phi(t, x)$, we seek a control function $u(t)$ which maximizes $R(t, x, u)$ (this is equivalent to minimizing J with respect to u, see eqn. 2.51). This procedure will give us an expression of the form $u = \tilde{u}(t, x)$, i.e., a function of the state x.

4. Finally, we need to solve the equations of motion (2.49) together with the requirement $\tilde{u}(t, x)$ in a self-consistent way, in order to find the new process $w = (x(t), u(t))$.

The intricate step in this procedure is to construct $\phi(t, x)$ so as to satisfy the condition (2). As shown in [94], this can be casted as a Hamiltonian problem,

where we define

$$h(t,x,u,y) \equiv R(t,x,u) - \frac{\partial \phi}{\partial t} = y\, f(t,x,u) - f^0(t,x,u), \tag{2.54}$$

where $y = \partial\phi/\partial x$ is taken as an independent variable. We then obtain

$$\left\{ \begin{array}{rcl} \dot{y} & = & -\frac{\partial}{\partial x} h(t,x,u,y) \\ y(T) & = & -\frac{\partial F(x(T),u)}{\partial x(T)} \end{array} \right. \text{ and } \left\{ \begin{array}{rcl} \dot{x} & = & \frac{\partial}{\partial y} h(t,x,u,y) \\ x(0) & = & x_0 \end{array} \right. \tag{2.55}$$

We now apply this method to solving the controlled Schrödinger equation. Nevertheless, the general treatment developed here will allow us to treat an optimal control problem in an open quantum system in Chapter 6. In an unitary evolution, we have

$$\frac{d}{dt} |\psi\rangle = -iH(u(t)) |\psi\rangle \text{ with } |\psi(0)\rangle = |\psi_0\rangle \tag{2.56}$$

Suppose now that we wish to maximize the probability of reaching a certain target state $|\psi_g\rangle$ at time $t = T$. Then, we can define the function F in (2.50) as

$$F(\psi(T)) = -\langle \psi(T)| P |\psi(T)\rangle, \text{ with } P = |\psi_g\rangle\langle\psi_g|. \tag{2.57}$$

As in the general treatment we have two conjugate state variables x and y, here we define $|\chi\rangle$ as the conjugate variable of $|\psi\rangle$. We also need to treat $\langle\psi|$ and $|\psi\rangle$ as independent variables. The (optimization) Hamiltonian h can be written down from expression (2.54),

$$\begin{aligned} h(t,\psi,u,\chi) &= -i \langle\chi| H(u) |\psi\rangle + i \langle\psi| H(u) |\chi\rangle - f^0(u) && (2.58) \\ &= 2 \operatorname{Im} \langle\chi| H(t) |\psi\rangle - f^0(u) && (2.59) \end{aligned}$$

and thus we can explicitly write equations (2.55)

$$\left\{ \begin{array}{rcl} \frac{d}{dt} |\chi\rangle & = & -iH(u) |\chi\rangle \\ |\chi(T)\rangle & = & P |\psi(T)\rangle \end{array} \right. \text{ and } \left\{ \begin{array}{rcl} \frac{d}{dt} |\psi\rangle & = & iH(u) |\psi\rangle \\ |\psi(0)\rangle & = & |\psi_0\rangle \end{array} \right. \tag{2.60}$$

Equations (2.60) then give us a method to systematically perform step 2 of the iterative algorithm. In the third step we obtain a rule to update the control field, via requiring $\partial h/\partial u = 0$. To obtain an explicit expression for this, we have to define $f_0(u)$, which via eq. (2.50) defines the intermediate-time cost function. This is usually defined as

$$f^0(u) = \alpha(t) u(t)^2. \tag{2.61}$$

This choice introduces a penalty on large field amplitudes, and forces the algorithm to optimize the direction of u instead of just its magnitude. Imposing an extrema

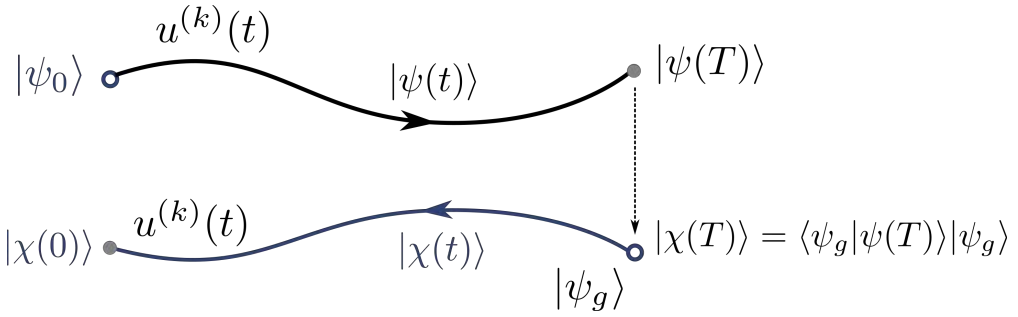

FIGURE 2.2: Schematic optimization algorithm. The initial state $|\psi_0\rangle$ is evolved using the current guess for the control field $u^{(k)}(t)$ from $t = 0$ to $t = T$. The final state is then projected to the target state to obtain a boundary condition for the adjoint state $|\chi(T)\rangle$. That state then is evolved backwards using the same field. Both trajectories are finally used to update the control field using expression (2.64).

the optimization Hamiltonian h with respect to u now gives

$$\frac{\partial}{\partial u}\left(2\,\mathrm{Im}\,\langle\chi|\,H(u)\,|\psi\rangle - u^2\right) = 0 \tag{2.62}$$

$$\Rightarrow \quad u(t) = \frac{1}{\alpha(t)}\mathrm{Im}\,\langle\chi|\,\frac{\partial H}{\partial u}\,|\psi\rangle\,. \tag{2.63}$$

In virtue of step (4), we need to solve this equation together with the equation of motion in a self-consistent way to obtain $u(t)$. Numerically, this can be done as explained in [23] with a delayed feedback procedure, which is schematically depicted in Fig. 2.2. We first evolve our initial state using the trial guess for the field $u^0(t)$, obtaining $|\psi^0(t)\rangle$. We then use the same field to the backwards evolution of $|\chi(t)\rangle$, c.f. eq. (2.60), using the same control function. We then use both trajectories to update the control field,

$$u^{(k)}(t) = u^{(k-1)}(t) + \frac{1}{\alpha(t)}\mathrm{Im}\,\langle\chi(t)|\left(\frac{\partial H}{\partial u}\right)_{u^{(k-1)}}|\psi(t)\rangle\,. \tag{2.64}$$

The new field is then used in the following iteration. The procedure stops when the functional J of eqn. (2.50) cannot be further minimized, or when a predefined threshold is achieved. Note that the function $\alpha(t)$ introduced in (2.61) can be chosen arbitrarily. In practice, it can be manipulated to ensure the stability of the algorithm, and also to enforce certain features of the control field. For example, if we want the field to turn on and off very slowly, we could propose $\alpha(t)$ to take large initial and final values [95].

2.3.2 Quantum control landscapes

Although optimization problems such as the one described in the previous section can be formally solved in theory, in practice almost all cases must be approached

numerically. There, a maximization procedure is generally done using local search algorithms, which systematically look for the direction where the objective functional grows, and stops when a maximum is reached, i.e. $\delta J = 0$. This is the case whether we have found a global or a local extremum. Note that once the k control fields $u_1(t), u_2(t), \ldots, u_k(t)$ are discretized into N time steps, we are left with a Nk-dimensional search space, and is thus reasonable to expect that if the space is filled with local and global extrema, a local search algorithm may easily converge to a poor-quality local control solution.

Surprisingly, when optimization methods began to be used to find control fields in quantum systems, numerous works reported finding optimal solutions with no "extra" efforts, as most control problems could be solved in small number of iterations to very large fidelity optimal solutions [96, 97, 98, 99, 100, 101] These results gave evidence of the benign nature of optimal control problems in quantum systems in general, which was pointed out for the first time in a seminal paper by Rabitz *et al.* [31]. There, the authors studied the usual functional to be maximized, $P_{i\to f} = |\langle i| U |f\rangle|^2$, where $|i\rangle$ and $|f\rangle$ are initial and target states, and U is the unitary evolution operator, which is a functional of the field $u(t)$, and defined the *control landscape* as the functional $P_{i\to f}[u(t)]$. Their main result is as follows: given a controllable system (in the sense described in Sect. 2.1), with no constraints in the control field, then for every $u(t)$ for which $\frac{\delta P_{i\to f}}{\delta u} = 0$, it must also hold that $P_{i\to f} = 1$. In words, this means that *the control landscape has no sub-optimal extrema*. The situation is depicted in Fig. 2.3. In this situation, every initial guess will be able to find, through local search, a global optimum, and thus no poor-quality controls (traps) are expected. This remarkable result about the topology of the control landscape motivated a number of detailed studies on structure of this object [34, 36, 102].

2.3.3 Connection with the quantum speed limit

In Sect. 2.2 we discussed the quantum speed limit problem and proposed methods to estimate a lower bound on the minimum evolution time in which a control process can be achieved. However, those bounds may not necessarily be tight, in the sense that there will generally be no specific control field which performs the control process successfully in that time. During the past decade, optimization methods have been proposed to explore and estimate the actual minimum control times in an *heuristic* fashion. The first proposal came in a work from Caneva *et al.* [54], in which it was shown that studying the performance (i.e.

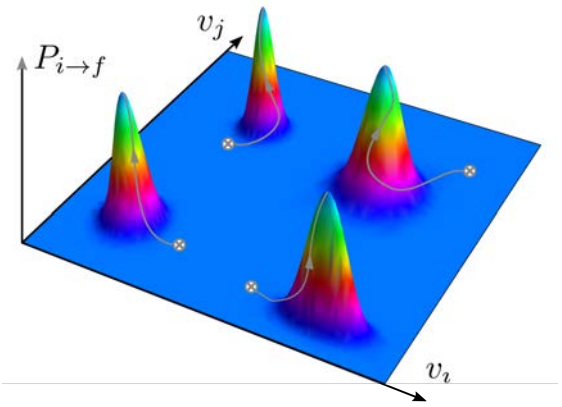

FIGURE 2.3: Simplified vision of the control landscape, which is defined as the probability of reaching the final state $P_{i\to f}$ as a functional of the control field. Here, the field $u(t)$ is discretized into just two time steps, so that $u = v_i$ for $t < T/2$ and $u = v_j$ for $t \geq T/2$. For unconstrained, fully controllable problems, Rabitz showed [31] that the landscape is trap-free, i.e. all extrema are global. This implies that all initial guesses (depicted in the figure by the symbols $\otimes$) will reach, upon local optimization, an equally good control solution.

the optimal achieved fidelity) of optimization methods as a function of the fixed evolution time T fed to the algorithm provided a method to estimate the minimum evolution time, which was termed the "quantum speed limit time"[1]. Since that proposal, numerous studies have implemented this methodology [57, 56, 103], including those presented in Chapter 4 of this Thesis. In particular, a work by Sorensen *et al.* [55] emphasized the fact that such methods could only give an upper bound to the QSL time, showing that different initial seeds for the optimization can lead to different estimates of the minimum evolution time. This is because most optimization algorithms perform a local search in the control landscape, and thus their results can depend strongly on the initial seed, specially in complex, high-dimensional systems. Evidence was also presented in [55] that optimization slows down when the evolution time is constrained, suggesting that the benign landscape topology predicted by Rabitz (for unconstrained scenarios) can suffer major changes, including the emergence of traps (local maxima). The study of these changes is currently a matter of active investigation.

[1]This nomenclature can be confusing since this magnitude is, in principle, unrelated to the original quantum speed limit results given by the Mandelstam-Tamm and Margolus-Levitin bounds (2.16) and (2.17). Nevertheless, it has been adopted in most of the literature on quantum optimal control

Aspectos generales del problema de control en sistemas cuánticos

En este capítulo presentamos una visión general sobre aspectos generales relacionados con el control en sistemas cuánticos. Hacemos esto antes de dirigir nuestra atención a modelos específicos con el fin de obtener un primer enfoque sobre las propiedades globales y las posibles limitaciones que se pueden encontrar cuando se tratan problemas de control cuántico.

En primer lugar, estudiamos el concepto de controlabilidad, que permite determinar con precisión, dado un determinado proceso de control y la estructura del sistema hamiltoniano, si es posible encontrar un campo de control que resuelva el problema o no. Este formalismo, que actualmente se encuentra desarrollado solo para sistemas que evolucionan unitariamente, se basa en el estudio del denominado álgebra de Lie dinámico, el cual puede caracterizarse de manera sistemática a partir del Hamiltoniano del sistema.

Luego, discutimos la existencia de tiempos de evolución mínimos para el control de sistemas cuánticos, e introducimos el concepto de límite de velocidad cuántico (QSL). Dado un problema de control, normalmente es de interés no sólo derivar el campo de control que realiza el proceso deseado, sino también hacerlo en el tiempo de evolución más corto posible. Esto es de interés típicamente en computación cuántica, por ejemplo, donde un gran número de operaciones tiene que realizarse secuencialmente, por lo que es esencial que cada una de ellas se realice lo más rápidamente posible, para evitar efectos ambientales indeseables que pueden destruir las propiedades de coherencia del sistema. En este contexto, durante la última década ha habido un renovado interés por estudiar los límites fundamentales a la velocidad de evolución de los sistemas cuánticos. Estas limitaciones fueron originalmente formuladas a través de las relaciones de incertidumbre de Heisenberg por Mandelstam y Tamm a mediados del siglo XX y, desde entonces, se han generalizado a una variedad de escenarios, como por ejemplo a sistemas cuánticos

abiertos, a la evolución de los estados mixtos y a hamiltonianos dependientes del tiempo. En la sección 2.2 presentamos una visión general de este problema, con especial énfasis en los resultados que son relevantes para nuestro trabajo.

En dicha sección también se discute la relación entre QSL y control cuántico, y mostramos que la formulación usual del límite cuántico de velocidad no es en general adecuada para obtener límites en el tiempo de evolución de un sistema cuántico controlado *a priori* (es decir, sin necesidad de resolver la ecuación de Schrödinger). Proponemos entonces varios métodos para superar esta limitación que, junto con su aplicación a diferentes modelos físicos en el capítulo 4, representan uno de los principales resultados de esta Tesis.

En la sección final de este Capítulo abordamos el problema central del control cuántico: ¿cómo encontrar un campo de control $u(t)$ necesario para manipular un sistema cuántico de una manera predefinida?. Si bien en algunas situaciones podemos hacerlo explotando nuestro conocimiento sobre la física del sistema, como lo haremos en el capítulo 3, en general se necesita un enfoque más sistemático. Este enfoque está dado por la teoría de control óptimo. En dicha sección desarrollamos el planteo general de esta teoría y mencionaremos sus características más importantes.

Aunque los problemas de optimización como el descrito en dicha sección anterior pueden ser formalmente resueltos de manera teórica, en la práctica casi todos los casos deben ser abordados numéricamente. Allí, un procedimiento de maximización se hace generalmente utilizando algoritmos de búsqueda local, que sistemáticamente buscan la dirección donde el objetivo funcional crece, y se detiene cuando se alcanza un máximo. Este es el caso si hemos encontrado un extremo global o local. Notar que una vez que los k campos de control se discretizan en N pasos temporales, se obtiene como resultado un espacio de búsqueda Nk - dimensional, por lo que es razonable esperar que si el espacio está lleno de extremos locales y globales, un algoritmo de búsqueda local puede converger fácilmente en una solución de control local de mala calidad. Sorprendentemente, cuando los métodos de optimización comenzaron a usarse para encontrar campos de control en sistemas cuánticos, numerosos trabajos informaron encontrar soluciones óptimas sin esfuerzos "extra" ya que la mayoría de los problemas de control podrían resolverse en un número pequeño de iteraciones a soluciones óptimas de gran fidelidad. Discutimos sobre el final del Capítulo algunos resultados previos relevantes sobre este tópico.

Chapter 3

Quantum control via navigation of the energy spectrum

In this Chapter we develop a method for implementing state-to-state control in quantum systems without using optimization techniques. The method is based on the knowledge of the spectrum of the system as a function of an external control parameter, and is suitable for systems which show well-defined avoided crossings in their energy spectrum. Although this characteristic may seem rather restrictive, it is, in fact, a general property of systems with interaction between its energy levels [104], at least in the low energy region. The method provides a way to derive a well–defined series of fast (diabatic) and sudden (step–like) variations of the control parameter, which allows us to evolve through the state space of the system and reach the desired target state. Although we will assess the time-optimality of the method in Chapter 4, this scheme indeed meets the quantum speed limit bound at each avoided crossing, and we will show that it can be applied successfully in the presence of decoherence.

3.1 Avoided level crossings and the Landau-Zener model

The building block of this method is the Landau-Zener (LZ) model [70, 71] for a quantum system with two interacting levels. The Hamiltonian of this system can be written as

$$H_{LZ} = \begin{pmatrix} \alpha\lambda & \frac{\Delta}{2} \\ \frac{\Delta}{2} & -\alpha\lambda \end{pmatrix} = \alpha\lambda\,\sigma_z + \frac{\Delta}{2}\sigma_x, \tag{3.1}$$

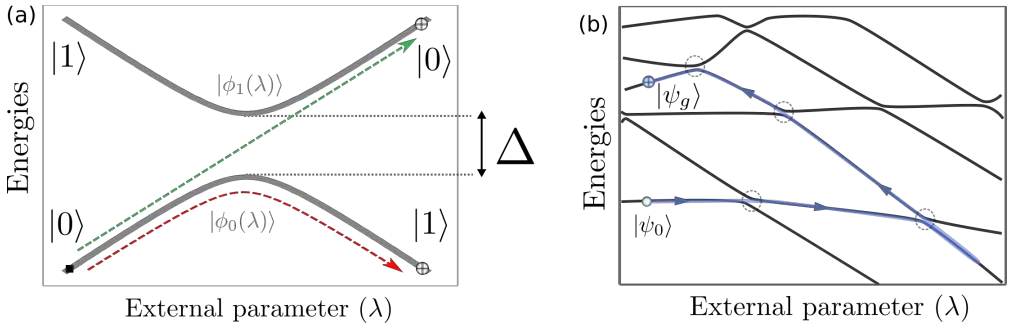

FIGURE 3.1: Energy spectrum as a function of parameter λ for (a) the LZ Hamiltonian (3.1). The dashed arrows represent the two limiting cases of the LZ formula (3.3): the red path is the adiabatic transition for which $P_1(t \to +\infty) = 1$, while the green path is the diabatic evolution where $P_1(t \to +\infty) = 0$. (b) idem (a) for a generic multilevel system. The control method allows us to derive the shape of $\lambda(t)$ required to navigate the energy spectrum in the indicated path, in order to connect states $|\psi_0\rangle$ and $|\psi_g\rangle$

where Δ is a constant, λ is the control parameter and we have set $\hbar = 1$. The eigenstates of σ_z form the so-called diabatic basis $\{|0\rangle, |1\rangle\}$. The eigenvalues of H_{LZ} form an hyperbola in the (λ, E) plane (as shown in Fig. 3.1 a), whose vertex represents an avoided crossing (AC) with an energy gap Δ. The eigenvectors of H_{LZ} form the adiabatic basis, $\{|\phi_0(\lambda)\rangle, |\phi_1(\lambda)\rangle\}$, where the notation makes explicit the asymptotic correspondence between both basis when $\lambda \to -\infty$, i.e.

$$|\phi_0(\lambda \to -\infty)\rangle \to |0\rangle\,, \;\; |\phi_1(\lambda \to -\infty)\rangle \to |1\rangle\,. \tag{3.2}$$

When $\lambda \to +\infty$, this correspondence is exchanged. The original LZ theory describes the transition probability of the system when the initial state is $|\psi(-\infty)\rangle = |0\rangle$ and the parameter λ is swept linearly in time, i.e. $\lambda(t) = v\,t$, yielding the famous LZ formula

$$P_1(t \to \infty) = 1 - \exp\left(-\frac{\pi\Delta^2}{4v|\alpha|}\right). \tag{3.3}$$

This result defines a critical velocity

$$v_c = \frac{\pi\Delta^2}{4|\alpha|} \tag{3.4}$$

which determines two limiting control scenarios. In the first place, we have the fast *diabatic* (D) transitions, in which $v \gg v_c$ in such a way that $P_1(t \to \infty) \simeq 0$, leaving the initial state unchanged. On the other hand, the *adiabatic* (A) transitions, in which $v \ll v_c$ and thus $P_1(t \to \infty) \simeq 1$, take place when the state evolves slowly following the adiabatic curve and finishes in state $|1\rangle$.

Let us now consider a many-level quantum system described by a Hamiltonian $H(\lambda)$, in which neighboring levels interact forming avoided crossings in its energy

spectrum, as depicted in Fig. 3.1 b. If we set the initial and target states as eigenstates of $H(\lambda)$, then we can derive the temporal shape for $\lambda(t)$ which would connect both states. We do this by drawing a "navigation path" in the spectrum, in which we eventually let the system jump to an adjacent energy curve only at avoided crossings, where the levels interact strongly. LZ theory then gives a binary recipe for determining the appropiate velocity of the driving field at each of the avoided crossings, which we can use for translating the path in the spectrum into a sequence of slopes of the resulting piecewise-linear control field. This method was proposed and thoroughly studied in [72, 105, 106, 107].

However, the use of adiabatic transitions implies a fundamental limitation of this method: in the presence of an environment, decoherence is bound to act within the long periods of time required by these transitions, rendering the effective dynamics of the system non-unitary and greatly diminishing the final fidelity of the protocol. This can be shown with a very simple model, which we describe in the following. We take a two level system described by the LZ Hamiltonian (3.1) and consider it weakly coupled to a high-temperature bosonic bath. It is then straightforward to write down the master equation for the reduced density matrix $\rho(t)$ of the system, which becomes independent of the particular election of time dependence of the control parameter. Assuming bilinear coupling of the form $\sigma_z \otimes \sum_j c_j q_j$ (the q_j's being the position operators of the environmental oscillators), we have [62]

$$\begin{aligned}\dot{\rho}(t) = &-i\left(H'(t)\rho(t) - \rho(t)(H')^{\dagger}(t)\right) - \frac{\gamma_0 T}{2}\left[\sigma_z,[\sigma_z,\rho(t)]\right] \\ &+ i\frac{\gamma_0\Delta}{4}\left(\sigma_y\rho(t)\sigma_z - \sigma_z\rho(t)\sigma_y\right),\end{aligned} \tag{3.5}$$

where γ_0 is the (dimensionless) coupling constant between the system and the environment at equilibrium temperature T (we set the Boltzmann constant $k_B = 1$). $H'(t) = \lambda(t)\sigma_z + \frac{\Delta}{2}\left(1 - i\frac{\gamma_0}{2}\right)\sigma_x$ is the renormalized non-hermitian effective Hamiltonian of the system. We wish to study how the non-unitary dynamic affects the fidelity of the control scheme, defined in this context as $\mathcal{F}(t) = \mathrm{Tr}\left(\rho(t)\rho_{goal}\right)$. It has been shown [108, 109] by different analytical approaches that while diabatic ($\rho_{goal} = |0\rangle\langle 0|$) transitions in a dissipative LZ evolution do not seem to suffer decoherence and thus achieve high fidelity, adiabatic ($\rho_{goal} = |1\rangle\langle 1|$) variations of the control parameter render poor final state fidelity even for weak coupling. This can be seen in Fig. 3.2 (b), where the fidelity as a function of time is plotted for different values of γ_0. As $\lambda(t)$, being swept slowly, reaches the AC, the system becomes extremely sensitive to decoherence and rapidly becomes mixed. The fidelity then fails to achieve the desired value of 1. For sufficiently large γ_0, the state losses its

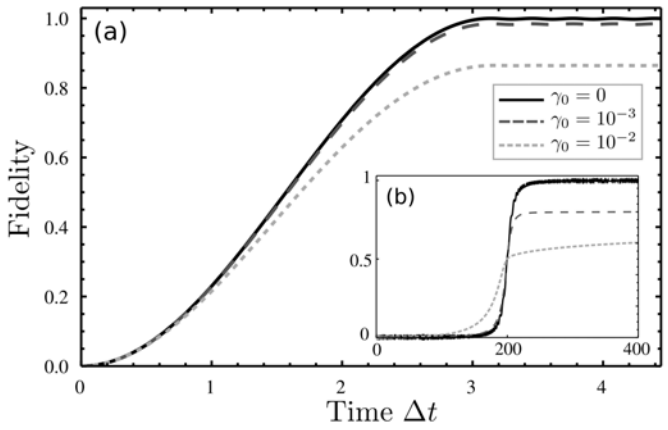

FIGURE 3.2: (a) Fidelity as a function of the dimensionless time Δt for sudden-switch variations of the control parameter (b) Fidelity as a function of Δt for adiabatic passages through the avoided crossing. In both fidelity plots, the solid line corresponds to the isolated system calculations, and the dashed curves to the system coupled to a bosonic environment. The temperature of the bath was fixed at $T = 10\Delta$.

purity and evolves to $\rho = \frac{\mathbb{I}}{2}$, for which $\mathcal{F}_{final} = \frac{1}{2}$.

To overcome this problem we propose an alternative method in which we use the so-called sudden-switch transitions [110]. Consider the LZ system prepared initially in the state $|\psi(0)\rangle = |0\rangle$. We now consider $\lambda(t)$ to be a piecewise constant function with initial value $\lambda(0) = -\lambda_0$, with $\lambda_0 \gg \Delta/|\alpha|$. In this way, the initial state is approximately an instantaneous eigenstate of the Hamiltonian $H_{LZ}(t = 0)$. If now $\lambda(t)$ undertakes a sudden variation to $\lambda = 0$ and the system is left to evolve for a time T, the final state is given by

$$|\psi(T)\rangle = \cos\left(\frac{\Delta}{2}T\right)|0\rangle + \sin\left(\frac{\Delta}{2}T\right)|1\rangle\,. \tag{3.6}$$

It is clear that choosing $T = \frac{\pi}{\Delta}$ yields $|\psi(T)\rangle = |1\rangle$. The final step in the evolution is a second sudden switch of the control parameter from 0 to $+\lambda_0$. Once again, the instantaneous eigenstates of the Hamiltonian will be approximately those of σ_z, in such a way that $|\psi(t)\rangle$ will be a stationary state for $t > T$, since $|\psi(T)\rangle = |1\rangle$. In sum, we have driven the system from $|0\rangle$ to $|1\rangle$ in a time $T = \frac{\pi}{\Delta}$ with a probability of 1. In this way, this scheme represents a sort of *shortcut* to adiabaticity, as the final state of the system is the same as if the parameter $\lambda(t)$ had been modified adiabatically. The total evolution time has been dramatically shortened, since an adiabatic passage through the AC requires a total time much larger than a critical time of the order of Δ^{-2} (recall the critical velocity expression from the LZ formula, c.f. eqn 3.4).

Note also that if we apply the Mandelstam-Tamm bound (2.16) to this case, with $|\psi_0\rangle = |0\rangle$, $|\psi_g\rangle = |1\rangle$ and $H = H_{LZ}(\lambda = 0) = \frac{\Delta}{2}\sigma_x$, we obtain

$$t_{QSL}^{MT} = \frac{\pi}{\Delta}. \tag{3.7}$$

The sudden-switch field protocol then saturates the quantum speed limit bound. This has been taken a proof of time-optimality [54]; however, as we discussed in Chap. 2, this result is actually telling us that the system is evolving through a geodesic in Hilbert space. Nevertheless, as we will see in Chap. 4 using optimization techniques, the control generated by the sudden-switch protocol is indeed time-optimal at each avoided-crossing, although it will not necessarily be so in a many level system.

We can now check the performance of the sudden-switch method in the presence of a dissipative environment. Taking again the master equation (3.5), we now observe that the desired transition to $\rho_{goal} = |1\rangle\langle 1|$ is indeed achieved with high probability in this case. In Fig. 3.2 (a) we show how the fidelity in this case evolves favorably even in the presence of the environment, making this method much more robust under the action of external influences, due to its increased speed as opposed to adiabatic method. In sum, this represents a relatively decoherence-resistant control recipe for achieving "adiabatic" ($P_1 \simeq 1$) transitions at an avoided crossing in the energy spectrum of a system. Together with the diabatic transitions, this updated binary control protocol (which we will refer to as S-D) renders a shorter control time and high fidelity at each AC, even in the presence of a dissipative environment.

3.1.1 Example: two-photon generation in the Jaynes - Cummings model

We will now apply the method presented in this section to an specific control problem in the Jaynes-Cummings model [111], which describes a two-level system coupled to single mode of the electromagnetic field. The Hamiltonian for the system reads

$$H_{JC}(\lambda) = \frac{\lambda}{2}\sigma_z + g\sigma_x(a^\dagger + a) + \Omega a^\dagger a, \tag{3.8}$$

where λ is the control field, g measures the coupling between both subsystems and Ω is the natural frequency of the oscillator. This model accurately describes the low energy behavior of a superconducting junction capacitively coupled to a transmission line, which is currently one of the most promising practical realizations of

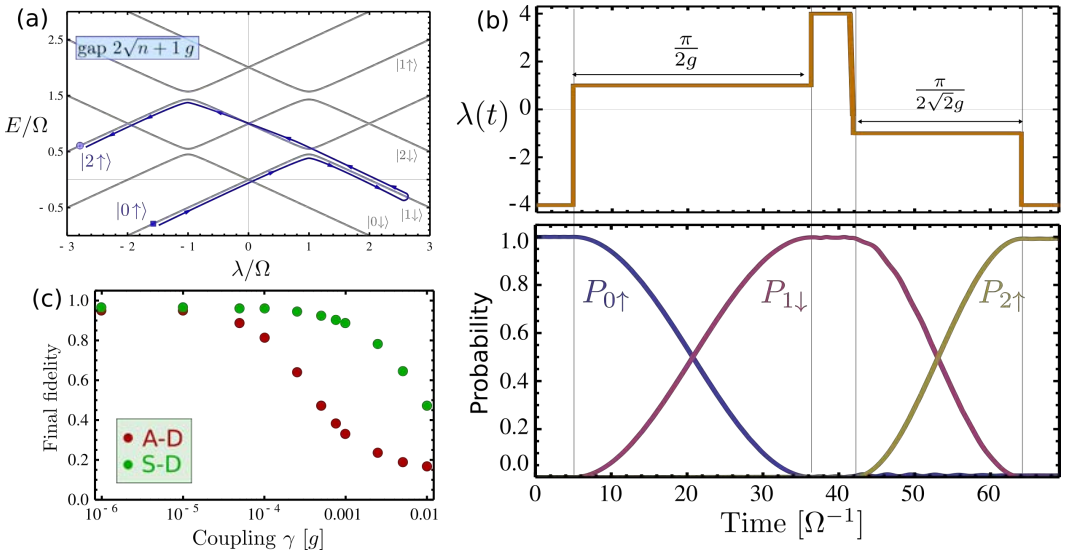

FIGURE 3.3: (a) Spectrum of Jaynes-Cummings model (3.8) as a function of the control parameter λ/Ω.The symbols ■ and ⊕ refer to the initial and target states, respectively, which are joined by a path following the energy levels. (b) Control field derived using the control method described in this section, together with the simulated time-dependent probabilities it generates. (c) Final fidelity $\mathcal{F}(T)$ as a function of the dimensionless coupling constant γ/g, for the dissipative model described by eqn. (3.9), both using S-D and A-D control methods.

a qubit for quantum computation applications [112, 113]. The energy spectrum of H_{JC} as a function of λ is shown in Fig. 3.3 a, where avoided level crossings appear as a result of qubit-oscillator interaction. Let us suppose that the system is initially prepared in state $|\psi_0\rangle = |\uparrow, 0\rangle$, where $|\uparrow\downarrow, n\rangle$ represents a separable state of the composite system, with the qubit in an eigenstate of σ_z and the oscillator in a Fock state $|n\rangle$. The initial state matches the ground state of the system for $\lambda \ll -\Omega$. We now intend to drive the system to the target state $|\uparrow, 2\rangle$, so that at the end of the process two photons will be generated in the cavity and the qubit will keep its initial configuration. In Fig. 3.3 a we draw a path connecting both states, from which we can infer the required control field $\lambda(t)$, shown in Fig. 3.3 b. The process requires two sudden-switch instances to transfer population at $\lambda/\Omega = 1$ and -1, with an intermediate diabatic passage through the second avoided crossing. The evolution of the diabatic state population is shown in Fig. 3.3 b, where it can be seen that the system evolves in the desired way.

Finally, we analyze the performance of the method in the presence of a dissipative environment. We again take a master equation approach to solve the reduced composite system dynamics when the oscillator couples to a high-temperature bosonic bath via $H_{int} = (a^\dagger + a) \otimes \sum_k c_k(b_k^\dagger + b_k)$, where $b_k^\dagger$, b_k are the creation / annihilation operators of the k-th environmental mode. The equation of motion

is given by [114]

$$\dot{\rho}(t) = -i\,[H_{JC}, \rho] + \frac{\gamma}{4}\,[Q, \{P, \rho\}] - \frac{\gamma T}{2\Omega}\,[Q, [Q, \rho]] \tag{3.9}$$

where H_{JC} is the Hamiltonian of eqn. (3.8), T is the temperature of the bath, $Q = a^\dagger + a$ and $P = a^\dagger - a$ and γ measures the coupling between the transmission line and the bath.

In order to obtain a comparison between the A-D method (which uses linear ramps of the control field to obtain adiabatic transitions) and the S-D method (in which we replace the linear ramps by sudden switches of λ), we studied the final fidelity for the control process described above as a function of the coupling strength γ, for both cases. Results are shown in Fig. 3.3 c. There, it can be seen that the performance of the control decreases much slower when using the S-D method, thus providing proof of the enhancement of the control methodology.

3.2 Time-periodic driving at avoided crossings

The method described in the previous section gives a robust strategy for control in quantum systems with many avoided crossings. However, the fields derived by means of this method have a temporal shape which is piecewise linear or constant, and may be complicated to realize in actual physical experiments. Typically, oscillating fields with fixed bandwidth are preferred in most experimental situations, for example in circuit QED. It is therefore desirable to study the dynamics of these systems under the influence of this type of fields.

In this section we will approach the problem of population transfer in the two-level model (3.1) using time-periodic fields. Beyond the control problem itself, this type of external driving has raised increasing interest over the past decades, as it leads to non-trivial steady state phenomena such as Landau-Zener-Stückelberg (LZS) interference [115], Floquet time crystals [116], Floquet topological insulators [117] and coherent destruction of tunneling (CDT). The latter is an striking phenomenon first predicted by Grossmann *et al.* [118] and later observed experimentally [119]. A particle in a symmetric double-well potential usually oscillates back and forth, if initially localized in one of the wells. However, if the depth of the wells oscillates in time, the tunneling rate may dramatically change. In fact, for certain combinations of the driving parameters, the rate vanishes, resulting in an effective localization of the particle in the initial well. Grossmann studied this problem using Floquet theory [120, 121], which states that for a time-periodic Hamiltonian $H(t) = H(t+$

T) a full set of orthonormal solutions for the corresponding Schrödinger equation exists, which are of the form

$$|\Psi_\alpha(t)\rangle = \exp\left(-i\epsilon_\alpha t\right)|\Phi_\alpha(t)\rangle\,,\ \alpha = 0,\ldots,n-1 \tag{3.10}$$

where n is the dimension of the system. The real-valued quantities $\{\epsilon_\alpha\}$ are called quasienergies, and the states $\{|\Phi_\alpha(t)\rangle\}$, which share the periodicity of $H(t)$, are called Floquet states. As shown in [118], CDT takes place only when some Floquet quasienergies are degenerate.

In the following, we will show that the Floquet spectrum of a two-level system under a sinusoidal driving in the regime of intermediate frequencies ($\omega \simeq \Delta$, being ω the driving frequency and Δ the characteristic frequency of the system) has a second kind of "special points", defined by the condition that the quasienergy separation is a local maximum, where population inversion is achieved after a time interval that only depends on the quasienergy difference, and where the full time-dependent evolution operator $U(t)$ can be obtained in a very simple analytical form.

We consider again a two-level system described by a Hamiltonian $H(t)$ of the form (3.1), where we now take the time-dependent field to be of the form

$$\lambda(t) = A\cos\left(\omega t\right), \tag{3.11}$$

such that $T = 2\pi/\omega$ is the period of $H(t)$. When dealing with this type of systems, it is customary to factorize the evolution operator as $U(t) = U_1(t)\,U_2(t)$, where $U_1(t) = \exp\left[-i\,\gamma_z(t)\,\sigma_z/2\right]$ can be regarded as a transformation to a rotating frame, since $\gamma_z(t) = 2\int\lambda(\tau)\,d\tau = (2A/\omega)\sin\left(\omega t\right)$. The remaining factor is obtained by the transformed Schrödinger equation $i\dot{U}_2(t) = H_2(t)\,U_2(t)$, where $H_2(t) = U_1^\dagger H U_1$ as

$$H_2(t) = \frac{\Delta}{2}\left\{\cos\left[\gamma_z(t)\right]\sigma_x + \sin\left[\gamma_z(t)\right]\sigma_y\right\} \tag{3.12}$$

The time dependence in this expression can be averaged out over one period of the driving field in the high frequency regime, i.e. $\omega \gg \Delta$, in what is usually referred to as the rotating wave approximation (RWA) [122]. This gives

$$U_2(t) = \exp\left(-i\frac{\Delta'}{2}t\,\sigma_x\right),\ \text{with}\ \Delta' = \Delta J_0\left(2A/\omega\right), \tag{3.13}$$

$J_0(x)$ being the first kind Bessel function For the values of $2A/\omega$ corresponding to the zeros of J_0, the evolution operator $U(t)$ is diagonal in the σ_z basis, , which explains the occurrence of the CDT phenomenon in the two-level approximation, where $\{|0\rangle, |1\rangle\}$ represent states localized in each one of the wells. For any other value of the amplitude A the population inversion between these states takes place

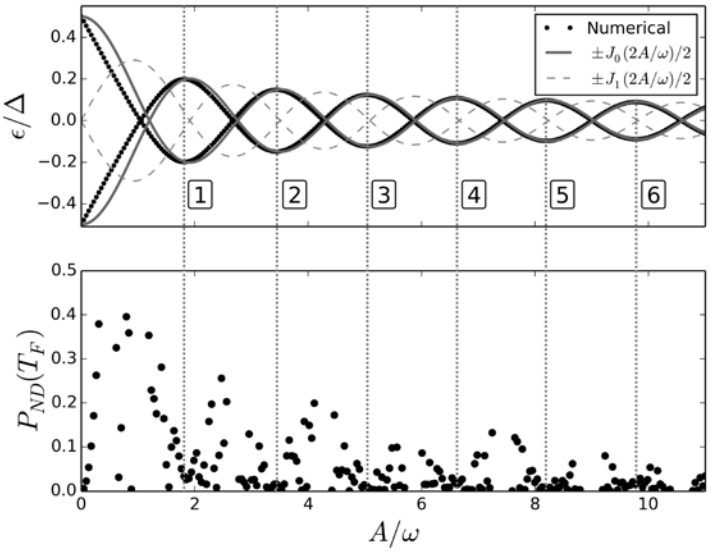

FIGURE 3.4: Top: Quasienergy spectrum for the two level Hamiltonian of eq. (3.1) with $\lambda(t) = A\cos(\omega t)$ as a function of A/ω. The boxed numbers $n = 1, 2, \ldots$ label the points of the spectrum in which the quasienergy separation is locally maximal. On top, we plot the analytical expression (3.15). Bottom: Non decay probability P_{ND} at time T_F, defined by eq. (3.14), calculated by numerical simulations of the system prepared in the initial state $|0\rangle$, as a function of A/ω. Near the degeneracies, where T_F diverges, results are not displayed. In all cases, the resonant case (i.e. $\omega = \Delta$) is studied.

in a finite lapse of time, given by

$$T_F = \frac{\pi}{\Delta'}. \tag{3.14}$$

When the RWA cannot be applied, we can resort to Floquet theory and study the quasienergy spectrum. The quasienergies can be obtained in an easy way by diagonalizing $U(T)$, something that can be done by numerically computing the time evolution from $t = 0$ to $t = T$ of an adequate basis set. In this way, the eigenphases of $U(T)$ give the desired quasienergies, which in the case $\omega \gg \Delta$, discussed above, simply correspond to

$$\epsilon_\pm = \pm\frac{\Delta'}{2}. \tag{3.15}$$

This expression implies that the spectrum contains an infinite set of degeneracies as A/ω increases, and also that expression (3.14) can be rewritten as $T_F = \pi/|\epsilon_+ - \epsilon_-|$. When computed for lower frequencies, the quasienergy spectrum changes considerably for small amplitudes [123], as shown in Fig. 3.4 (top) for the case $\omega = \Delta$. However, the results still show the typical ribbon structure [124], and expression (3.15) remains a reasonable approximation for $A/\omega \gtrsim 3$. To asses the validity of expression (3.14) in this regime, we simulate the evolution of the system starting from $|0\rangle$ for different values of amplitude, calculating the non probability

$P_{ND}(t) = |\langle 0|\psi(t)\rangle|^2$ at time $t = T_F$, in each case. The results that are shown in Fig. 3.4 (bottom) reflect a more complex behavior than that predicted by the high frequency model, in which $P_{ND}(T_F) = 0$ is expected for every value of A corresponding to finite T_F. More interesting is the fact that the results of Fig. 3.4 reveal the existence of a new outstanding feature: the points for which $P_{ND} \simeq 0$ pack around certain values of A, which correspond to the points of local maximum separation between quasienergies, i.e. the "peaks" of the spectrum. We have labeled these points by $n = 1, 2, \ldots$ in the figure.

To analyze this behavior in more detail we consider the time evolution of $P_{ND}(t)$ for different values of the driving amplitude. Some representative numerical results are shown in Fig. 3.5, where it can be seen that P_{ND} shows a "ladder"-type structure, decreasing through a series of steps, in each of which the probability oscillates rapidly around a constant mean value. Moreover, as n grows, the frequency of these oscillations increases,while the corresponding amplitude decreases. These steps occur whenever the field $\lambda(t)$ reaches a maximum or a minimum, and then their amount can be estimated by the ratio $2\omega/\Omega$, with $\Omega = 2\pi/T_F$.

The singular behavior shown by the dynamics at the extrema of the quasienergy spectrum admits a deeper analytical analysis. Hamiltonian H_2 in eq. (3.12) can be regarded as equivalent to the interaction of a spin-1/2 particle with a unit intensity magnetic field $\vec{B(t)}$ rotating periodically but non-uniformly in the $x - y$ plane, such that the instantaneous Larmor frequency is Δ. The components of this field can be expanded in Fourier series

$$B_x(t) \equiv \cos(\gamma_z) = J_0(\nu) + 2\sum_{n=1}^{\infty} J_{2n}(\nu)\cos(2n\omega t) \tag{3.16}$$

$$B_y(t) \equiv \sin(\gamma_z) = 2\sum_{n=1}^{\infty} J_{2n-1}(\nu)\sin[(2n-1)\omega t], \tag{3.17}$$

where $\nu = 2A/\omega$. If considered separately, the time integrals of both components give the accumulated phase throughout the evolution. Note that integrating $B_y(t)$ shows that the leading term vanishes when $J_1(2A/\omega) = 0$, which results in a small phase contribution of the whole series. Also notice that, because of the relation $J_0'(x) = -J_1(x)$, the zeros of J_1 match the extrema of J_0, also giving the position of the spectrum peaks mentioned above, as long as approximation (3.15) holds. In this situation, $U_2(t)$ is well approximated by $U_2(t) = \exp\left[-\frac{i}{2}\gamma_x(t)\sigma_x\right] =$

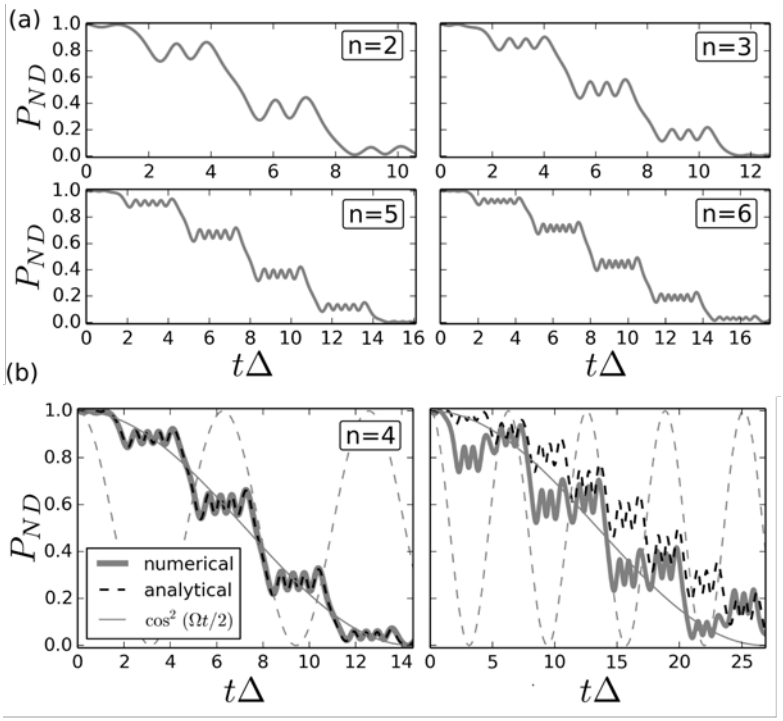

FIGURE 3.5: Time evolution of the non-decay probability for the system starting in state $|0\rangle$, in the resonant ($\omega = \Delta$) regime. (a) Amplitudes corresponding to peaks $n = 2, 3, 5, 6$. (b) Left: Amplitude corresponding to $n = 4$. Right: $A = 4.5\omega$, between $n = 2$ and $n = 3$. Thick lines show the results given by numerical simulations,while the black dashed curve is given by the analytical solution (see text for details). For comparison, we show the solution predicted in the high frequency regime (solid light gray line), and a cosine function with the frequency of the driving field, ω (dashed light gray line).

$\exp\left\{-\frac{i}{2}\left[\Delta' t + \delta(t)\right]\sigma_x\right\}$ with

$$\delta(t) = \frac{\Delta}{\omega}\sum_n \frac{J_{2n}(2A/\omega)}{n}\sin\left(2n\omega t\right), \tag{3.18}$$

which is T-periodic and can be seen to vanish in the limit $\Delta/\omega \to 0$, as expected.

This result for $U_2(t)$ approximates very well the population dynamics when the field parameters are set at the extrema of the quasienergy spectrum. A representative example is shown in Fig. 3.5. In this case the full evolution operator becomes

$$U = U_1 U_2 = \exp\left[-i\gamma_z(t)\sigma_z/2\right]\exp\left[-i\gamma_x(t)\sigma_x/2\right]. \tag{3.19}$$

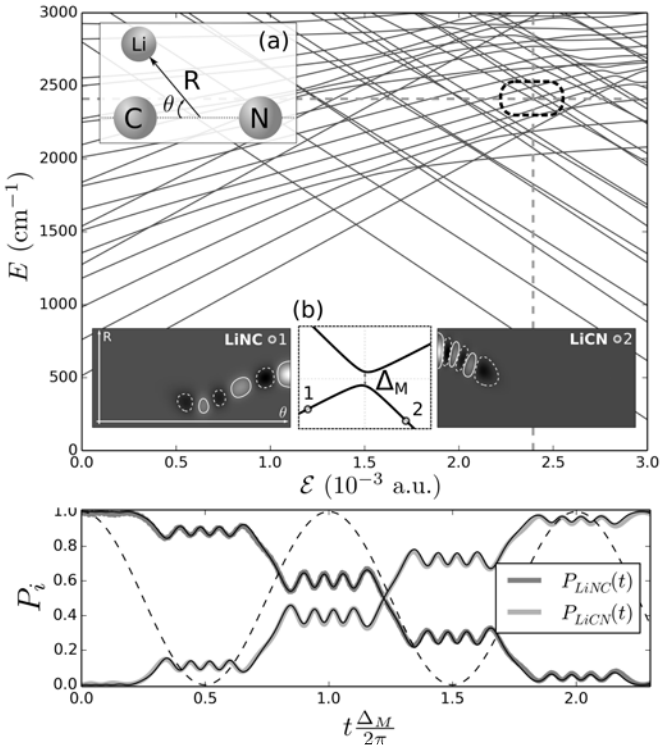

FIGURE 3.6: Top: (main) energy spectrum of the LiNC/LiCN molecular system as a function of the electric field intensity E. (a) Schematic diagram of the LiCN molecule, including the set of coordinates (R, θ) used. (b) Enlarged view of the squared zone of the spectrum, showing the avoided crossing considered. At both sides, density plots of the wave functions far from the crossing, which represent excited isomerized states. The axis ranges are $0 < \theta < 180°$ and $3 < R < 5.5$ a.u. Bottom: numerically simulated population evolution, starting in state $|1\rangle$ and setting $\omega = \Delta_M$ and $A = (1.23 \times 10^{-2})\Delta$. Full black lines show the result predicted by the two-level analytical solution (3.19) applied to this system.

3.2.1 Application to a multilevel system

As seen in the previous paragraphs, the degree of population transfer is related to the quasienergy spectrum of a periodically-driven system. As was studied in [123], such spectrum usually depends on the ratio between the driving amplitude and frequency, A/ω. One thus has to be careful when studying this type of phenomena in a two-level model derived from a more complicated system, since the two-level approximation holds when the field amplitude remains on the vicinity of the avoided crossing. For example, high-frequency results typically hold when $\omega \gg \Delta$, and so the first degeneracy in the quasienergy spectrum is bound to appear for values of $A \gg \Delta$. In that regime, however, the two-level approximation may break down. Thus, our analysis of the intermediate frequency regime becomes specially relevant for multilevel systems.

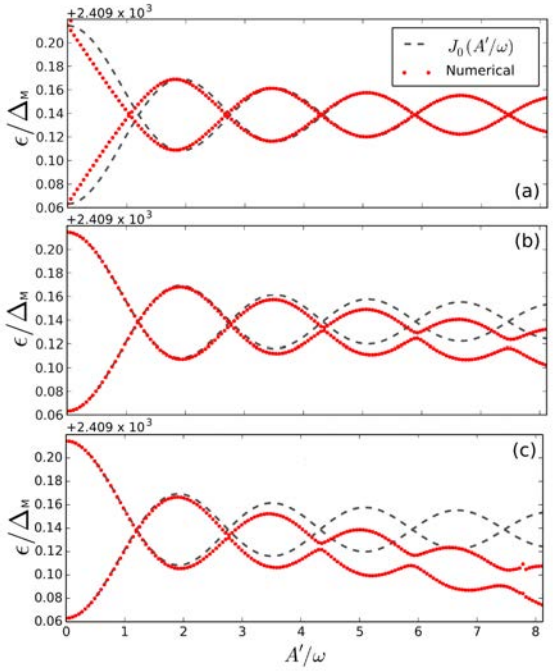

FIGURE 3.7: Quasienergy spectrum for the LiNC/LiCN molecular system, focused in the energy range of the avoided crossing under study (see Fig. 3.6). The values of driving field frequency used in each case are: (a) $\omega = \Delta_M$, (b) $\omega = 20\Delta_M$, (c) $\omega = 30\Delta_M$.

Here, we study a molecular model to to test our results: the LiNC/LiCN isomerizing system, which presents two stable isomers at the linear configurations: Li–N–C and Li–C–N. We present a detailed description of this system in Appendix B. We consider the system to be driven by a time-periodic electric field in the dipole approximation, and compute the energy spectrum as function of the field value in Fig. 3.6. We obtain a complex multilevel structure where, as a rule of thumb, positive-slope energy lines correspond to LiNC states (that is, those localized in the $\theta = 180°$ well) and the negative-slope lines to LiCN states ($\theta \sim 0$).

A careful analysis of the spectrum shows that most avoided crossings (ACs) in the low-energy region are very narrow and thus correspond to interactions too weak to be useful in controlling the isomerization. However, there is an AC centered at $\mathcal{E} = \mathcal{E}_{\rm dc} \equiv 2.39 \times 10^{-3}$ a.u., with a spectral gap of $\Delta_M = 0.15$ cm^{-1} which seems suitable for achieving such control. Indeed, far for from the AC, the involved eigenstates, termed $|\text{LiNC}\rangle$ and $|\text{LiCN}\rangle$, show localization in opposite wells (see Fig. 3.6 b). We then use an electric field of the form: $\mathcal{E}(t) = \mathcal{E}_{\rm dc} + A\cos(\omega t)$ and study the population dynamics.

In Fig. 3.7 we show the quasienergy spectrum of our molecular system as a function of A'/ω [1], for different values of driving frequency ω. Note that only the region of the spectrum corresponding to the marked AC in the Fig. 3.6 is displayed here. As discussed in the beginning of this subsection, the typical ribbon structure becomes clearly distorted as the frequency increases. Therefore, we propose to work in the intermediate frequency regime discussed before, so that the main results of the previous sections become relevant for this problem. Actually, setting ω equal to Δ_M make expression 3.19) straightforwardly applicable. As an illustration, we show in the bottom panel of Fig. 3.6 the evolution obtained starting from state $|LiNC\rangle$ for $A = (1.23 \times 10^{-2})\Delta$ (corresponding to $n = 4$). As can be seen, the total control time is approximately $2.3 \times 2\pi/\Delta_M \simeq 0.51$ ps, which is well below the 400 ps reported in Ref. [**?**]. Moreover, the results predicted by the analytical model proposed in this subsection are in full agreement with the numerical results, as can be seen in the Figure.

In summary, in this section we have shown the existence of a set of special points in the quasienergy spectrum of a periodically driven TLS, where the evolution of the populations takes place with maximum probability transfer, and show the relevance of these results in a realistic multilevel model. We also develop an analytical treatment for this model, which will be useful when we address time-optimal control in Chap. 4.

[1] Note that the AC in model (3.1) is symmetrical; in the general case, the slopes of the diabatic branches must be taken into account. This leads to the rescaling $A \to A' = \frac{\Delta\alpha}{2}A$, where $\Delta\alpha$ is the difference of slopes between the branches (in absolute value).

Control cuántico via navegación del espectro de energías

En este capítulo desarrollamos un método para implementar control en sistemas cuánticos sin utilizar técnicas de optimización. El método se basa en el conocimiento del espectro de energías del sistema en función de un parámetro de control externo y es adecuado para sistemas que muestren cruces evitados bien definidos en su espectro. Aunque esta característica puede parecer bastante restrictiva, es, de hecho, una propiedad general de sistemas con interacción entre sus niveles de energía, al menos en la región de bajas energías. El método proporciona una forma de deducir una serie bien definida de variaciones rápidas (diabáticas) y repentinas (escalonadas) del parámetro de control, lo que nos permite evolucionar a través del espacio de estados del sistema y alcanzar el estado objetivo deseado. Si bien evaluaremos la optimalidad del método en el capítulo 4, este esquema de hecho cumple con el límite de velocidad cuántica en cada cruce evitado, y por lo tanto demostraremos que puede aplicarse con éxito en presencia de decoherencia.

En la sección 3.1 presentamos el modelo de Landau-Zener para un sistema de dos niveles, el cual analizamos en detalle en distintos escenarios a lo largo de la Tesis. Asimismo realizamos un resumen de un método de control desarrollado previo a este trabajo en [72] y discutimos sus propiedades mas importantes. Luego proponemos un método modificado que permite efectuar protocolos de control en tiempos mas cortos, y presentamos un estudio comparativo sobre la performance de ambas variantes del método en un sistema abierto, en particular el modelo de Jaynes Cummings acoplado a un entorno térmico. Mostramos que la variante propuesta permite mejorar sustancialmente el éxito del control en presencia de un entorno.

El método descrito anteriormente da una estrategia robusta para el control en sistemas cuánticos con muchos cruces evitados. Sin embargo, los campos derivados por medio de este método tienen una forma temporal que es lineal o constante

por piezas, y puede ser complicado de realizar en experimentos físicos reales. Típicamente, los campos oscilantes con ancho de banda fijo son deseables en la mayoría de las situaciones experimentales, por ejemplo en circuit QED. Por lo tanto, es deseable estudiar la dinámica de estos sistemas bajo la influencia de este tipo de campos. En la sección 3.2 abordamos el problema de la transferencia de población en el modelo de dos niveles usando campos periódicos. Allí mostramos la existencia de un conjunto de puntos especiales en el espectro de cuasienergías donde la evolución de las poblaciones es tal que probabilidad de transferencia es máxima. También mostramos que para estas combinaciones particulares de los parámetros de control, el operador de la evolución del sistema puede ser aproximado por una expresión analítica simple. Al estudiar un modelo realista para la dinámica vibracional de una molécula triatómica, mostramos que estos resultados son particularmente relevantes cuando el espectro de energía presenta varios cruces evitados, donde el uso de los campos oscilantes de gran amplitud invalidaría la aproximación de dos niveles.

Chapter 4

Optimal control of quantum systems

In this chapter we will use the optimization tools introduced in Chapter 2 to further analyze control problems in systems with one and with many avoided crossings in their energy spectrum, such as the ones discussed in Chapter 3. We will first revisit the two-level system described by the Landau-Zener Hamiltonian (3.1), where we will see that it is possible to solve the problem of time-optimal control analytically. This will allow us to confirm the time-optimality of the sudden-switch protocol introduced earlier, as well as test the methods presented in Section 2.2 to obtain lower bounds for the minimum control time. We will then tackle the general multilevel problem with the spectrum navigation method, and use numerical optimization tools to further minimize the required evolution time.

4.1 Optimal evolution time in a two-level system

We go back to the two-level Hamiltonian originally presented in Sect. 3.1,

$$H(\lambda) = \begin{pmatrix} \lambda & \frac{\Delta}{2} \\ \frac{\Delta}{2} & -\lambda \end{pmatrix} = \lambda\, \sigma_z + \frac{\Delta}{2}\sigma_x. \tag{4.1}$$

We now redefine the notation $|g_\gamma\rangle \equiv |\phi_0(\gamma)\rangle$, which refers to the ground state of $H(\gamma)$ (i.e. its eigenstate with negative eigenvalue, see Fig. 4.1 a). Pursuing the motivation of Chapter 3, we will focus on the following control problem: we start in the initial state $|\psi_0\rangle = |g_{-\gamma}\rangle$ and we wish to drive the system to the target state $|\psi_g\rangle = |g_{+\gamma}\rangle$ (here $\gamma > 0$). Moreover, we wish to do so in the minimum possible time. First of all, let us point out that this system is completely controllable in the sense defined in Chap. 2. We can prove this computing the dimension of

the dynamical Lie algebra $\mathcal{L}$ in the following way. We first take the zero-depth operators in H_{LZ} which are σ_x (the drift term) and σ_z (the control term). The commutator gives

$$[\sigma_z, \sigma_x] = i\sigma_y \tag{4.2}$$

Of course, there is no need to continue computing the nested commutators associated with this system, since we have already found a set of $n^2 - 1 = 3$ linearly independent elements of $\mathcal{L}$, $\{\sigma_x, \sigma_y, \sigma_z\}$, and thus we can assert that $\mathcal{L} = su(2)$.

The problem of finding the required control field for this process was solved by Hegerfeldt in 2013 [125], which proved that different protocols arise whether we place constraints on the amplitude $|\lambda(t)|$ of the control field or not. In the unconstrained case, the optimal field is

$$\lambda(t) = \begin{cases} +\lambda_0 & \text{for} \quad 0 < t < t_0 \\ 0 & \text{for} \quad t_0 < t < t_0 + T \\ -\lambda_0 & \text{for} \quad t_0 + T < t < 2t_0 + T \end{cases}, \tag{4.3}$$

where $\lambda_0 \gg \Delta$, $\lambda_0 t_0 = \pi/4$, and as $|\lambda(t)|$ has no restrictions, we can choose $\lambda_0 \to \infty$ so as to have $t_0 \to 0$. The total evolution time is then given by

$$T_{min} = T + 2t_0 \to T = \frac{2}{\Delta}\arctan\left(\frac{2\gamma}{\Delta}\right) \tag{4.4}$$

The control sequence in (4.3) was in fact derived previously in [126] by numerical methods for an specific value of γ, and received the name "composite pulse protocol". In the constrained case, where $|\lambda(t)| \leq \Lambda$, the optimal solution is similar,

$$\lambda(t) = \begin{cases} +\Lambda & \text{for} \quad 0 < t < T_\Lambda \\ 0 & \text{for} \quad T_\Lambda < t < T_\Lambda + T_{off} \\ -\Lambda & \text{for} \quad T_\Lambda + T_{off} < t < 2T_\Lambda + T_{off} \end{cases} \tag{4.5}$$

The optimal time here is given by $T_{min} = T_{off} + 2T_\Lambda$. The expressions for T_Λ and T_{off} differ whether the maximum field Λ is smaller or larger than $\frac{\Delta^2}{4\gamma}$. For $\Lambda \geq \frac{\Delta^2}{4\gamma}$, we have

$$\begin{aligned} T_\Lambda &= \frac{1}{\sqrt{\Lambda^2 + \frac{\Delta^2}{4}}}\arcsin\left(\frac{\Lambda^2 + \frac{\Delta^2}{4}}{2\Lambda(\Lambda + \gamma)}\right) \\ T_{off} &= \frac{2}{\Delta}\arctan\left(\frac{\Lambda\gamma - \frac{\Delta^2}{4}}{\frac{\Delta}{2}\sqrt{\Lambda^2 + 2\Lambda\gamma - \frac{\Delta^2}{4}}}\right), \end{aligned} \tag{4.6}$$

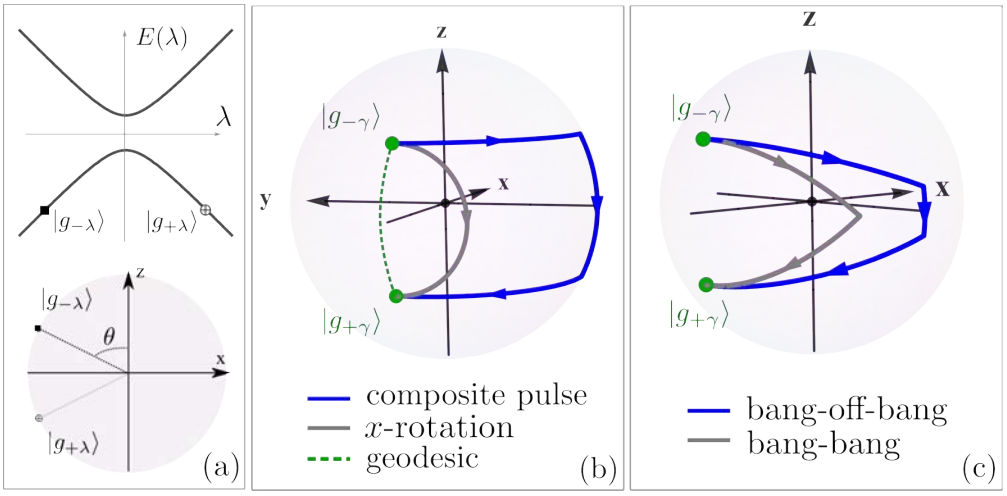

FIGURE 4.1: (a) Energy spectrum of Hamiltonian (4.1) as a function of λ. Initial and final states for the control problem are shown with symbols ■ and $\oplus$, and are shown in Bloch sphere in the bottom drawing. (b) Bloch sphere representation of the two-level system state space. Blue line shows the evolution generated by the composite pulse protocol, the gray line shows the evolution for $\lambda = 0$ and the dashed line represents the geodesic path linking $|g_{-\gamma}\rangle$ and $|g_{+\gamma}\rangle$. (c) Bloch sphere trajectories for the protocol with constrained λ. Bang-off-bang protocol is shown with $c = 1.5\frac{\Delta^2}{4\gamma}$, while for the bang-bang protocol, $c = 0.5\frac{\Delta^2}{4\gamma}$ was used.

while for $\Lambda < \frac{\Delta^2}{4\gamma}$, the result is

$$\begin{aligned} T_\Lambda &= \frac{1}{\sqrt{\Lambda^2 + \frac{\Delta^2}{4}}} \arcsin\left(\frac{\Lambda\left(\Lambda^2 + \frac{\Delta^2}{4}\right)}{\frac{\Delta^2}{2}(\Lambda + \gamma)}\right) \\ T_{off} &= 0 \end{aligned} \tag{4.7}$$

Although expressions (4.4) through (4.7) may be rather involved, the evolutions generated in this three scenarios are easy to visualize and interpret in Bloch sphere. In Fig. 4.1 we draw the initial and final states, which can be parametrized by an angle θ, such that

$$|g_{-\gamma}\rangle = \cos\left(\frac{\theta}{2}\right)|0\rangle - \sin\left(\frac{\theta}{2}\right)|1\rangle \tag{4.8}$$

$$|g_{+\gamma}\rangle = \sin\left(\frac{\theta}{2}\right)|0\rangle - \cos\left(\frac{\theta}{2}\right)|1\rangle\,, \tag{4.9}$$

where

$$\tan(\theta) = \frac{\Delta}{2\gamma} \tag{4.10}$$

As seen in Fig. 4.1 (b), the composite pulse protocol (4.3) generates a rotation around the x axis preceded and followed by instantaneous z-rotations, thanks to the unconstrained magnitude of the control field. In the constrained case, however,

optimality is reached by generating rotations about a tilted axis in the x-z plane, as seen for the bang-bang and the bang-off-bang evolutions in 4.1 (c).

Before we continue, let us look at these results in the limit $\gamma \to \infty$. In virtue of eqn. (4.10) we have that $\theta \to 0$ in this limit, and thus the initial and target states are $|\psi_0\rangle = |0\rangle$ and $|\psi_g\rangle = |1\rangle$, as was considered for the control problem in Chap. 3. In this case, all three solutions (4.3) and (4.5) coincide and we get exactly the sudden-switch protocol, with the optimal evolution time given by, for example, eqn. (4.4)

$$T_{min} \to \frac{\pi}{\Delta} \text{ when } \gamma \to \infty, \tag{4.11}$$

which is consistent with what we saw in Chap. 3. This confirms the time-optimality of the sudden-switch protocol for a two-level system. As we will see at the end of this Chapter, this will not hold for a multilevel system, although we can modify the method in order to further minimize the total evolution time.

4.2 Analysis of the quantum speed limit bounds

In Sect. 2.2.3 we presented the quantum speed limit (QSL) formalism based on Mandelstam-Tamm relation (2.16) and mentioned that obtaining a bound on the evolution time for a time-dependent Hamiltonian would require solving Schrödinger equation. We also proposed a number of expressions of the form (2.27) which, in principle, allow us to bound the evolution time with minimal knowledge about the system evolution. Here we apply all those results to the controlled two-level system presented in the previous paragraphs.

As mentioned in Sect. 2.2.3 there is more than one way to extract a bound on the evolution time from the Anandan-Aharonov relation

$$s(\psi_0, \psi(\tau)) \leq \int_0^\tau \Delta E(t')\, dt'. \tag{4.12}$$

One of them follows a proposal in [84], also later used in [87]. For that we set $|\psi(\tau)\rangle = |\psi_g\rangle$ in the l.h.s. of eq. (4.12), set T_{Q1} as the upper bound of the integral in the r.h.s., and impose the equality. We can then solve the integral for T_{Q1}, which is the desired the evolution time bound. Note that, in this case, the QSL time T_{Q1} is interpreted as the time required by the process to traverse a distance equal to $s(\psi_0, \psi_g)$ in state space, regardless of the states being actually connected in the evolution. An alternative method, proposed in Ref. [82] was mentioned in

Chap. 2, c.f. eqn. (2.25), which we rewrite here

$$T \geq \frac{\arccos\left(|\langle\psi_0|\psi_g\rangle|\right)}{\overline{\Delta E}} \equiv T_{Q2} \tag{4.13}$$

As already described, in this case $T_{Q2} = \frac{s}{s_p} T \leq T$, where s is the distance between ψ_0 and ψ_g measured by Fubini-Study metric, s_p is the length of the actual path traversed by the system during the evolution and clearly $s_p \geq s$.

Let us begin by analyzing the composite pule protocol of eq. (4.3) in the unconstrained case. In order to obtain the bounds T_K (with $K = Q1, Q2$) it is necessary to calculate the integral on the r.h.s. of expression (4.12). To do so, we express the state of the system at time t using the usual Bloch parametrization

$$|\psi\rangle = \cos\left(\frac{\chi}{2}\right)|0\rangle + \mathrm{e}^{i\varphi}\sin\left(\frac{\chi}{2}\right)|1\rangle\,, \tag{4.14}$$

where $\chi = \chi(t)$ and $\varphi = \varphi(t)$ are the usual polar and azimuthal angles used in spherical coordinates. The variance of Hamiltonian (4.1) can then be expressed as

$$\begin{aligned}\Delta E^2 &= \lambda^2 \sin^2(\chi) + \left(\frac{\Delta}{2}\right)^2 \left(1 - \sin^2(\chi)\cos^2(\varphi)\right) \\ &\quad -\lambda\,\Delta \sin(\chi)\cos(\chi)\cos(\varphi)\,.\end{aligned} \tag{4.15}$$

Due to the piecewise-constant time-dependence of $\lambda(t)$, i.e. expression (4.3), this protocol has three steps. In the first one, $t \in [0, t_0]$ and the last one $t \in [T + t_0, T + 2t_0]$, we have $\chi = const. = \theta$ and φ varies fromπ to $\frac{3}{2}\pi$ (or in reverse) with angular velocity $2\lambda_0$. This results in

$$2\int_0^{t_0} \Delta E(t')\,dt' = 2\int_{T+t_0}^{T+2t_0} \Delta E(t')\,dt' = \frac{\pi}{2}\sin(\theta)\,, \tag{4.16}$$

which, naturally, is the length of the path travelled by the system in each step. For $t \in [t_0, T + t_0]$, we have $\varphi = \frac{3}{2}\pi = const.$ and the polar angle runs from θ to $\pi - \theta$ with velocity Δ, so we get

$$2\int_{t_0}^{t_0+T} \Delta E(t')\,dt' = \int_{t_0}^{t_0+T} \Delta\,dt' = \Delta T. \tag{4.17}$$

As was discussed in before, to obtain the bound T_{Q1} we have to solve

$$s(\theta) = 2\int_0^{T_{Q1}} \Delta E(t')\,dt', \tag{4.18}$$

in which different results are be obtained depending on the values of θ, yielding

$$T_{Q1}(\theta) = \begin{cases} 0 & \text{if } \frac{\pi}{2}\sin(\theta) \geq s(\theta) \\ \frac{s(\theta) - \frac{\pi}{2}\sin(\theta)}{\Delta} & \text{if not} \end{cases}\,, \tag{4.19}$$

We remark that, in order to obtain eq. (4.19), the integral on the r.h.s. of eq. (4.18) is computed along the composite trajectory generated by the field in eq. (4.3) in the limit $\lambda_0 \to \infty$. As discussed above, T_{Q1} is equivalent to the time

required by the process to traverse a distance equal to $s(\psi_0, \psi_g)$. Note that, in light of expression (4.9), here the distance is given by

$$s(\psi_0, \psi_g) = \pi - 2\theta \equiv s(\theta). \tag{4.20}$$

Since in the first z-rotation the system covers a distance $(\pi \sin\theta)/2$ with infinite speed, it is easy to see that, for $s(\psi_0, \psi_g) \leq (\pi \sin\theta)/2$, we have $T_{Q1} = 0$. Otherwise, the lengths covered in the first and second rotation both contribute, while the length from the third step of the procedure does not need to be computed. It can be seen by comparing expression (4.19) to eq. (4.4) that $T_{Q1} < T_{min}$ for all θ. The bound T_{Q2}, given by eq. (4.13), can also be evaluated directly and gives

$$T_{Q2}(\theta) = \frac{s(\theta)}{s_{path}(\theta)} T(\theta) = \frac{s(\theta)}{s(\theta) + \pi \sin(\theta)} T_{min}(\theta). \tag{4.21}$$

Before we go on to compare the actual minimum evolution time T_{min} of eq. (4.4) with the QSL bounds of eqns. (4.19) and (4.21), we will use the methods proposed in Sect. 2.2.3 and analyze the new bounds t^X_{min} with X=B, P, R1 and R2 which are of the form

$$T \geq t_{min}\left(H, \lambda_{max}, |\psi_0\rangle, |\psi_g\rangle\right). \tag{4.22}$$

We stress that, since these expressions are independent of the actual dynamics of the system, we will derive them for the constrained and unconstrained protocols in the same way. This is a key aspect of the approach we propose, since we should be able to obtain some information about the minimum evolution time without any knowledge about the actual optimal protocol. Let us start with t^B_{min} of eqn (2.28), for which we calculate the norm of H

$$H^2 = \left(\frac{\Delta^2}{4} + \lambda^2\right)\mathbb{I} \Rightarrow \|H\| = \sqrt{\mathrm{tr}\left(H^2\right)} = \sqrt{2\left(\frac{\Delta^2}{4} + \lambda^2\right)} \tag{4.23}$$

We bound this expression to obtain

$$t^B_{min} = \frac{\frac{\pi}{2} - \theta}{\sqrt{\frac{\Delta^2}{4} + \lambda^2_{max}}} \tag{4.24}$$

For computing the bound (2.38) obtained via Pfeifer's theorem, t^P_{min}, we need to evaluate the variance ΔE of (4.15) in both the initial and final states. This can be done in a straightforward way, and we obtain

$$\Delta E|_{\psi_0/\psi_g} = \frac{\Delta}{2}\cos(\theta)\,|1 \pm \frac{2\lambda}{\Delta}\tan(\theta)|, \tag{4.25}$$

which in turn gives

$$h(t) = \frac{\Delta}{2}\cos(\theta)\int_0^t \min\left\{|1 + \frac{2\lambda}{\Delta}\tan(\theta)|, |1 - \frac{2\lambda}{\Delta}\tan(\theta)|\right\} \tag{4.26}$$

In this way we obtain

$$t^P_{min} = \frac{\frac{\pi}{2} - \theta}{\frac{\Delta}{2}\cos(\theta) + \lambda_{max}\sin(\theta)} \tag{4.27}$$

We finally consider t^{R1}_{min}, which was defined in eq. (2.47) to be of the form,

$$t^{R1}_{min} = \frac{1 - \sum_j^n |\langle\psi_g|\phi^c_j\rangle\langle\phi^c_j|\psi_0\rangle|}{\|H_0\|}. \tag{4.28}$$

We recall that here $H_0 = \frac{\Delta}{2}\sigma_x$ is the free term of the Hamiltonian, and $|\phi^c_j\rangle$ refer to $|0\rangle$ and $|1\rangle$, i.e. the eigenstates of the control operator σ_z. Straightforward calculation gives

$$t^{R1}_{min} = \frac{1 - \sin(\theta)}{\frac{\sqrt{2}}{2}\Delta}. \tag{4.29}$$

We point out that t^{R2}_{min} defined in eq. (2.48) as

$$t^{R2}_{min} = \frac{1 - \sum_j^n |\langle\psi_g|\phi^0_j\rangle\langle\phi^0_j|\psi_0\rangle|}{\lambda^{max}\|\sigma_z\|} \tag{4.30}$$

gives 0 for this problem since the numerator of this expression can be seen to vanish for all θ.

Up to this point we have computed five bounds for the evolution time in this control problem: (4.19) and (4.21) derived from the geometrical QSL formulation, for which we had to use the optimal solution derived by Hegerfeldt; in addition to (4.24), (4.27) and (4.29) which are computed without knowledge of such solution. Let us first compare this expressions with the optimal time T_{min} for the case of full population transfer, i.e. $\gamma \to \infty$ or $\theta \to 0$. In this case, $T_{min} = \frac{\pi}{\Delta}$, while

$$T_{Q1} = T_{Q2} = \frac{\pi}{\Delta} \tag{4.31}$$

Since these were the geometrical expressions, it is reasonable to have obtained a tight bound: when $\theta = 0$, the optimal evolution (which is generated by setting $\lambda = 0$) is along a geodesic, which is precisely when the Anandan-Aharanov relation is saturated. For the other expressions, we obtain $t^B_{min} = 0$ due to the dependence on $\lambda_{max} \to \infty$ and

$$t^P_{min} = \frac{\pi}{\Delta} > \frac{\sqrt{2}}{\Delta} = t^{R1}_{min}. \tag{4.32}$$

It is interesting to see that Pfeifer's bound t^P_{min} matches the optimal evolution time also, although we didn't use any information about the optimal solution itself to compute it. This result gives us confidence about the usefulness of this method to bound evolution times in optimal control problems.

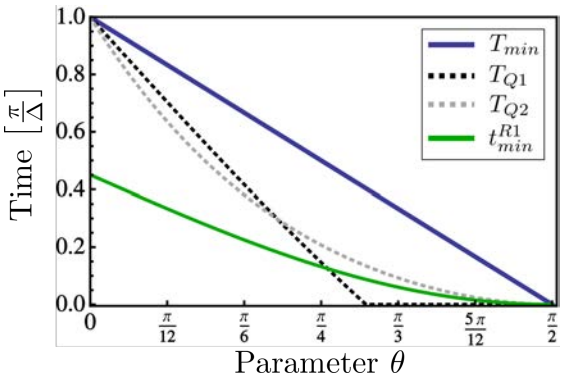

FIGURE 4.2: Optimal evolution time T_{min} and bounds T_{Q1}, T_{Q2}, t_{min}^{R1} obtained from eqs. (4.19), (4.21) and (4.29) for the composite-pulse protocol (with unconstrained λ) as a function of parameter θ.

Let us now analyze the general case of finite γ. For the unconstrained control, we have that $\lambda_{max} \to \infty$. Note that this immediately gives $t_{min}^{B} = t_{min}^{P} = 0$, but t_{min}^{R1} remains finite since it does not depend on the control field constraints, as we pointed out in Chap. 2. In Fig. 4.2 we plot this quantity along with the actual optimum time T_{min} and the QSL estimates T_{Q1} and T_{Q2} as a function of angle θ, which defines the initial and target states (see Fig. 4.1 a). Note that for $\theta = \pi/2$ ($\gamma = 0$) both states are the same, and thus $T_{min} = 0$. From the figure we can observe that the T_{Q1} and T_{Q2} curves (in dashed lines) cross for certain value of a θ, so we cannot assert that one gives a tighter bound than the other. Moreover, T_{Q1} vanishes for a certain range of θ, meaning that in that regime, it does not give a meaningful limitation for the evolution time. Note that in the time-independent case, the MT bound (eq. 2.16) gives zero only if $\psi_0 = \psi(\tau)$ (which is trivial) or if $\Delta E \to \infty$, which means that the system evolves uniformly with infinite velocity. In the time-dependent formulation, the velocity of the system in state space is not constant, and the QSL time can vanish if, for some period, $\Delta E \to \infty$. Note also that t_{min}^{R1}, which was computed without knwoledge of the optimal evolution, is never tight (except for $\theta = \frac{\pi}{2}$, which is trivial). However, its interesting to point out that it is nonzero in spite of the fact that the control field is unconstrained (and is infinite in this case), and thus gives a meaningful bound as opposed to t_{min}^{P} and t_{min}^{B}.

We now compare the bounds for the case of constrained control, where $|\lambda(t)| \leq \Lambda$. As already mentioned, here the optimal solution depends on the relation between Λ and γ. For $\Lambda \geq \frac{\Delta^2}{4\gamma}$, we have the bang-off-bang protocol described by expressions (4.5) and (4.7),while for $\Lambda < \frac{\Delta^2}{4\gamma}$, the solution is the bang-bang protocol, c.f. eqns. (4.5) and (4.6). For both cases, we can compute T_{Q1} and T_{Q2} as described before; the calculations are a bit more tedious than in the unconstrained case and we show

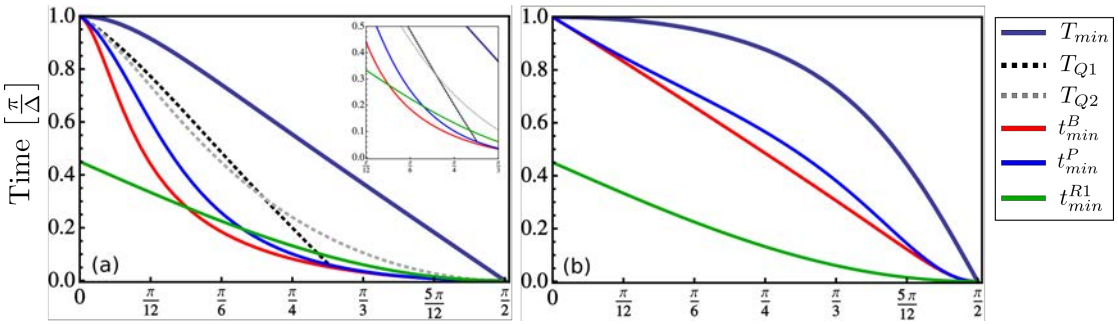

FIGURE 4.3: Optimal evolution time T_{min} and its bounds obtained from the expressions discussed in the text for: (a) Bang-off-bang protocol, where $\Lambda > \frac{\Delta^2}{4\gamma}$ (in this calculations $\Lambda = 6\frac{\Delta^2}{4\gamma}$). In the inset we show a zoom of the zone where curves cross. (b) Bang-bang protocol, where $\Lambda \leq \frac{\Delta^2}{4\gamma}$ (in this calculations $\Lambda = 0.2\frac{\Delta^2}{4\gamma}$). Note that in this last case, $T_{Q1} = T_{Q2} = t^P_{min}$.

the analytical expressions in Appendix A.2.

In Fig. 4.3 (a) we show the results for the bang-off-bang case. All the bounds considered yield different curves in general, and all coincide for $\theta = 0$ (except for t^{R1}_{min}). Moreover, there is no bound tighter than another for all θ. Of all the bounds computed without the optimal protocol, t^P_{min} stands out as the better one (although its in general less tight than the QSL bounds T_{Q1} and T_{Q2}).

In Fig. 4.3 (b) we show results for the bang-bang case. Interestingly, in this case ΔE is constant throughout the evolution, albeit the Hamiltonian being time-dependent itself (see Appendix A.2). As a result, we have $T_{Q1} = T_{Q2}$. In this case, they also coincide with t^P_{min}, all of them being equal to the Mandelstam-Tamm bound from the time-independent case. These three are in turn tighter than t^{R1}_{min} as before. Notably, however, the bound derived from Pfeifer's theorem t^P_{min} is bigger or equal than all of the others for all θ, and results in the tighter bound, albeit being computed without knowledge of the optimal protocol. This result provides further evidence about the usefulness of this particular expression for bounding minimal evolution times in quantum control problems. In the last part of the following section we will continue to explore the bounds given by this expressions, but in more complicated systems.

4.3 Optimal evolution time for systems with many avoided crossings

We will now use quantum optimal control (QOC) as a tool to study the quantum speed limit in many-level systems which show several avoided-crossings (ACs) in their energy spectrum, as the ones described in Chap. 3. There, we saw that we could engineer control fields by a series of sudden variations of the control parameter, which turned out to generate time-optimal evolution at each AC. In the remainder of this chapter we will show that the minimum evolution time for processes involving more than one AC is in general smaller than the algebraic sum of the optimal times for each crossing, even when they appear to be well-isolated. Then, through an analysis of the optimal fields derived by QOC, we will study the physical mechanism involved in such speed up. Finally we will discuss the importance of the spectrum navigation method in generating the initial seeds for the optimization.

4.3.1 Multilevel model

The two-level model of eqn. (4.1) studied in the beginning of this chapter can be extended and generalized to account for the presence of several ACs in a many-level scenario. Here we construct a model for such situation. Consider an N-level system with the following Hamiltonian

$$\begin{aligned} H_N(\lambda) &= \sum_{n=0}^{\left[\frac{N-1}{2}\right]} (\lambda - n\,\varepsilon_0)\,|2n\rangle\langle 2n| + \sum_{n=0}^{\left[\frac{N-2}{2}\right]} n\,\varepsilon_0 |2n+1\rangle\langle 2n+1| \\ &\quad + \sum_{n=0}^{N-2} \frac{\Delta_n}{2}\left(|n\rangle\langle n+1| + |n+1\rangle\langle n|\right), \end{aligned} \tag{4.33}$$

where $[x]$ denotes the integer part of x and $\{|n\rangle\}$ is the basis of diabatic states. When $\Delta_n = 0$ for $n = 0, 1, \ldots, N-2$, the Hamiltonian is diagonal in that basis, and the energy spectrum consists merely on a series of horizontal and diagonal straight branches with degeneracies at values of $\lambda_{ij} = (i+j)\varepsilon_0$ corresponding to states $|2i\rangle$ and $|2j+1\rangle$. If one of the couplings is non-zero, say $\Delta_n \neq 0$, the degeneracy at $\lambda_n = n\varepsilon_0$ is lifted and an AC is generated with a minimum energy gap of Δ_n. As a consequence, transitions between the states $|n\rangle$ and $|n+1\rangle$ become permitted. The overall shape of the energy spectrum for this model is schematically depicted in Fig. 4.4 (e). There, it can be seen that ε_0 measures how far apart are

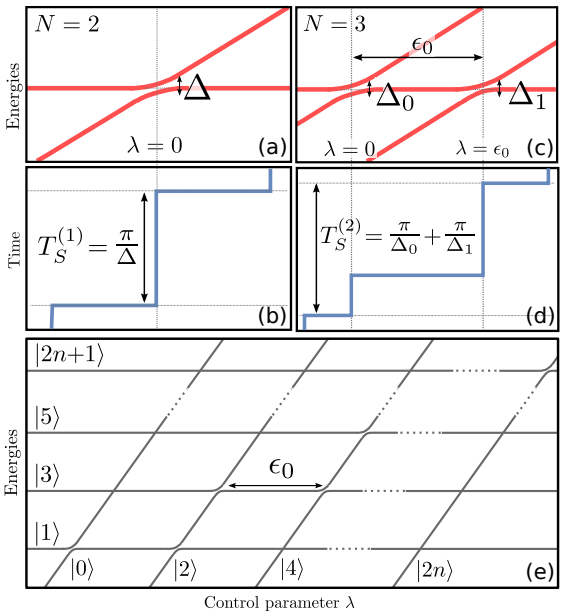

FIGURE 4.4: (a) A single avoided crossing as a function of the control parameter λ. (b) Control field $\lambda(t)$ as a function of time for a simple realization of complete population transfer between the diabatic states. Note that time is represented on the vertical axis. (c) and (d) same as (a) and (b) but for the three-level Hamiltonian (4.34). (e) Schematical representation of the energy spectrum of Hamiltonian $H_N(\lambda)$, c.f. Eq. (4.33), as a function of control parameter λ. In the most general setting, the spectrum shows $N-1$ avoided crossings separated by ε_0, each of which generate a coupling between states $|n\rangle$ and $|n+1\rangle$ with $n < N-1$.

the locations of the ACs. Note that, when all the interaction rates are non-zero, the number of ACs equals $N-1$. In a regime where $\varepsilon_0 \gg \Delta_n$ for all n, this model is very convenient for analyzing dynamical processes which are dictated by local two-level interactions. This can be seen as follows: if the system is initially preparred in some state $|n\rangle$ and the control parameter λ does not deviate much from the position of the corresponding AC (i.e. $|\lambda - \lambda_n| \ll \Delta_n$ [104]), then the dynamics of the system is effectively confined to a two-dimensional subspace, as the remaining $N-2$ levels can be adiabatically eliminated [127]. This is the key characteristic of this model, and we will expand on its consequences on the QSL analysis later on.

Evaluating Eq. (4.33) for $N = 2$ we recover the two-level (one AC) Hamiltonian similar to eq. (4.1). Taking the next step in complexity, the case $N = 3$ renders the following Hamiltonian matrix

$$H_3(\lambda) = \begin{pmatrix} \lambda & \frac{\Delta_0}{2} & 0 \\ \frac{\Delta_0}{2} & 0 & \frac{\Delta_1}{2} \\ 0 & \frac{\Delta_1}{2} & \lambda - \varepsilon_0 \end{pmatrix}, \tag{4.34}$$

which has two ACs, one at $\lambda_0 = 0$ and other at $\lambda_1 = \varepsilon_0$. The corresponding gaps are Δ_0 and Δ_1 when $\varepsilon_0 \gg \Delta_0, \Delta_1$. The energy spectrum for this case is depicted in Fig. 4.4 (c). This model has been widely studied in many different contexts [127, 128, 129], as it is suitable for describing a three-level atom in a Λ configuration. Note that, in that case, the parameters Δ_0 and Δ_1 correspond to detunings between the energy levels and the frequencies of two external laser fields, which are generally regarded as the control paraneters, while λ and ε_0 are related to the bare energy splittings. In this work this is not the case, as the off-diagonal couplings are fixed and we implement control protocols by variying solely $\lambda(t)$.

For this multiple AC model, we are interested in control processes which connect diabatic states of the system. Without loss of generality, we consider the initial state $|\psi_0\rangle = |0\rangle$ and define the process $\mathcal{P}_K$ as the one which drives the system to the state $|K\rangle$, with $0 \leq K \leq N-1$ (generalization to a different diabatic initial state is straightforward). Our goal will be to find the control field $\lambda_K(t)$ which generates $\mathcal{P}_K$ in a time T with maximum fidelity. Note that, if the ACs are sufficiently isolated, we can use the method introduced in Chap. 3 to solve the problem. By succesively setting the control field $\lambda(t) = \lambda_n$ constant during time intervals of length π/Δ_n, with $0 \leq n \leq K-1$ the dynamics navigates through the K ACs turning them on and ensuring full population transfer one at the time. The system then evolves through the sequence $|0\rangle \to |1\rangle \to \ldots \to |K\rangle$. The control field $\lambda_K^{(S)}(t)$ is depicted for $K = 1$ and $K = 2$ in Fig. 4.4 (b) and (d), respectively. The total evolution time for this protocol equals

$$T_S^{(K)} \equiv \sum_{n=0}^{K-1} \frac{\pi}{\Delta_n}. \tag{4.35}$$

Note that we have constructed the model in Eq. (4.33) in such a way that the degeneracies between states $|n\rangle$ and $|n+k\rangle$ (for $k \neq 1$) are exact, and cannot be lifted. For this protocol, this means that there is only one path in the energy spectrum between $|0\rangle$ and $|K\rangle$, which involves exactly K ACs. We point out that we do not lose generality by making this assumption: if there were a shorter path between those states, it would be equivalent to a process $\mathcal{P}_L$ with $L < K$, which is accounted for in our model.

4.3.2 Exploring the quantum speed limit with optimal control

We now numerically investigate the QSL or minimum evolution time[1] for the control processes described in the previous section. For that purpose we use optimal control techniques, inspired by the basic idea introduced by Caneva *et al.* [54] that the optimization performance is limited by the maximum speed allowed by quantum evolution. The basic procedure is as follows. First, we fix the state dimension N and choose a control process $\mathcal{P}_K$ (which starts in $|0\rangle$ and targets $|K\rangle$) for the model described the previous subsection. Then, we run the optimization algorithm developed in Chap. 2 in order to find the control field $\lambda_K(t)$ which generates the desired process, for different values of the total evolution time T. In each run, this procedure takes as an input the value of T and an initial guess for the field $\lambda_K^{(0)}(t)$. In order to choose these inputs, we take advantage of the physical features of the model discussed in the previous section. The values of T were taken from an interval centered around $T_S^{(K)}$, cf. Eq. (4.35). Note that, if the ACs are well isolated, we are certain that the sudden switch field generates the desired process when $T = T_S^{(K)}$. Similarly, the initial guess for the control function were chosen to be close to the sudden switch field. Actually, we used

$$\lambda_K^{(0)}(t) = a(t)\lambda_K^{(S)}(b\,t) + c(t) \tag{4.36}$$

where b is a parameter which shrinks or expands the shape of the function to fit the total evolution time (i.e. $b = 1$ when $T = T_S^{(K)}$), while $a(t)$ is a function which smooths the discontinuities of $\lambda_K^{(S)}$ and $c(t)$ is a small linear correction. The latter functions are introduced in order to force the algorithm to take a minimum number of steps (of the order of 100) before the required convergence is achieved.

Each run of the algorithm finishes after a fixed number of steps, or when the process is sufficiently converged. This is determined by evaluating the value of the infidelity at each step m, which is defined as

$$\mathcal{I}_m \equiv 1 - \left|\left\langle \psi_g | \psi^{(m)}(T)\right\rangle\right|^2, \tag{4.37}$$

where $\left|\psi^{(m)}(t)\right\rangle$ is the state of the system obtained at step m of the algorithm. The function $\mathcal{I}_m$ decreases monotonically as m increases, but its shape and asymptotic

[1] In this section we will take "quantum speed limit time" and "minimal evolution time" as synonyms, regardless of the discussion about the geometrical QSL formulation, so as to be consistent with the optimal control literature

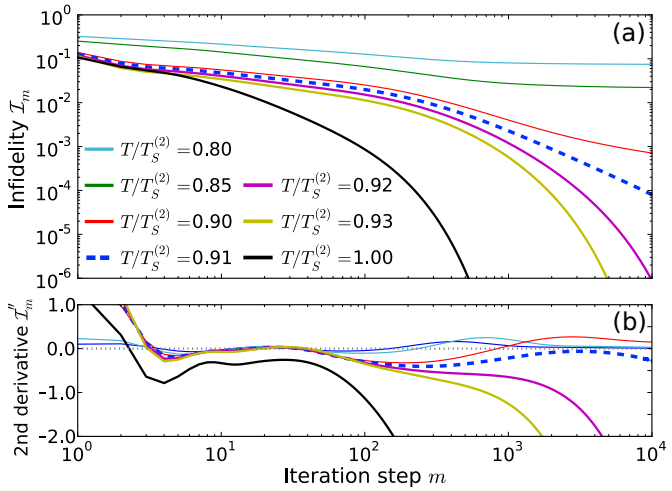

FIGURE 4.5: A typical procedure for determining the QSL time T_{QSl} for a particular control process. This example corresponds to a $P_{K=2}$ process in a Hilbert space of dimension $N = 3$, cf. Eq. (4.34), where $\varepsilon_0 = 10\Delta_0$ and $\Delta_1 = \Delta_0$. (a) Infidelity $\mathcal{I}_m$ as a function of the step number m for each optimization. (b) Second derivative $\mathcal{I}''_m$ of the curves in (a). The dotted line corresponds to the minimum value of T which asymptotically renders $\mathcal{I}''_m < 0$ and so is identified as T_{QSL} within error margin. Thin full lines correspond to $T < T_{QSL}$ while, thick full lines to $T > T_{QSL}$.

behaviour depends critically on the input parameters. In Fig. 4.5 (a) we plot this function for a particular case, as an example. We argue, as in Ref. [54] that the infidelity cannot decrease indefinitely if the fixed evolution time T is smaller than the QSL time. In that case, $\mathcal{I}_m$ should look asymptotically flat. We use this feature to obtain the estimator of the QSL time $T_{QSL}^{(K)}$. Formally, for each value of T we look at the second derivative of $\mathcal{I}_m$ (with respect to m), see Fig. 4.5 (b), and analyze its sign. Then, the minimum value of T which gives $\mathcal{I}''(k) < 0$ asymptotically, is chosen as the QSL time.

We now turn our focus to the model of Eq. (4.34) which presents two ACs. We begin by considering the QSL time for process $\mathcal{P}_1$, for which the system starts in state $|0\rangle$ and evolves to $|1\rangle$, in the minimum possible time. Note that this process involves just one AC, as seen from the sudden-switch protocol mentioned earlier. In Fig. 4.6, we plot the calculated QSL time $T_{QSL}^{(1)}$ for this case as a function of ε_0, the parameter which measures the distance between the ACs in the energy spectrum (see Fig. 4.4), for fixed values of interaction parameters Δ_0, Δ_1. There, it can be seen that $T_{QSL}^{(1)}$ is larger than $T_S^{(1)} = \pi/\Delta_0$ for small values of ε_0. This is reasonable in this regime, since the ACs are closer together and thus interact considerably, which leads to significant variations of the interaction rates (see Ref. [127] for more details). Away from that regime, $T_{QSL}^{(1)}$ converges to $T_S^{(1)}$, which is

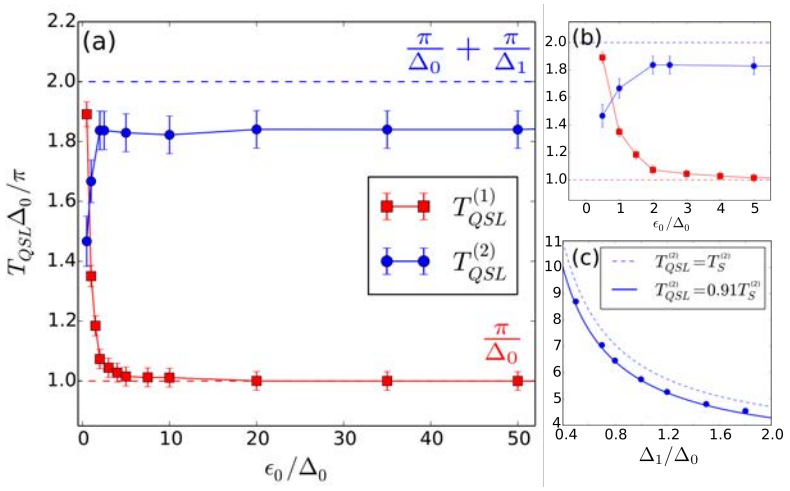

FIGURE 4.6: (a) QSL time calculated from the optimal control procedure (see text for details) as a function of ε_0/Δ_0, for processes P_1 (crossing one AC) and P_2 (crossing two ACs). Dashed lines correspond to expression (4.35), i.e. the time required by the sudden-switch protocol in each case, $T_S^{(1)}$ and $T_S^{(2)}$. (b) Close-up of (a) in the region of low ε_0/Δ_0, where the ACs strongly interact. (c) QSL time for the case $\varepsilon_0/\Delta_0 = 5$ as a function of Δ_1/Δ_0, for process P_2.

the well-known result for the two-level system. This is a sound result, since only the states $|0\rangle$ and $|1\rangle$ are involved in the process. However, it is interesting to point out that this behavior allows us to identify the regime in which the ACs are well isolated. In the case shown in the figure, for which $\Delta_0 = \Delta_1$, this is achieved for $\varepsilon_0/\Delta_A \gtrsim 5$.

Next, we discuss control process $\mathcal{P}_2$, which involves both ACs. Following the same procedure as for the previous case, we get the results of Fig. 4.6 (a). There, it can be seen that the estimated QSL time $T_{QSL}^{(2)}$ is smaller than the sudden switch evolution time $T_S^{(2)}$. Remarkably, this result holds in all cases, even for large ε_0. The difference between $T_{QSL}^{(2)}$ and our prediction is larger for small ε_0, and decreases as the ACs are brought apart. However, for ε_0/Δ_0 as large as 100, the difference is still larger than 7%. This striking behaviour indicates that the QOC optimization can generate successful (i.e., with arbitrary fidelity) control processes which are significantly shorter in time than the double sudden-switch, a process wich is time-optimal at each AC, as discussed above. We point out that this behaviour persists even when the relative magnitude of the gap sizes Δ_0, Δ_1 is modified as we can see in Fig. 4.6 (c). We will analyze the physical mechanisms that cause this speed-up in the next section.

Finally, we address the results obtained for the QSL time for control processes

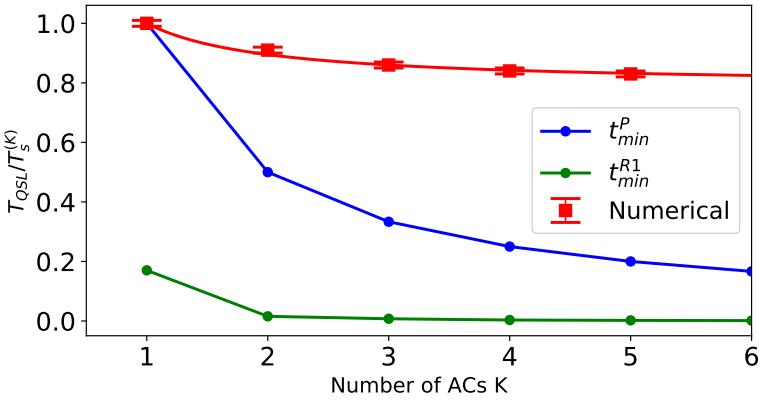

FIGURE 4.7: Ratio between the calculated QSL time T_{QSL} and $T_S^{(K)}$ as a function of the number of avoided crossings K involved in the control process. Full red line corresponds to the estimation in ec. (4.39). The parameter τ was chosen so to fit the data. For all cases, the distance between the ACs was set to $\varepsilon_0 = 10\Delta$, where $\Delta = 1$ is minimum gap for all the ACs.

involving more than two ACs, i.e. $\mathcal{P}_K$ with $K > 2$. Applying the same procedure outlined in the previous paragraphs, we obtained T_{QSL} for various values of the number of avoided crossings K involved in the process. In Fig. 4.7 we plot the ratio between T_{QSL} and $T_S^{(K)}$ as a function of K. There, it can be seen that the optimal evolution time (measured with respect to the corresponding sudden switch protocol evolution time) decreases as the number of ACs involved increases. This means that, as more ACs get involved in the evolution, the connection between diabatic states can be performed faster. However, the improvement reaches a saturation point for large values of K.

4.4 Analysis of optimal control fields

We now turn to analyze the shape of the control fields derived via the optimization procedure outlined in the previous section. We will focus on the optimal fields obtained for $T = T_{QSL}$, but for larger evolution times its description is similar. In Fig. 4.8 (a) and (b) we plot the optimized field $\lambda(t)$ together with the evolution of the populations for two particular cases: processes involving two ACs ($K = 2$) and three ACs ($K = 3$). At first sight, it can be seen that the field shows oscillations wich are mounted on a step-like function. The latter feature is preserved from the sudden-switch field, wich we used as an initial guess for the optimization. Fourier transform of the driving signal reveals that there is only one dominant frequency f_ε, which together with the maximum amplitude A_{max}, characterizes the overall

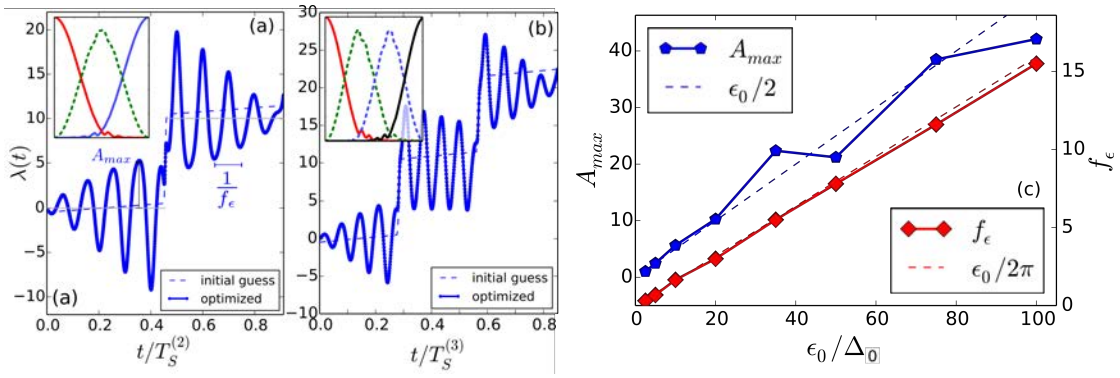

FIGURE 4.8: (a) Initial and optimized control fields $\lambda(t)$ for process P_2, using $\Delta_1/\Delta_0 = 1$ and $\varepsilon_0/\Delta_0 = 10$. Inset show the time evolution of the populations for each one of the diabatic states $|k\rangle$ $(k = 0, 1, 2)$, given by the optimized field. Evolution time is set at $T = T^{(2)}_{QSL} \simeq 0.91 T^{(2)}_S$. (b) same as (a) for process P_3, with same parameter values and $\Delta_2/\Delta_0 = 1$ as well. Evolution time is set at $T = T^{(3)}_{QSL} \simeq 0.85 T^{(3)}_S$. (c) Frequency f_ε (right axis) and maximum oscillation amplitude A_{max} (left axis) of the optimal field for process P_2 as a function of ε_0. Dashed lines indicate lineal dependences of both quantities with ε_0.

shape of the field. Remarkably, this behaviour is common to all high-order control processes studied in our model, even for $K > 3$. In order to quantitatively analyze the driving field, we studied the dependance of f_ε and A_{max} as a function of the distance ε_0 between the ACs. Results are shown in Fig. 4.8 (c) for $K = 2$, where the linear dependence of both quantities with ε_0 is clear and can even be regarded as exact for the frequency, for which we can write $f_\varepsilon = \varepsilon_0/2\pi$. Note that, from the insets of Fig. 4.8 (a) and (b), it can be seen that the diabatic states which do not correspond either to the intial nor the target state do not get fully populated, as opposed to the dynamics of the sudden-switch protocol discussed in Chap. 3. We remark here that a similar result for the optimized evolution of the populations was shown in Ref. [130]. There, the authors investigated control in a system of bosonic atoms in a double-well potential. Interestingly, they show that this type of dynamics is present even for piecewise-constant control fields and for strong interaction between the ACs, as opposed to our case where we allow for any waveform for the field and considere isolated ACs.

We will now describe how the particular shape of the optimized fields provides the physical mechanism for the overall speed-up of the evolution. As pointed out before, the field preserves the step-wise feature of the original sudden-switch field but with the novelty of showing oscillations. This behaviour can be understood in terms of navigation of the energy spectrum (Fig. 4.4). At the beginning of the protocol, the field activates the $|0\rangle \leftrightarrow |1\rangle$ interaction by setting $\lambda = \lambda_0 = 0$.

As a consequence, the initial population of state $|0\rangle$ starts to move to state $|1\rangle$. Simultaneously, the control parameter λ starts to oscillate both rapidly (i.e. with a frequency $f_\varepsilon \sim \varepsilon_0 \gg \Delta_A$) and with large amplitude (again, of the order of ε_0). This makes the control parameter λ navigate areas of the spectrum close to the adjacent avoided crossing. As a consequence, the previously uncoupled state $|2\rangle$ starts to get populated. Note that this is the target state $|\psi_g\rangle$ for this process. When the first *step* is finalized, i.e. when the mean value of λ switches to λ_1, the three diabatic states have non-zero population. This is the key of the speed-up with respect to the sudden-switch field: the target state is already activated in the first half of the evolution. The protocol finishes by activating the dominant interaction $|1\rangle \leftrightarrow |2\rangle$, so that the population of $|2\rangle$ continues to grow to 1. As happened in the first half of the evolution, the field also oscillates, now to drive λ close the previous AC with the purpose of depopulating state $|0\rangle$.

The previous analysis allows us to quantify the speed-up produced by the optimization as a function of the number of avoided crossings involved in the protocol. As seen above, the key to the speed-up is that in each step, the control field draws a small population to an adjacent level, originally not coupled to the AC. Also, given the shape of the spectrum, there cannot be more than three ACs simultanously active during the protocol: the one activated by the sudden-switch field and its adjacent neighbors. As a consequence, the QSL time will be smaller or equal than $T_S^{(N-1)}$ for all $N \geq 2$, and the difference is proportional to N, so that we can write

$$T_{QSL} = T_S^{(N-1)} - (N-2)\tau \tag{4.38}$$

for some value of $\tau < T_S^{(N-1)}$. This leads to

$$\beta = 1 - \frac{N-2}{N-1}\frac{\tau\Delta}{\pi}. \tag{4.39}$$

The parameter $\beta(N)$ is then found to decay with N to a constant value below 1, thus proving the existence of a speed-up for this control process. The proposed form for T_{QSL} is plotted in Fig. 4.7, and it can be seen that it describes the numerical findings with good accuracy.

For this problem we can also explore how is the behavior for the minimum time bounds t_{min} already discussed in this Chapter. Since this is, in principle, an unconstrained control problem, were do not pose explicit restrictions for $\lambda(t)$, we

get two non-zero bounds, t^P_{min} and $tmin^{R1}$, which we plot as a function of the number of ACs in Fig. 4.7. The expression derived from Pfeifer's theorem, eqn. (2.38) is computed as described in Appendix A.2, yielding the simple result

$$t^P_{min} = \frac{\pi}{\min\left(\Delta_0, \Delta_{K-1}\right)} \tag{4.40}$$

which is independent of λ. This is because the initial and target states are eigenstates of the control Hamiltonian, a feature already pointed out in Chap. 2. Also in the Appendix we show that

$$t^{R1}_{min} = \frac{1}{\|H^{(0)}_N\|}. \tag{4.41}$$

In Fig. 4.7 we can see that both expressions are in general well below the actual optimal time, albeit t^P_{min} being optimal for $K = 1$ as we saw at the beginning of this Chapter. In general, the information given by this expressions becomes less significant as the number of levels increases, specially for t^{R1}_{min} as was already pointed out in [93]. However, they both give a non-zero bound even when there is no constrain on the control field amplitude.

4.4.1 Analytical approximate solution for the time-dependent problem

The regular behavior shown by the numerically optimized control field has some interesting consequences. First, note that as ε_0 increases and the avoided crossings get further apart, the driving field will require a bigger intensity and a larger bandwidth in order to be implemented. In practice, at some point this requirement will no longer be fulfilled, and most likely the QSL time will tend to $T^{(K)}_S$ for all practical purposes. This is indeed reasonable, since technical limitations would then imply that the ACs are effectively isolated, with no possible coupling between them. However, from a theoretical standpoint, this is a much different scenario than the one usually obtained in QOC optimizaton, where the broad bandwidth requirements originates from the highly irregular features of the optimized field. In our case the control function $\lambda(t)$ can be readily described by a few parameters. We associate this remarkable feature with the special characteristics of our model, which shows localized two-level interactions in a many-level spectrum, a scenario which is common in many different physical setups, as previously mentioned.

Remarkably, we found that an analytical approximation for the time-dependent evolution can be drawn inspired from the results of the optimization process. We will show this solution in the following for the case $K = 2$, although the idea can

extended higher order processes. Recall the Hamiltonian $H_3(\lambda)$ from Eq. (4.34), which can be written as the sum of its non-diagonal and diagonal parts

$$H_3(\lambda) = H_{ND} + H_D(\lambda), \tag{4.42}$$

in such a way that H_{ND} depends on the coupling parameters Δ_0 and Δ_1 while the dependence on the control parameter is concentrated in $H_D(\lambda)$. We propose the following expression for the driving field

$$\lambda(t) = \begin{cases} \lambda_A \cos(\omega t + \phi) & , \quad 0 \leq t < t_m \\ \varepsilon_0 + \lambda_A \cos\left(\omega(t - t_m) + \tilde{\phi}\right) & , \quad t_m \leq t \leq T \end{cases} . \tag{4.43}$$

This field has the form of a step-wise constant function with oscillations of angular frequency ω mounted on each step (note that, from the previous analysis, we can infere that $\omega = \varepsilon_0$). The field then oscillates around a fixed value at each step, corresponding to the localization of the two ACs: a $t = 0$ it begins at $\lambda = \lambda_0 = 0$, and then turns to $\lambda = \lambda_1 = \varepsilon_0$ at some $t = t_m$. The overall shape of $\lambda(t)$ then emulates the optimized field seen in Fig. 4.8 (a) and (b), with the difference that we use a constant amplitude λ_A for the oscillating term, for convenience. We recall that this situation is very similar to what we studied in Chap. 3 (section 2) for a single avoided crossing.

Let us first consider the dynamics from $t = 0$ to $t = t_m$. We propose that the total evolution operator for this evolution can be factorized as

$$U_0(t, 0) = U_0^{(A)}(t) U_0^{(B)}(t), \tag{4.44}$$

where $U_0(A)(t) = \exp\left(-i \int_0^{t_m} H_D(t')dt'\right)$ is diagonal in the diabatic basis and the superscript emphasizes the fact that we are working on the AC located at $\lambda = \lambda_0 = 0$. The problem is then to find the unitary operator $U^{(B)}(t)$, which satisfies the Schrödinger equation in the interaction picture $i\dot{U}^{(B)}(t) = \tilde{H}_{ND}(t) U^{(B)}(t)$, with $\tilde{H}_{ND} \equiv U_0^{(A)\dagger} H_{ND} U_0^{(A)}$ being the corresponding transformed Hamiltonian, which takes the form

$$H'_{ND}(t) = \frac{\mathrm{e}^{-i\lambda_i}}{2} \begin{pmatrix} 0 & \mathrm{e}^{2i\lambda_i}\Delta_0 & 0 \\ \Delta_0 & 0 & \mathrm{e}^{i\varepsilon_0 t}\Delta_1 \\ 0 & \mathrm{e}^{2i(\lambda_i - \varepsilon_0 t)}\Delta_1 & 0 \end{pmatrix}, \tag{4.45}$$

where we have defined $\lambda_i \equiv \lambda_i(t) = \int_0^{t_m} \lambda(t')dt' = \frac{\lambda_A}{\omega}\sin(\omega t + \phi) - \phi_0$ and $\phi_0 = \frac{\lambda_A}{\omega}\sin(\phi)$. The unitary evolution problem is then casted in terms of this time-dependent Hamiltonian. The key to consider here is that the exponentials that appear in the previous expression can be written in Fourier series using the identity

$$\mathrm{e}^{iz\sin\gamma} = \sum_{n=-\infty}^{n=\infty} J_n(z)\, \mathrm{e}^{in\gamma}, \tag{4.46}$$

where $J_n(z)$ symbolyzes the Bessel J-function of order n. The results we obtained from the QOC procedure indicates us that the frequency of the driving at each step ω is much larger than Δ_0, Δ_1. Then, most of the terms in Eq. (4.45) oscillate very quickly and can thus be neglected.

$$\begin{aligned} \mathrm{e}^{-i(\lambda_i(t)-\varepsilon_0 t)} &= \mathrm{e}^{i\phi_0}\sum_n J_n\left(\frac{\lambda_A}{\omega}\right)\mathrm{e}^{-i(n\omega-\varepsilon_0)-in\phi} \\ &\simeq \mathrm{e}^{i(\phi_0-\phi)}J_1\left(\frac{\lambda_A}{\omega}\right), \end{aligned} \tag{4.47}$$

where we used the argument of the previous paragraph to identify the term $n = 1$ as the resonant one and set the field angular frequency $\omega = \varepsilon_0$, which was expected from the numerical analysis of the optimal fields. Its straightforward to calculate the rest of the elements of Hamiltonian of Eq. (4.45), which can be approximated by a time-independent expression

$$H'_{ND} = \frac{1}{2}\begin{pmatrix} 0 & \mathrm{e}^{-i\phi_0}\Delta'_0 & 0 \\ \mathrm{e}^{i\phi_0}\Delta'_0 & 0 & \mathrm{e}^{i(\phi_0-\phi)}\Delta'_1 \\ 0 & \mathrm{e}^{-i(\phi_0-\phi)}\Delta'_1 & 0 \end{pmatrix}, \tag{4.48}$$

where we have introduced the renormalized interaction rates

$$\begin{aligned} \Delta'_0 &\equiv J_0\left(\frac{\lambda_A}{\varepsilon_0}\right)\Delta_0 \\ \Delta'_1 &\equiv J_1\left(\frac{\lambda_A}{\varepsilon_0}\right)\Delta_1 \end{aligned} \tag{4.49}$$

Then, the evolution of the system for $0 \leq t < t_m$ is completely determined by the evolution operator in Eq. (4.44) where $U_0^{(B)}(t) = \exp\left(-iH'_{ND}t\right)$. Note that this factor introduces the couplings between the diabatic states which generate the time evolution of the operators. The role of the driving in this process is clear. In the absence of the oscillatory field, i.e. $\lambda_A = 0$, Eq. (4.49) gives $\Delta'_0 = \Delta_0$ and $\Delta'_1 = 0$, and so only states $|0\rangle$ and $|1\rangle$ can be connected in this evolution. This is exactly what we expected from the sudden-switch protocol and the adiabatic elimination procedure discussed in the previous section. When the oscillatory field is turned on, Δ_0 decreases and Δ_1 takes a non-zero value, thus coupling weakly states $|1\rangle$ and $|2\rangle$. This generates an evolution where the target state of the protocol $|2\rangle$ can draw a portion of the population of the other levels even when the dynamics is mainly dictated by the first AC. Thanks to this feature, the evolution towards the target state is accelerated, thus providing the overall enhancement of the QSL time shown in the previous Section. Note that Eq. (4.49) formalizes the fact that the amplitude λ_A cannot be neglected with respect to ε_0. Moreover, setting λ_A/ε_0 to a constant value is consistent with the analysis shown in Fig. 4.8 (c), where both quantities showed a linear correlation.

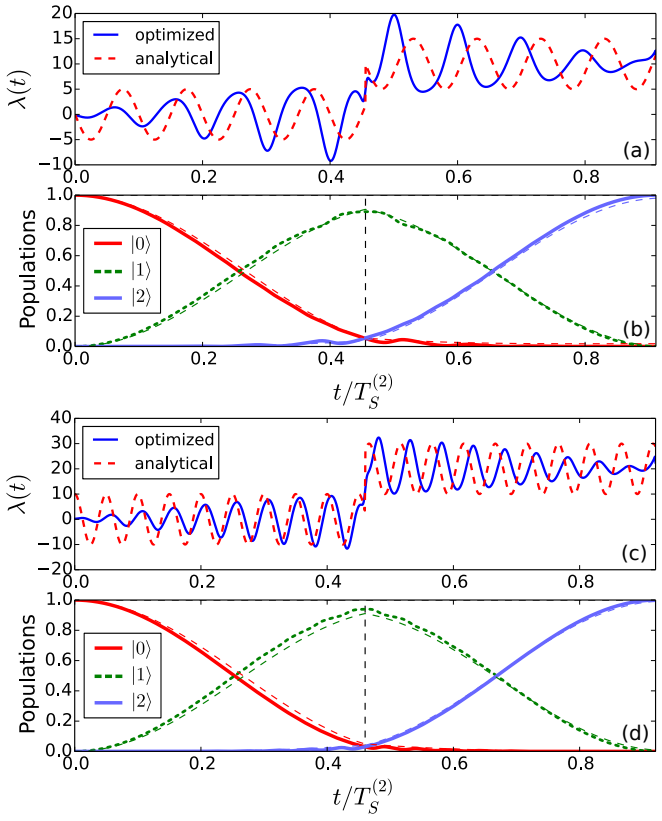

FIGURE 4.9: (a) and (c) Optimized and analytical proposal of Eq. (4.43) for the control field as a function of time. (b) and (d): time-evolution of the populations for each of the diabatic states. Thin dashed lines corresponds to the analytical solution of Eq. (4.50). (a) and (b) Case $\varepsilon_0 = 10\,\Delta_0$. (c) and (d) Case $\varepsilon_0 = 20\,\Delta_0$.

An analogous procedure can be done for the evolution between $t = t_m$ and $t = T$, in such a way that we can finally write for the whole evolution as

$$U(t) = \begin{cases} U_0^{(A)}(t)U_0^{(B)}(t) & , \quad 0 \leq t < t_m \\ U_1^{(A)}(t)U_1^{(B)}(t)U_0^{(A)}(t_m)U_0^{(B)}(t_m) & , \quad t_m \leq t \leq T \end{cases} , \tag{4.50}$$

where we have defined $U_1^{(A)}(t) = \exp\left(-i\int_{t_m}^{T} H_D(t')dt'\right)$ and $U_1^{(B)}(t) = \exp\left(-iH''_{ND}(t-t_m)\right)$ with an effective time-independent Hamiltonian given by

$$H'_{ND} = \frac{1}{2}\begin{pmatrix} 0 & \mathrm{e}^{-i(\tilde{\phi}_0-\tilde{\phi})}\Delta''_0 & 0 \\ \mathrm{e}^{i(\tilde{\phi}_0-\tilde{\phi})}\Delta''_0 & 0 & \mathrm{e}^{i\tilde{\phi}_0}\Delta''_1 \\ 0 & \mathrm{e}^{-i\tilde{\phi}_0}\Delta''_1 & 0 \end{pmatrix}. \tag{4.51}$$

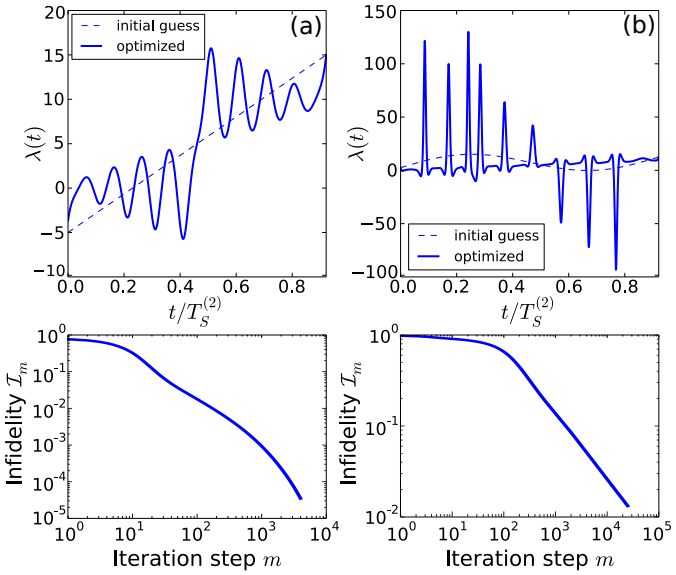

FIGURE 4.10: Results of the optimization procedure using different initial guesses for the control field. Top: Optimized control field as a function of time. Bottom: Infidelity $\mathcal{I}_m$ as a function of the step number m for each optimization. (a) Initial guess is a linear function. (b) Initial guess is a sinusoidal function. For both cases, we used the same parameter values as in Fig. 4.8 (a).

The renormalized interaction rates are now interchanged with respect to the previous case,

$$\begin{aligned} \Delta_0'' &\equiv J_1\left(\frac{\lambda_A}{\varepsilon_0}\right)\Delta_0 \\ \Delta_1'' &\equiv J_0\left(\frac{\lambda_A}{\varepsilon_0}\right)\Delta_1, \end{aligned} \tag{4.52}$$

which is natural since in the second step the dominant interaction is due to the AC between states $|1\rangle$ and $|2\rangle$. In Fig. 4.9 we show the time evolution of the populations for different cases, as predicted by the analytical formula (4.50). There, it can be seen how this expression approximates very well the optimized evolution, even though the driving fields are not exactly equal. Finally, we point out that the solution we provide here is based on the process $P_{K=2}$, being the next step in complexity of the two-level case, where these novel effects are, of course, absent. We believe that a similar procedure could be applied to find analytical expressions for higher-order processes.

4.4.2 Initial guess and performance of the optimization

We recall that the previous analytical discussion was motivated by the fact that the control field obtained from QOC had a simple shape. This, in turn, related with the fact that the optimized field preserved certain features of the initial guess $\lambda_0(t)$ we employed, for example, the step-wise structure. We will now briefly discuss the role of the initial guess in the optimization. In Fig. 4.10 we show the infidelity and optimized field obtained for two choices of $\lambda_0(t)$ different from the one shown in Fig. 4.8. In one of the cases, Fig. 4.10 (a), the field has a linear dependence and connects the positions of the ACs. The corresponding optimized field develops fast oscillations and overall looks very similar to the one in Fig. 4.8. Moreover, the frequency of the oscillations f_ε is the same for both cases, and the total number of iterations required for the convergence of the algorithm is also of the same order (around 4000). On the other hand, in Fig. 4.10 (b) we used as an initial guess a sinusoidal field, with initial and final value at $\lambda = \lambda_0 = 0$, and for which we deliberately change the parity with respect to the other cases. In that case, the number of iterations required by the optimization to converge raises by a factor of 10. Moreover, the optimized fields has a very irregular shape, showing peaks of very large amplitude (50 times bigger than the other cases).

As we mentioned previously, the fact that the QSL time for control processes can be drawn from the optimization procedure enforces the power of QOC as a tool in this context. The results we show here also tell us that the performance of QOC, and its ability to give us information about the physical mechanisms involves in a control processes can be enhanced by properly providing the optimization with a good initial guess. In this case we have done so by analyzing the characteristics of the system, and more precisely by studying the structure of the energy spectrum.

Control óptimo en sistemas cuánticos

En este capítulo utilizamos las herramientas de optimización presentadas en el capítulo 2 para analizar más a fondo los problemas de control en sistemas con uno y con muchos cruces evitados en su espectro de energía, como los discutidos en el capítulo 3. En primer lugar volvemos a analizar el sistema de dos niveles descrito por el hamiltoniano de Landau-Zener (3.1) en la sección 4.1. Allí veremos que es posible resolver analíticamente el problema de controlar el sistema en un tiempo óptimo. Esto nos permite confirmar la optimización temporal del protocolo de control introducido en el capítulo anterior.

En la sección siguiente aplicamos los métodos presentados en la sección 2.2 para obtener cotas inferiores para el tiempo de control mínimo. Un conjunto de ellos se desprenden de la relación geométrica de Anandan-Aharonov (2.20), y comparten la característica de que es preciso conocer la evolución completa del sistema para ser calculadas. El resto de los métodos forman parte de un nuevo enfoque para obtener estas cotas, que implica necesariamente no tener que resolver la ecuación de Schrödinger, ni conocer la forma exacta de los campos de control. Este enfoque fue desarrollado en el Capítulo 2. En dicha sección concluimos que estos nuevos métodos pueden proveer un grado de información similar a los primeros, a pesar de requerir menos información. Sin embargo, cuando los campos de control no poseen restricciones en su amplitud, su utilidad se ve disminuida.

En la sección 4.3 utilizamos control óptimo como herramienta para estudiar el QSL en los sistemas de muchos niveles que muestran varios cruces evitados (ACs) en su espectro de energía, como los descritos en el Cap. 3. En ese caso vimos que podíamos diseñar campos de control mediante una serie de variaciones repentinas del parámetro de control, que resultó en una evolución óptima en cada AC. En el resto de este capítulo mostramos que el tiempo mínimo de evolución para procesos que involucran más de un AC es en general menor que la suma algebraica de

los tiempos óptimos para cada cruce, incluso cuando parecen estar bien aislados. Luego, a través del análisis de los campos óptimos derivados por control óptimo, estudiamos el mecanismo físico implicado en dicha mejora. Inclusive mostramos que podemos resolver la dinámica completa del sistema proponiendo una forma cerrada para los campos de control, inspirada en los resultados de la optimización.

Finalmente, concluimos que el hecho de que el tiempo QSL para los procesos de control se puedan extraer del procedimiento de optimización muestra la potencia de las técnicas de control óptimo (OC) como una herramienta en este contexto. Los resultados que mostramos aquí también nos dicen que el desempeño de OC, y su capacidad para darnos información sobre los mecanismos físicos implica que un proceso de control se puede mejorar proporcionándole a la optimización una buena semilla inicial. En este caso lo hemos hecho analizando las características del sistema y, más precisamente, estudiando la estructura del espectro energético.

Chapter 5

Complexity and control in quantum systems

In the last section of Chap. 4 we showed that by analyzing the shape of optimal control fields, we could gain information about the physical mechanisms involved in the controlled dynamics of a quantum system. In this Chapter we will revisit this idea but in a much more complex scenario: performing control on many-body quantum systems. Our goal is to investigate the connection between the complexity of a quantum system and its controllability. To this end, we study control protocols in a chain of spin-1/2 particles with short-range interactions, both in the few- and many-body regimes. By using this model, we are able to tune the physical complexity of the system in two different ways: by adding excitations to the system, we can increase the effective state space dimension; and by tuning the interparticle coupling, we can drive the system through a transition from a regular energy spectrum to a chaotic one. We will start by briefly reviewing some important features of quantum chaos, and then we will turn our attention to the spin chain model and the problem of performing optimal control on that system.

5.1 Signatures of quantum chaos

As already mentioned, here we will study the structure of the energy spectrum of a quantum system in relation to its complexity. Interestingly, this link takes place in connection to quantum chaos, i.e. the study of the quantum mechanical properties of systems which classical analogs display a chaotic behavior [131, 132, 133]. Here we give an overview of the spectral properties of such systems.

An n-dimensional quantum system described by some Hamiltonian H has an energy spectrum given by the eigenvalues of H: $\{E_1, E_2, \ldots, E_n\}$. We define the (nearest-neighbor) level spacing distribution $P(s)$ is as the probability that the spacing between two neighboring levels is s,

$$\bar{E}_{n+1} - \bar{E}_n = s. \tag{5.1}$$

Here, the set $\{\bar{E}_n\}$ is called the *unfolded* spectrum of H, and its calculated by locally rescaling the energies so that the mean level density of the new spectrum is equal to 1 [134, 135]. The resulting distribution satisfies

$$\int_0^\infty P(s)\, ds = 1 \text{ and } \int_0^\infty s\, P(s)\, ds = 1. \tag{5.2}$$

Berry and Tabor proved [131] that quantum systems for which the corresponding classical dynamics is regular, exhibit a Poissonian level spacing distribution

$$P_P(s) = \mathrm{e}^{-s} \text{ (Regular)}. \tag{5.3}$$

This behavior implies that level spacings can be seen as randomly distributed in an uncorrelated fashion: the amount of levels with different spacings are independent from each other. Another property derived from this conjecture is that, since $p(s)$ is maximum at $s = 0$, then the energy levels show clustering, in the sense that many of them will be close together. As opposed to the type of systems studied in Chap. 3, here the energy levels do not repel to form avoided crossings, and instead are prone to exhibit degeneracies.

On the other hand, Bohigas, Giannoni and Schmidt (BGS) [136] conjectured in 1984 that quantum systems whose classical analogs are chaotic should display a different level spacing distribution. In particular, the BGS conjecture says that the statistical properties of the energy spectra of such systems is the same as predicted for the Gaussian Orthogonal Ensemble (GOE), an specific type of random matrices. Random matrix theory (RMT) was put forward by Wigner [137] in the context of nuclear physics and the main idea behind it is that the Hamiltonian describing a complicated many-level system such as heavy nucleus should be similar to some element of an ensemble of matrices which, apart from having some defined symmetry properties (like, for example, being hermitian), have completely random elements [138]. In particular, it can be seen that the level spacing statistics for the GOE is given by the Wigner-Dyson distribution

$$P_{WD}(s) = \frac{\pi}{2} s \exp\left(-\frac{\pi}{4} s^2\right) \text{ (Chaotic)}. \tag{5.4}$$

Note that, in clear contrast with the regular case, c.f. eqn. (5.3), the distribution vanishes for $s = 0$, which is a sign of level repulsion and thus of the appearance of avoided crossings in the energy spectrum. In this way, we can argue that a

quantum system with a chaotic energy spectrum is more complex than a regular one, since in the former there is a degree of correlation between the energy levels, which is absent in the latter.

The above characterization was proposed by Percival as a way to distinguish the quantum mechanical properties of classically regular or chaotic systems [139]. An elegant way to quantify the level of chaoticity in a quantum system is to employ the Brody parameter β. This number is obtained by fitting the actual level spacing distribution $P(s)$ with the Brody distribution [140]

$$P_B(s) = (\beta+1)bs^{\beta}\exp(-bs^{\beta+1}),\ b = \left[\Gamma\left(\frac{\beta+2}{\beta+1}\right)\right]^{\beta+1}. \tag{5.5}$$

Note that $\Gamma(x)$ refers here to the usual gamma function. The function $P_B(s)$ tends to a Poisson distribution $P_P(s)$ for $\beta \to 0$, while for $\beta \to 1$ resembles the Wigner-Dyson distribution $P_{WD}(s)$.

5.2 Spin chain model

We will now turn our attention to a quantum many-body model in which we will study control problems. Let us consider a one-dimensional chain of L spin-1/2 particles that interact through nearest-neighbor (NN) and next-to-nearest-neighbor (NNN) homogeneous couplings with open boundary conditions. The Hamiltonian for this models reads

$$H_{01} = H_0 + \Gamma H_1, \tag{5.6}$$

$$H_0 = \frac{J}{2}\sum_{i=1}^{L-1} \sigma_i^x\sigma_{i+1}^x + \sigma_i^y\sigma_{i+1}^y + \alpha_z\sigma_i^z\sigma_{i+1}^z, \tag{5.7}$$

$$H_1 = \frac{J}{2}\sum_{i=1}^{L-2} \sigma_i^x\sigma_{i+2}^x + \sigma_i^y\sigma_{i+2}^y + \alpha_z\sigma_i^z\sigma_{i+2}^z, \tag{5.8}$$

where $\sigma_i^{x,y,z}$ are the Pauli matrices for the i-th particle and we have taken $\hbar = 1$. The Hamiltonian H_0, which has only NN couplings, is the usual XXZ Heisenberg model, which can be exactly solved via the Bethe ansatz [141]. The parameter Γ measures the ratio between the NNN exchange and the NN couplings. Although the full Hilbert space of this system has dimension $\dim(\mathcal{H}) = 2^L$, the Hamiltonian (5.6) has a block-diagonal structure due to it symmetry properties.

5.2.1 Symmetries and sources of complexity

The most evident symmetry of the system arises from the conservation of the total magnetization in the z direction $S_z = \frac{1}{2}\sum_{i=1}^{L}\sigma_i^z$, since $[H_{01}, S_z] = 0$ for all values of α_z as we show in Appendix C. This conserved quantity allows us to break up the total state space into subspaces $\mathcal{S}_K$ of fixed number K of spins up which will not mix under the evolution of Hamiltonian (5.6). We refer to the number of spins up in each subspace as "excitations", and note that the following relation holds

$$\mathcal{H} = \bigoplus_{K=0}^{L} \mathcal{S}_K \tag{5.9}$$

In this way, the single-excitation subspace $\mathcal{S}_1$ will contain states such as

$$\mathcal{S}_1 : \ |\uparrow\downarrow\downarrow \ldots \downarrow\rangle\,,\ |\downarrow\uparrow\downarrow \ldots \downarrow\rangle\,,\ \ldots \tag{5.10}$$

while $\mathcal{S}_2$ will be spanned by

$$\mathcal{S}_2 : \ |\uparrow\uparrow\downarrow \ldots \downarrow\rangle\,,\ |\downarrow\uparrow\uparrow\downarrow \ldots \downarrow\rangle\,,\ \ldots \tag{5.11}$$

and so on. The dimension of each subspace can be easily computed by combinatorial considerations, since its equal to the number of ways we can choose K sites out of a L long chain, that is

$$D_K \equiv \dim(\mathcal{S}_K) = \binom{L}{K} = \frac{L!}{K!(L-K)!}. \tag{5.12}$$

Note that the dimension of the effective state space will grow from 0 for $K = 1$ to its maximum value at $K = \frac{L-1}{2}$ (for odd L). Up to that point, we will take the number of excitations K as a parameter which increases the complexity of the dynamics since it allows the system to evolve in a larger manyfold.

The model in (5.6) may also preserve the value of total spin S^2 depending on the value of α_z, since for example we have that

$$\left[H_0, S^2\right] = \frac{J}{4}(\alpha_z - 1)\left(\sum_{n=1}^{L} 2\sigma_n^z\sigma_{n+1}^z - \sigma_n^x\sigma_{n+1}^x - \sigma_n^y\sigma_{n+1}^y\right) \tag{5.13}$$

and a similar result is obtained for $[H_1, S^2]$. We deliberately take $\alpha_z = \frac{1}{2} \neq 1$ in order to avoid conservation of S^2.

Finally, let us consider the parity symmetry of the system. For that, let us define the permutation operator P_{ij} between sites i and j as

$$P_{ij} = \frac{1}{2}\left(\mathbb{I} + \vec{\sigma}_i.\vec{\sigma}_j\right). \tag{5.14}$$

P_{ij} acts on the two-site basis exchanging the state of spins i and j, in such a way that for example $P_{12}\,|\uparrow\downarrow\rangle = |\downarrow\uparrow\rangle$. The parity operator Π is then defined as the

collective permutation of mirrored sites in the chain. For example, in a chain of length 5 it would act as

$$\Pi\,|\uparrow\downarrow\downarrow\uparrow\downarrow\rangle = |\downarrow\uparrow\downarrow\downarrow\uparrow\rangle \tag{5.15}$$

For odd L we can write the general form of Π as

$$\Pi = P_{1,L}P_{2,L-1}\ldots P_{\frac{L-1}{2},\frac{L+3}{2}}. \tag{5.16}$$

Given that the interparticle couplings in Hamiltonian (5.6) are homogeneous, it is obvious to see that $[H_{01},\Pi] = 0$ for all values of σ_z and Γ and thus parity is preserved. Taking it into account, each subspace $\mathcal{S}_K$ is further divided into two subspaces of definite (positive or negative) parity $\mathcal{S}_{K,\pm}$. The dimension of each of those is such that $D_{K,\pm} \simeq D_K/2$.

The model described in the previous paragraphs has been extensively studied in the literature in many contexts, including the analysis of thermal entanglement [142] and quantum phase transitions [143], but it has attracted much attention as a model of quantum chaos. Albeit lacking a semiclassical counterpart, this spin model displays a transition in its level spacing distribution as Γ changes. Following the discussion of the previous Section, we computed the level spacing distribution $P(s)$ for the (unfolded) energy spectrum of Hamiltonian (5.6) for various values of the NNN coupling parameter Γ. From this, we then calculated the Brody parameter β by fitting the corresponding distribution (5.5) to $P(s)$. Results are shown in Fig. 5.1, where it can be seen that for $\Gamma \lesssim 0.5$, $\beta \to 0$ and thus level spacings follow a Poisson distribution as in (5.3); in this case the energy spectrum is regular. On the other hand, for $\Gamma \gtrsim 0.5$ we have $\beta \to 1$, the distribution follows Wigner-Dyson statistics, eqn. (5.4), and the spectrum is deemed chaotic.

Note that results are shown in Fig. 5.1 for different subspaces $\mathcal{S}_{K,+}$ of fixed excitation number K and positive parity. The dimension of such subspaces range from $D_{2,+} \simeq 52$ to $D_{5,+} \simeq 1500$. The distinction between regular and chaotic spectra can be effectively seen for K larger or equal than 3, where the state space dimension becomes large enough so that we can draw sufficient statistics to see the full distribution.

5.2.2 Control processes

For this model we are interested in studying control problems for various regimes of state space dimension (given by parameter K) and chaoticity in the energy spectrum (measured by parameter Γ). In order to do so, we first need to define a

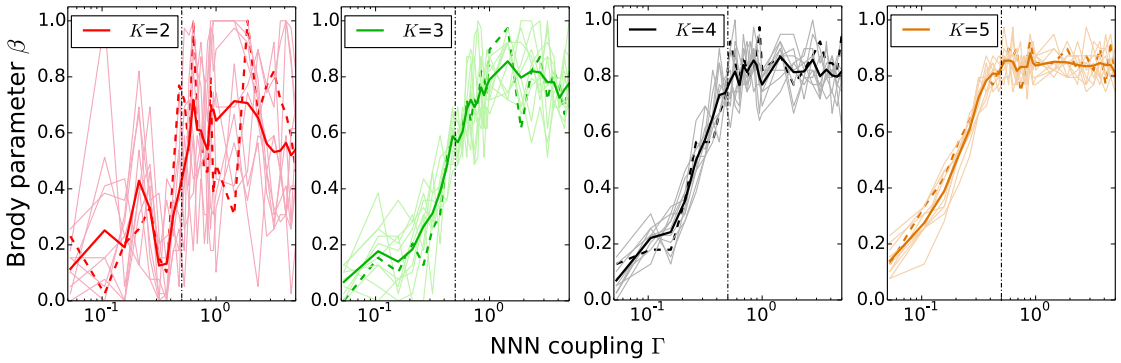

FIGURE 5.1: Dashed lines: Brody parameter β as a function of the NNN coupling Γ for the free spin chain Hamiltonian (5.6). The four plots correspond to various values of the number K of excitations in the chain. In each case, curves in light colors correspond to the results obtained by fixing the adimensional control parameter ϵ to values in the range $[-3, 3]$ in the full Hamiltonian (5.19). Thick full lines denote the mean value of all curves. The dash-dotted vertical line shows the critical value of Γ for the regular-chaotic transition in the energy spectrum. In all cases we consider only the eigenenergies corresponding to positive eigenstates of the parity operator Π.

control Hamiltonian by means of which we intend to steer the free chain Hamiltonian H_{01}. Many different alternatives have been studied in the literature. For example, in Ref. [144], the author proposed using a global parabolic magnetic potential to control the transfer of excitations from one end of the chain to the other. Later, the same configuration was used to study the optimal evolution time for such processes in the single excitation subspace [54, 145]. Other control configurations have also been proposed in scenarios where only one [146] or two [147, 148, 149] sites are locally addressed by external fields. Here, we will consider time-dependent magnetic fields in the z direction which are locally applied at each site of the chain, i.e.

$$H_c = \frac{J}{2} \sum_{i=1}^{L} \epsilon_i(t) \sigma_i^z \tag{5.17}$$

Note that, since we want to explore in particular the relation between the chaotic properties of the system and its controllability, the control Hamiltonian we introduce must comply with the symmetries of the free Hamiltonian H_{01}. This is because if the interaction where to mix subspaces with different symmetry properties, then the full level statistics may have no dependence on Γ, as discussed in Ref. [150]. Clearly the expression in (5.17) preserves the total magnetization, since $[H_c, \sum_i \sigma_i^z] = 0$. On the other hand, when analyzing the parity operator

defined in eqn. (5.16), we obtain (derivation can be found in Appendix C)

$$[H_c, \Pi] = \frac{J}{2} \sum_{i=1}^{L} [\epsilon_{L-i+1}(t) - \epsilon_i(t)]\, \sigma_i^z \Pi, \tag{5.18}$$

which indicates us that the commutator vanishes only if the fields applied on mirrored sites of the chain are equal. So, in order to preserve parity we will consider the situation where the first and last spin of the chain are affected by the same field $\epsilon(t)$, whereas all the other spins do not interact with any external field. Consequently, the full Hamiltonian can be written as

$$H(t) = H_{01} + \epsilon(t) H_c, \text{ where } H_c = \frac{J}{2} \left(\sigma_1^z + \sigma_L^z\right). \tag{5.19}$$

We point out that we have explicitly checked that for any fixed value of the field, the full Hamiltonian H still shows a transition between a regular and a chaotic spectrum for $\Gamma \simeq 0.5$. Numerical results are shown in Fig. 5.1, where we computed the Brody parameter for different fixed values of $\epsilon(t)$.

The next step is to define the control processes we aim to perform. We will consider two different protocols (A and B) in order to obtain general results about the controllability of the system. In both cases, we define initial and target states which we denote $|\psi_0^\alpha\rangle$ and $|\psi_f^\alpha\rangle$, where $\alpha = A, B$. These states are deliberately defined to allow the system to evolve within a particular subspace with fixed (positive) parity and number of excitations K of the complete Hilbert space, as discussed previously. First, process "A" involves the system initially prepared in a state with all excitations in the middle sites of the chain (in this scheme, the central site has no excitations if K is even). We then intend to drive this configuration into a coherent superposition as defined by

$$|\psi_0^A\rangle = |\downarrow \ldots \downarrow\uparrow\uparrow\downarrow \ldots \downarrow\rangle \tag{5.20}$$

$$|\psi_f^A\rangle = \frac{1}{\sqrt{2}} \left(|\uparrow\uparrow\downarrow \ldots \downarrow\rangle + |\downarrow \ldots \downarrow\uparrow\uparrow\rangle\right). \tag{5.21}$$

Process A then represents and ordered control process in which entanglement is generated between both ends of the chain.

On the other hand, we define a disordered process B, where the system starts from the ground state of H_0 and is steered into a random superposition of excited states (with positive parity).

$$|\psi_0^B\rangle = |\text{g.s.}_0\rangle \tag{5.22}$$

$$|\psi_f^B\rangle = \sum_{n=1}^{D_{K,+}-1} a_n |n_0\rangle \tag{5.23}$$

where $\{|n_0\rangle\}$, $n = 0, \ldots, D_{K,+}$ are the positive eigenvectors of H_0 in the subspace

of K excitations and $|\text{g.s.}_0\rangle \equiv |0_0\rangle$. The coefficients $\{a_n\}$ are a set of random complex numbers so that $\sum_i |a_n|^2 = 1$.

For these two processes, we applied the same optimal control algorithm described in Chap. 2 and already used in Chap. 4. As we intend to compare the control fields obtained by this procedure, we fix the input parameters of the optimization as follows. For the total evolution time T we set $T = 15 \times T_L$ where $T_L = (L-1)\frac{\pi}{J}$ can be regarded as the typical evolution time required for transferring a single excitation from one end of the chain to the other [145]. We have checked that using this value we are operating well beyond the quantum speed limit [54], and so that fidelities up to 0.99 or greater can be achieved, for both control processes and every value of the number of excitations K and the NNN coupling Γ considered. Also, we used a constant initial guess $\epsilon^{(0)}(t) = 0.1$ in all cases. We have checked that the results we present in the next section hold for other choices of this function, and also for larger values of the evolution time T.

Note that the optimal control algorithm requires to propagate forward and backward the state of the system at each iteration. This can be computationally expensive especially for large values of K, since for example for $K = 4$ the relevant subspace of state space has dimension $D_4 = 1365$. We avoid having to explicitly diagonalize the Hamiltonian at each iteration by employing the split-operator technique which is outlined in Appendix C.2.

We point out that previous works have studied the relationship between optimal control and the dimension of the quantum system under analysis [60, 61]. There, a suitable measure for the control field complexity was defined, related with the number of frequencies in the field, as allowed by the optimization procedure. Then, it was shown that the complexity required to achieve control scaled polynomially with the dimension of the manifold supporting the dynamics. Here, we focus on studying the complexity of the control fields regardless of the details of the optimization method itself. We do this by deliberately allowing many frequency components in the control fields, and then analyzing which of those components are required to effectively drive the system. Other studies relating chaos and control can be found in [151, 152].

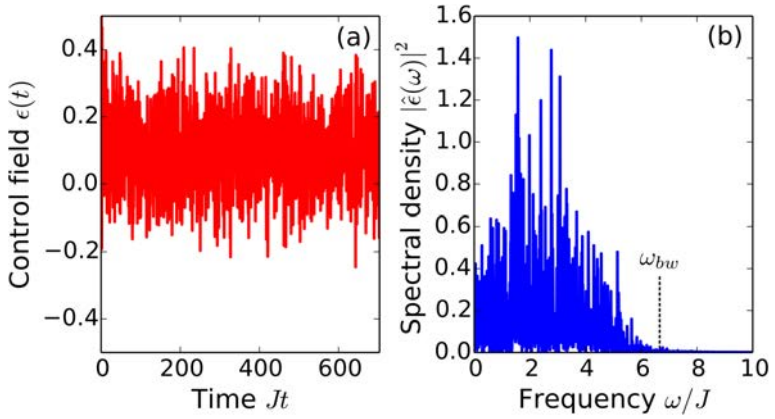

FIGURE 5.2: (a) A typical optimized control field $\epsilon(t)$ obtained for process A and $\Gamma = 1$ and (b) its normalized Fourier transform.

5.3 Optimal control fields

In Fig. 5.2 (a) we show a typical example of the control field $\epsilon(t)$ obtained by optimal control methods, together with its Fourier spectrum in Fig. 5.2 (b). The time signal shown can be seen to be complex and have many spectral components up to certain frequency threshold. In order to characterize quantitatively these features, we define two measures of complexity for the control fields: the frequency bandwidth and the spectral inverse participation ratio (sIPR). In the following we investigate these quantities.

5.3.1 Frequency bandwidth

Given a time-varying signal $\epsilon(t)$ and its Fourier transform $\hat{\epsilon}(\omega)$, we first define its frequency bandwidth as the value ω_{bw} such that

$$\int_0^{\omega_{bw}} d\omega \, |\hat{\epsilon}(\omega)|^2 = 1 - \beta, \tag{5.24}$$

where $0 < \beta < 1$ and the frequency distribution is normalized

$$\int_0^{\infty} d\omega \, |\hat{\epsilon}(\omega)|^2 = 1. \tag{5.25}$$

By this definition, the frequency interval $[0, \omega_{bw}]$ concentrates the $[(1-\beta)\times 100]\%$ of the power spectrum (here, we use $\beta = 10^{-2}$). In other words, ω_{bw} is a measure of the maximum frequency present in $\epsilon(t)$.

In Fig. 5.3 (a) we show the frequency bandwidth ω_{bw} as a function of the NNN or chaos parameter Γ, for different number K of excitations in the chain. Results obtained for both processes A and B are shown in the same plot. Remarkably, we

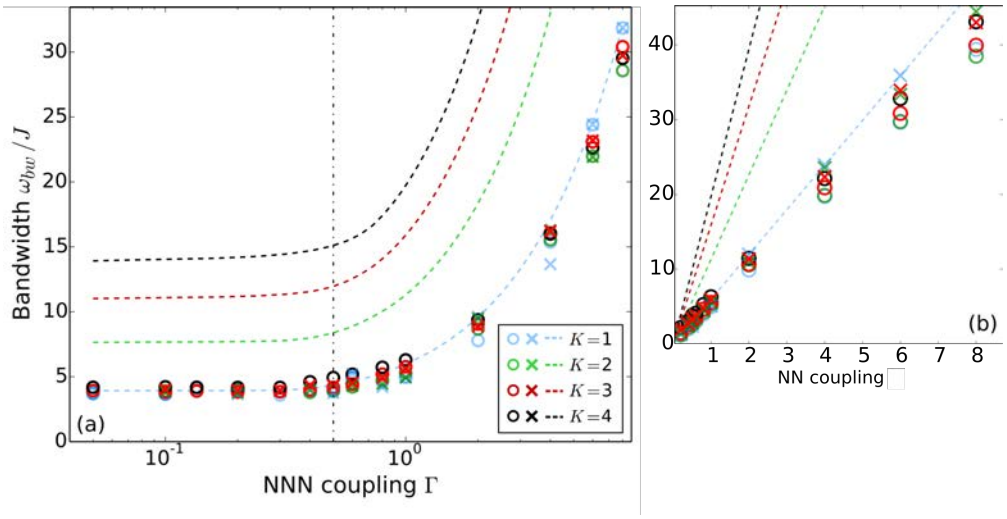

FIGURE 5.3: (a) Spectral bandwidth of the optimized control fields (in units of J) as a function of the adimensional NNN coupling Γ, for various values of K (the number of excitations in the spin chain). Data shown is for both control processes A and B. State space dimension ranges from 15 (K=1) to 1365 (K=4). The dashed curves show the energy spread (in units of J) of the free Hamiltonian H_{01} (5.6) for different values of K. The dash-dotted vertical line indicates the critical value of $\Gamma = 0.5$ for which the regular-chaotic transition occurs in the energy spectrum of H_{01}. (b) same as in (a), but plotted as a function of the NN coupling J, for a fixed value of $\Gamma = 1$.

find that all data roughly coincides in the same curve. This result indicates that the bandwidth is independent not only of the control processes considered, but also of the state space dimension. Note that, in each case, ω_{bw} is approximately constant for $\Gamma < 0.5$ and then increases steadily for $\Gamma > 0.5$. Although this behavior correlates with the onset of chaos in the system (as discussed in the previous section), we must first consider that increasing the interparticle coupling Γ necessarily increases the energy of the chain. As previously discussed in the context of quantum optimal control [96, 153], we expect the frequency distribution of the control fields to present peaks located at the resonances of the free Hamiltonian H_{01}. Following this criterion, the maximum frequency is bounded by the energy spread ΔE of H_{01}, defined as

$$\Delta E = E_{max} - E_0, \tag{5.26}$$

where E_{max} and E_0 are the maximum and minimum (ground state) energies of the Hamiltonian. Note that ΔE is a function of the interparticle interaction parameters J and Γ and of the number of excitations K. We show such functions as dashed lines in Fig. 5.3 (a). It is clear that the dependence of the bandwidth with Γ closely resembles the energy spread with $K = 1$. The same observation can be

drawn by studying both quantities as a function the NN coupling J (for fixed Γ). There, the behaviour is obviously linear, as shown in Fig. 5.3 (b).

Note, however, that the surprising independence of the bandwidth with the space dimension cannot be explained by its relation with the energy spread of the free Hamiltonian, since ω_{bw} is in every case significantly smaller than ΔE for $K > 1$. In order to gain a deeper insight about this result, we turn to investigate the role of the control Hamiltonian H_c, defined in eq. (5.19). We first study the structure of the matrix H_c written in the basis of (positive) eigenvectors of the free chain Hamiltonian H_{01}. In Fig. 5.4 (a) and (b) we plot the absolute value of such matrix elements for fixed values of Γ and K. From this plots we can see that H_c does not connect eigenstates which distant energies: for example, the ground state is not connected with excited states beyond the middle of the spectrum. This explains the absence of such high transition frequencies in the spectrum of the control fields. In order to provide numerical proof about this feature, we studied the implementation of one of the control processes with a different choice of control operator H_c' which presents a higher connectivity [134] between distant states in the spectrum. Such Hamiltonian matrix is shown in Fig. 5.4 (c) and (d). Results for the new optimized fields are shown in Fig. 5.4 (e), where we show the frequency bandwidth as a function of Γ for this case. It can be seen that ω_{bw} is greater for $K = 2$ than for $K = 1$, for all values of Γ considered. We point out that, by looking at the representation of H_c' in the computational basis, Fig. 5.4 (c), we can see that this alternative control procedure would involve tuning a complex combination of multi-spin interactions, in clear contrast with the simple structure of H_c.

The results shown so far allow us to assert that the control bandwidth, which measures the range of frequencies present in the fields is determined exclusively by the energy spread of the free Hamiltonian and the structure of the control Hamiltonian. This gives us a measure of the physical complexity of the control field which turns to be independent of the number of particles in the system. We point out here that we are not interested in analyzing the complexity of the optimization itself, as has been done in previous works which have obtained interesting results [60, 61]. We work our way around this issue by fixing the time step of our numerical implementation to very small values, $J\Delta t = 10^{-2}$. This determines that the maximum allowed frequency in the fields is in every case at least on order of magnitude higher than the actual physical frequencies found by Fourier analysis in the control fields.

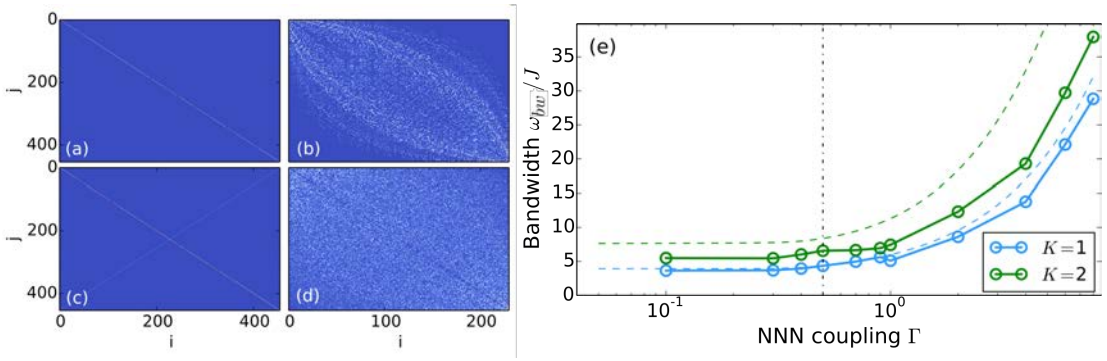

FIGURE 5.4: (a)-(d) Absolute values of the matrix elements for the control Hamiltonian (in units of J) in the computational basis (left panels) and in the energy eigenbasis with positive parity (right panels). Top panels: local control with H_c as in eq. 5.19. Bottom panels: long-range control with H_c' described in text. (e) Frequency bandwidth of the optimized control fields (in units of J) as a function of the adimensional NNN coupling Γ, for $K = 1$, 2 (the number of excitations in the spin chain). Data shown is for process A, using the long range control Hamiltonian H_c'.

5.3.2 Spectral localization

We now turn our attention to another measure of the control field complexity. In this case, we study how the number of frequencies which appear in the spectrum of the field varies as the system complexity is increased. For this purpose, we define the following quantity

$$\text{sIPR} = \left(\int_0^\infty d\omega \, |\hat{\epsilon}(\omega)|^4 \right)^{-1}, \tag{5.27}$$

which we call "spectral inverse participation ratio" (sIPR) as it is inspired in the commonly known IPR [154, 155] used to study eigenstate localization in many-body quantum systems. Here, the sIPR quantifies the localization in the Fourier transform of a time signal, and thus allows us to asses how complex the control field is inside its bandwidth. Note that localized frequency spectra give sIPR$\to$ 0, and complex signals with delocalized spectrum tend to higher sIPR. As an example, take a completely random signal with frequency components up to ω_{bw}. We expect such a signal to have a flat Fourier transform $\hat{\epsilon}(\omega) = 1/\omega_{bw}$ for $0 < \omega < \omega_{bw}$ and $\hat{\epsilon}(\omega) = 0$ for $\omega > \omega_{bw}$. Calculating the sIPR in that case is straightforward and gives ω_{bw}. We point out that here we intend to quantify the optimal control field complexity regardless of the frequency distribution width. For this purpose, we evaluate the normalized sIPR

$$\text{sIPRn} = \frac{\text{sIPR}}{\omega_{bw}}. \tag{5.28}$$

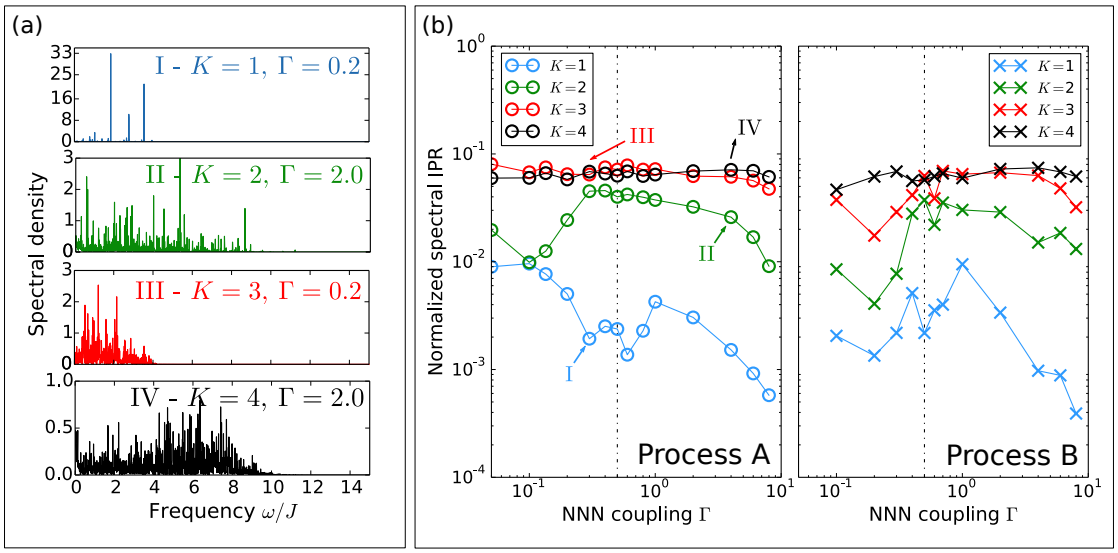

FIGURE 5.5: (a) Various normalized spectral densities of the optimal control fields found for process A. Values for the excitation number K and the adimensional next to nearest-neighbour (NNN) coupling Γ are shown for each case I-IV. (b) Normalized spectral inverse participation ratio (sIPRn), which measures the control field complexity, as a function of Γ, for various values of K (the number of excitations in the spin chain). Data shown is for process A (left) and B (right). The points indicated by labels I-IV correspond to the spectra shown in (a). State space dimension ranges from 15 ($K = 1$) to 1365 ($K = 4$). The dash-dotted vertical line shows the critical value of Γ for the regular-chaotic transition in the energy spectrum. All quantities shown are dimensionless.

Following the discussion in the previous paragraph, we expect sIPRn to range between 0 and 1, and we can interpret it as a measure of resemblance between the signal under study and a completely random time signal.

In Fig. 5.5 we plot the normalized spectral IPR as a function of the NNN exchange Γ for different values of the number K of excitations in the spin chain, and for both control processes A and B. We show also some examples of the frequency spectra we obtained, and it can be corroborated that sIPRn effectively measures how localized the spectrum is in Fourier space. More generally, it can be seen from the figure that sIPRn takes small values for $K = 1$ and then grows with K, and thus with state space dimension of the system. This is in sharp contrast with the behavior of the frequency bandwidth ω_{bw}, which was found to be independent of K. We point out that this behavior is common to both control processes. It is interesting to note that the high-dimensional cases ($K = 3, 4$) roughly converge to the same value of sIPRn, indicating that there maybe an upper bound for this measure which is below its maximal theoretical sIPRn= 1, which is achieved when the frequency spectrum is flat. Physically, the existence of an upper bound < 1 means that optimal control fields can always be distinguished from completely

random, white noise type fields.

Despite the dependence of normalized spectral IPR with the space dimension, it can be seen also that this indicator does not exhibit any clear trend with the NNN parameter Γ. We observe that, for small values of K, this parameter shows large fluctuations which tend to attenuate when for larger space dimensions. We recall that, for $K \geq 3$, the system exhibits a clear transition from a regular energy spectrum to a more complex (chaotic) one at $\Gamma = 0.5$. As can be seen from Fig. 5.5, there is no evidence of such leap in complexity in our numerical study. In this way, we can assert that the optimal fields required to control the dynamics of regular or chaotic Hamiltonians display a similar spectral complexity.

As a final remark, we point out that it would not be correct to claim that the spectral properties analyzed in this section are completely independent of the choice of initial and final state. This can be easily seen by considering a processes where we intend to connect the ground state of the free Hamiltonian H_{01} and one of its excited states $|n(\Gamma)\rangle$. If the control Hamiltonian H_c connects both states, we expect that the bandwidth of the control field will be given by the energy difference between both levels $E_n(\Gamma) - E_0(\Gamma)$, which can be significantly lower than the obtained ω_{bw} for processes A and B if $|n\rangle$ lies in the low-energy region. Nevertheless, our results do apply to general linear combinations of energy eigenstates, which is the more common scenario.

5.3.3 Control fields and energy spectrum

We will now look more closely at the connection between the spectral features of the optimal control fields and the structural properties of the system energy spectrum. We have already pointed out in the previous Section that the free chain Hamiltonian H_{01} (5.6) shows a transition in its level spacing distribution $\{\delta E_n\}$ as the NNN coupling parameter Γ changes, where

$$\delta E_n = E_{n+1} - E_n, \tag{5.29}$$

and E_n is the nth ordered eigenvalue of H_{01}. If the space dimension is high enough ($K \geq 3$), the level spacings statistics show a Poisson distribution for $\Gamma \lesssim 0.5$, and a Wigner-Dyson distribution $\Gamma \gtrsim 0.5$. We have also discussed at the beginning of this Section that we observed a connection between the frequency components present in the optimized control field and the resonances of the free Hamiltonian H_{01}. Thus, an interesting point arises: if the energy spectrum of H_{01} changes its structure with Γ, why is there no evidence about those changes in the frequency

distribution of the optimal control fields?

The key point here is to note that the resonances of H_{01}, which feed the frequency distribution of the control field, are not only formed by the difference of two consecutive energies δE_n (5.29). If connected by the control Hamiltonian, every energy difference present in the spectrum is also a suitable candidate for appearing the control field frequency spectrum. Following this discussion, we studied the distribution of the energy differences defined as

$$\delta E_{n,m} = E_{n+m} - E_n \text{ with } 0 < m \leq M, \tag{5.30}$$

such that $\delta E_{n,1} \equiv \delta E_n$. Note that, for every n, the value of M indicates how many levels above E_n are considered, and is thus bounded by the space dimension $D_{K,+}$. In Fig. 5.6 we show the distributions of normalized energy differences for different values of M, using $\Gamma = 0$ and $\Gamma = 1$. There, it can be seen that both distributions show the expected Poisson and Wigner-Dyson shapes when $M = 1$ (as discussed in the previous paragraph), but start to converge to a common form when M grows. As an example, for $K = 4$ we have that dimension of the positive subspace is $D_{4,+} \simeq 700$, and already taking $M \simeq D_{4,+}/10$ already gives near perfectly matching distributions for both values of the chaos parameter Γ. This analysis indicates that, while consecutive level spacing distributions are quite different for regular and chaotic spectra, the overall energy difference distributions converge to a same shape. This interesting behavior determines that the frequency spectrum

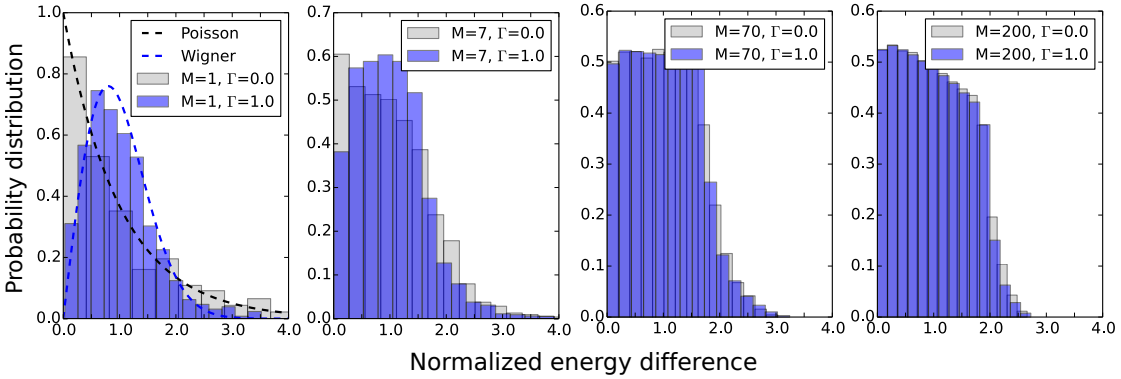

FIGURE 5.6: Distribution of energy differences $\delta E_{n,m}$ defined in eq. (5.30) for $\Gamma = 0$ (regular) and $\Gamma = 1$ (chaotic), where Γ is the NNN coupling parameter. All cases are normalized such that their mean value is 1. In the top left plot, we show the $M = 1$ case corresponding to the standard level spacing distribution. Poisson and Wigner-Dyson distributions are shown on top of the histograms. In all cases, we consider the positive subspace with $K = 4$ excitations in the chain ($D_{4,+} \simeq 700$). All quantites shown are dimensionless.

of the optimal field which control both type of systems have the same complexity.

Complejidad y control en sistemas cuánticos

En la última sección del Cap. 4 mostramos que el análisis de la forma de los campos de control óptimos nos permitió obtener información sobre los mecanismos físicos involucrados en la dinámica controlada de un sistema cuántico. En este capítulo volvemos a utilizar este enfoque, pero en un escenario mucho más complejo: realizar control en un sistema cuántico de muchos cuerpos. Nuestro objetivo es investigar la conexión entre la complejidad del sistema y su controlabilidad. Para ello, estudiamos protocolos de control en una cadena de partículas de espín 1/2 con interacciones de corto alcance, tanto en el regímen de pocos y muchos cuerpos. Usando este modelo, podemos ajustar la complejidad física del sistema de dos maneras diferentes: en primer lugar, agregando excitaciones al sistema podemos aumentar la dimensión eficaz del espacio de estados; también, variando el acoplamiento entre sitios, podemos conducir el sistema a través de una transición de un espectro de energía regular a uno caótico.

En la primera parte del Capítulo mostramos algunas características importantes del caos cuántico y luego nos centraremos en el modelo de la cadena de espines. Luego, discutimos distintas variantes propuestas en la literatura para controlar el estado de la cadena, y definimos dos tipos de procesos de interés que pretendemos obtener aplicando campos locales que afectan a cada sitio por separado. En la sección 5.3 proponemos y desarrollamos un estudio sistemático de los campos óptimos obtenidos. Con el fin de caracterizar cuantitativamente dichos campos, definimos dos medidas de complejidad para ellos: el ancho de banda de frecuencia ω_{bw} y la coeficiente de participación espectral inversa (sIPR). Mientras que ω_{bw} mide la frecuencia máxima presente en el espectro de Fourier del campo, el sIPR mide cuantas componentes distintas surgen en dicho espectro.

Los resultados principales del capítulo se hallan en la Fig. 5.3 y 5.5. En la primera

mostramos que el ancho de banda de los campos depende del acoplamiento a segundos vecinos de la cadena Γ pero no la dimensión K del sistema, ni del proceso de control considerado. También observamos que la dependencia con Γ no muestra correlación con las características caóticas del espectro, y por lo tanto deducimos que esta característica de los campos no permite evaluar la complejidad del sistema. Existe, sin embargo, una excepción interesante a estos resultados, que surge cuando variamos el tipo de control que proponemos. De hecho, si acoplamos el campo a un operador que actua de manera no local sobre la cadena, podemos observar que ω_{bw} si depende de la dimensión del sistema.

En la Fig. 5.5 mostramos el IPR espectral normalizado como una función de Γ nuevamente para diferentes valores del número K de excitaciones en la cadena. Allí mostramos que sIPR toma valores pequeños para $K = 1$ y luego crece con K, y por lo tanto con dimensión de espacio de estado del sistema. Esto contrasta claramente con el comportamiento del ancho de banda de frecuencia ω_{bw}, que se encontró que era independiente de K. Señalamos que este comportamiento es común a ambos procesos de control. Es interesante observar que los casos de dimensión alta ($K = 3, 4$) convergen aproximadamente al mismo valor de sIPRn. A pesar de la dependencia del IPR espectral normalizado con la dimensión espacial, puede observarse también que este indicador no muestra ninguna tendencia clara con el parámetro Γ. Observamos que, para valores pequeños de K, este parámetro muestra grandes fluctuaciones que tienden a atenuarse cuando para dimensiones espaciales mayores. Dado que para $K \geq 3$, el sistema muestra una clara transición de un espectro de energía regular a uno más complejo (caótico) en $\Gamma = 0.5$, podemos ver que no hay evidencia de tal salto en complejidad en nuestro estudio numérico. De esta manera, podemos afirmar que los campos óptimos requeridos para controlar la dinámica de hamiltonianos regulares o caóticos muestran una complejidad espectral similar.

En la última sección del capítulo nos centramos en explicar este último resultado estudiando distintas distribuciones asociadas al espectro de energías del Hamiltoniano. Encontramos que la distribución de niveles de energía se vuelve independiente de la naturaleza regular o caótica del sistema a medida que consideramos niveles cada vez mas alejados en el espectro. Dado que es esta distribución, y no la de niveles consecutivos, la que determina las frecuencias presentes en los campos de control, este análisis nos permite entender nuestros resultados.

Chapter 6

Control in open quantum systems and non-Markovian effects

In this Chapter we turn our attention to controlling open quantum system dynamics. Although we already studied some control problems in dissipative systems in Chap. 3, in that case we focused on how to speed up the evolution in order to reduce the impact of environmental effects, which could not be manipulated. Here we will take a more general approach, and discuss to what extent we can control open quantum systems depending on the features of their environments. After presenting an overview about open quantum systems and control under Markovian evolutions, we will focus completely on non-Markovian quantum maps, which show a more fertile (and also less explored) ground for quantum control.

6.1 Open quantum systems and dynamical maps

A quantum system $\mathcal{S}$ is said to be *open* if it interacts with a (typically larger) system, its environment $\mathcal{E}$, which is formed by degrees of freedom which are not available for measurements and in general unreachable to the observer. In this way, the state $\rho_{\mathcal{SE}}$ of the total system $\mathcal{S}\otimes\mathcal{E}$ evolves unitarily according to

$$\rho_{\mathcal{SE}}(t) = U(t)\rho_{\mathcal{SE}}(0)U^{\dagger}(t) \quad \text{with} \quad \frac{d}{dt}U(t) = -iH\,U(t) \tag{6.1}$$

where H describes the full system-environment Hamiltonian and is of the form

$$H = H_{\mathcal{S}}\otimes\mathbb{I}_{\mathcal{E}} + \mathbb{I}_{\mathcal{S}}\otimes H_{\mathcal{E}} + H_{int}^{\mathcal{SE}}. \tag{6.2}$$

By definition we may only access information about the *reduced* density matrix ρ of the system $\mathcal{S}$, which is defined as

$$\rho \equiv \mathrm{tr}_{\mathcal{E}}\left(\rho_{\mathcal{SE}}\right), \tag{6.3}$$

and which will in general evolve non-unitarily. The goal of open quantum systems theory is to describe the evolution of reduced dynamics of the system $\mathcal{S}$ by means of, for example, effective equations of motion for $\rho(t)$ [62, 63].

We can characterize the dynamics of the reduced system in the following way. If we consider the initial state of the full system to be uncorrelated, i.e. of the form

$$\rho_{\mathcal{SE}}(0) = \rho(0) \otimes \rho_{\mathcal{S}}(0) \tag{6.4}$$

then it is easy to see that we can combine expressions (6.1), (6.3) and (6.4) to write down a general expression for $\rho(t)$

$$\rho(t) = \mathrm{tr}_{\mathcal{E}} \left[U(t)\rho(0) \otimes \rho_{\mathcal{E}}(0)U^{\dagger}(t) \right]. \tag{6.5}$$

From this we see that the relation between $\rho(t)$ and $\rho(0)$ at each fixed $t \geq 0$ is given by a linear map $\Phi(t, 0)$ such that

$$\rho(0) \to \rho(t) = \Phi(t, 0)\rho(0) \tag{6.6}$$

These objects are called CPTP (completely positive trace preserving) maps since they satisfy the important properties of preserving hermiticity, trace and positivity[1]. In this way, a CPTP map applied to a density operator gives also a density operator.

6.1.1 Markovian quantum maps and control

An important type of dynamical maps $\Phi(t, 0)$ are those forming a semigroup, meaning that

$$\Phi(t + s, 0) = \Phi(t, 0)\Phi(s, 0) \tag{6.7}$$

for all $t, s \geq 0$. This property also implies that the dynamical map is divisible, in the sense that there exists a map $\Phi(t_2, t_1)$ such that $\Phi(t_2, 0) = \Phi(t_2, t_1)\Phi(t_1, 0)$. This property is taken as the definition of a *Markovian* dynamical map. The analogy with the classical version of a Markovian process originates because in both cases the process is memoryless, as seen by looking at the following identity derived from the divisibility property:

$$\rho(t_2) = \Phi(t_2, t_1)\rho(t_1). \tag{6.8}$$

There we see that the state of the system at time t_2 depends only on the state at time t_1, and thus does not have any memory of its state before that time [157].

[1] These maps are in fact completely positive, meaning that an extended map $\Phi \otimes \mathbb{I}_n$ acting over S and an auxiliary system of dimension n is still positive [156].

We will later on discuss more in detail the definition and quantification of Markovianity in dynamical maps.

The semigroup property in turn implies the existence of a generator $\mathcal{L}$ such that we can always write $\Phi(t,0) = \exp(\mathcal{L}t)$ [156]. We can also cast this expression in master equation form for the reduced density matrix $\rho(t)$

$$\frac{d}{dt}\rho(t) = \mathcal{L}\rho(t). \tag{6.9}$$

The most important result about quantum dynamical semigroups is a theorem due to Gorini, Kossakowski, Sudarshan [158] and Lindblad [159] that tells us that $\mathcal{L}$ is a generator of a semigroup of CPTP maps if and only if it can be written in the following form

$$\mathcal{L}\rho = -i\left[H_s, \rho\right] + \sum_k \gamma_k \left[L_k \rho L_k^\dagger - \frac{1}{2}\left\{L_k^\dagger L_k, \rho\right\}\right]. \tag{6.10}$$

Combination of eqns. (6.9) and (6.10) yields the famous GKSL equation (or, simply, Lindblad equation). This result is of tremendous practical importance since it provides a unified mathematical framework to simulate divisible (Markovian) dynamical maps to any degree of precision.

This useful mathematical framework has enabled thorough investigations over the past decade and a half about quantum control problems in open systems undergoing Markovian dynamics. Here we review the most salient features and results of this subject [25, 66]. First of all, let us consider a generic quantum control problem where we intend to steer a system from some initial to some target state by means of a control field $u(t)$. The system is coupled to an environment as described in eqn. (6.2) and the $H_\mathcal{S}$ is now of the form

$$H_\mathcal{S} = H_\mathcal{S}(u(t)). \tag{6.11}$$

Deriving an equation of motion for the reduced density matrix is, in general, hard without making any further approximations, specially if $u(t)$ is a generic control function of time [68]. One of two approaches can be followed: on one hand, we can model the effects of the environment phenomenologically by using Lindblad equations (6.9), in which case such effects will be independent of the way we drive the system by construction [156]. Or we can propose a microscopical model for the environment and its coupling to the system and work out an equation for $\rho(t)$. This approach generally relies on the Born and Markov approximations, which consider that the coupling between system and environment is weak, and also that correlations in the environmental degrees of freedom have a characteristic duration which is much shorter than the timescale in which the system state

changes appreciably. This is usually the case for large, unstructured at high temperatures. These considerations (in some cases in addition to the rotating wave approximation) allows us to derive a master equation of Lindblad form for various types of systems and environments [62].

In these cases, having an equation of motion to simulate the dynamics of the open system allows for properly formulating and solving optimal control problems. Note that the Krotov scheme discussed in Chap. 4 can be applied to Markovian evolutions in a straightforward way, since it is derived for general dynamical systems. However, it is key to note that the dissipation and decoherence generated by the interaction between system and environment are set by the structure of the Lindblandian (6.10). It is also worth pointing out that the problem of determining whether a system is controllable or not (in the sense discussed in Chap. 2) is much more complicated in open quantum system dynamics [66], and up to now it has only been addressed for specific cases [160, 161, 162]. With these considerations in mind, the most likely scenario is that control fields affecting solely the unitary terms of Lindblad equations may not suffice to perform arbitrary control over the reduced dynamics of the system.

For Markovian dynamics, then, it is generally considered that there are two basic scenarios which encompass control problems; those where the environmental effects are detrimental to the objective, and those in which it is favorable to the objective [66]. In the first case, in which for example we may consider driving the system between pure states or generating unitary gates, the usual approach consists in combining the usual unitary control protocol and one of the following

- driving the system to the target as fast as possible, so as to minimize decoherence and dissipation effects. This brings about the question about what is the minimum time required to perform a certain process and the quantum speed limit, which we have discussed extensively in this Thesis. Note that this scenario for control in open systems was studied in Chap. 3.
- if possible, shielding the system from environmental effects by operating in a subset of its Hilbert space commonly known as decoherence-free subspace [163]. This subspace is composed by states which are invariant under the system-bath Hamiltonian. A famous example is given by the problem of two interacting qubits which can be combined to yield one decoherence-free two-level effective system [164].

- introducing and additional driving field which effectively reduces the magnitude of the coupling between system and environment, in an scheme commonly known as dynamical decoupling [165, 166]. In general, this implies appliying high-frequency pulses on the system that prevent it from interact with the environment. We will come back to this phenomenon when analyzing a particular model in the next section.

In all of these cases, the use of optimization techniques can improve the performance of the control [66, 167, 168].

On the other hand, there may be cases where the environment may have a "good" or even vital effect on controlling a system. This is the case, for example, when we want to drive a mixed state to a pure state, since purity is invariant under unitary evolution. A famous example of a control process where this happens is laser cooling [68, 169]. A more general approach to this subject was layed out by Cirac and Verstraete [67], which showed that robust state preparation of strongly correlated states can be performed via coupling of subsystems to dissipative environments, whose dynamics are described by Lindblad equations. This can be easily seen if we consider that eqn. (6.9) admit the existence of an steady state, i.e. $\dot{\rho}(\rho_0) = \mathcal{L}\rho_0 = 0$ to which the system relaxes asymptotically irrespective of its initial configuration [170]. Although the asymptotic state may sometimes be thermal or even of maximum entropy, careful engineering of the environment via its Lindblad operators $\{L_k\}$ can steer the system to any desired configuration. Of course, this scheme requires control over the environment itself (which, in a way, contradicts the very definition of environment) and although it seems to be too difficult to perform in condensed matter experiments, it has been demonstrated in quantum optics.

6.1.2 Non-Markovian quantum maps

Non-Markovian dynamical maps encompass all cases where the semigroup property (6.7) is not fulfilled [156] and thus describe a more general kind of open quantum system evolutions. Numerous interesting effects signature the onset of non-Markovianity (NM) such as backflow of coherence from the environment back to the system, non-steady asymptotic states and correlation revivals [65, 66]. Unfortunately, there is currently no unified mathematical framework to study these type of evolutions. Different approaches have been studied, such as stocastic Schrödinger equations, time-local master equations and path-integral methods

[65]. We will later on describe a particular method usually referred to as hierarchy equations of motion [171].

Over the past decade, numerous works have studied the role of NM in a variety of scenarios in open quantum system evolution, and there is currently a debate about whether NM is a useful resource for quantum technologies such as computing, simulation and communication [66, 172]. For instance, the task of generating steady entangled states in open quantum systems has been showed to rely upon non-Markovian effects in some cases [173], but not in others [174], where NM does act as catalyst to speed up the process. Also, the problem of the maximum speed of evolution for open quantum systems or quantum speed limit [83], has also been linked with NM. In particular, it was argued that non-Markovian effects could actually speed up the system evolution and thus reduce the QSL time [82, 175]. A recent work on the subject revealed that non-Markovian effects could not be inferred from the QSL bounds [87].

Regarding quantum control, studies which assessed the effectiveness of optimal control methods in open quantum system evolutions showed that NM allowed for an improved controllability [68, 176, 177]. However, non-Markovian effects were also related to reduction of efficiency in dynamical decoupling schemes [178]. Besides investigations on particular systems, there has been no rigorous studies about controllability in non-Markovian evolutions, and currently there is very limited knowledge about which features of NM can be exploited for control [25, 66].

Whether NM is a valuable resource or an unwanted effect, it is important to be able to quantify non-Markovian effects in an open quantum system evolution. This allows to study quantitatively the relation between NM and other physical quantities involved in any dynamical process. Given that there are many aspects which characterize non-Markovian dynamics, during the last few years there have been a large number of proposals of NM measures, a complete review of which can be found in [179]. The two most popular approaches for measuring NM were proposed by (i) Rivas, Huelga and Plenio (RHP) [180], who proposed to measure the amount of non-divisibility of a dynamical map, and (ii) Breuer, Laine and Piilo (BLP), who propose to quantify revivals of distinguishability between quantum states during the dynamics [181, 64]. Here we explore in more detail the latter. For that we define the trace distance between states ρ_1 and ρ_2 as

$$D(\rho_1, \rho_2) = \frac{1}{2}||\rho_1 - \rho_2||, \text{ with } \|A\| = \mathrm{tr}(\sqrt{A^\dagger A}) \tag{6.12}$$

This quantity fulfills the requirements of a distance measure (i.e. the ones already mentioned in Sect. 2.2.2) and has important additional properties:

1. $0 \leq D(\rho_1, \rho_2) \leq 1$
2. Unitary transformations leave D invariant: $D(U\rho_1 U^\dagger, U\rho_2 U^\dagger) = D(\rho_1, \rho_2)$
3. CPTP maps contract D: $D(\Phi\rho_1, \Phi\rho_2) \leq D(\rho_1, \rho_2)$

If we look at the last property as a function of time we can write

$$D(\rho_1(t), \rho_2(t)) \leq D(\rho_1(0), \rho_2(0)) \tag{6.13}$$

where $\rho(t) = \Phi(t, 0)\rho(0)$. It is important to point out that relation (6.13) does not exclude the existence of time intervals during which $D(\rho_1(t), \rho_2(t))$ increases (although it can never exceed its initial value).

Note that the first property stated above also entails that that $D(\rho_1, \rho_2) = 0$ if and only if $\rho_1 = \rho_2$ and $D(\rho_1, \rho_2) = 1$ if ρ_1 and ρ_2 are orthogonal; thus D quantifies how different the states are, as expected from a distance measure. Moreover, it can formally interpreted as the distinguishability between such states in the sense of being a measure of the bias in favor of the correct identification of states ρ_1 and ρ_2 [181].

The BLP criterion states that a map $\Phi_t \equiv \Phi(t, 0)$ is non-Markovian if there exists at least a pair of initial states $\rho_1(0)$, $\rho_2(0)$ such that

$$\sigma(\rho_1(0), \rho_2(0), t) = \frac{d}{dt} D(\rho_1(t), \rho_2(t)) > 0 \tag{6.14}$$

for some time interval. Note that $\sigma > 0$ implies that the states $\rho_1(t)$ and $\rho_2(t)$ are moving away from each other in state space, thus becoming momentarily more distinguishable. This means that information about the initial state of the system, which had been partly lost at the beginning of the evolution due to the inequality (6.13), is re-gained: information has flowed from the environment back to the system. In Markovian dynamics, the opposite occurs: since $\sigma \leq 0$ for all times, information is continuously lost to the environment, and the map ultimately bears no memory of the initial state of the system.
The BLP criterion can also be naturally extended to define a measure of the degree of NM in a quantum process. The original proposal aims at quantifying the total amount of information backflow during the evolution of the system, and its calculated via

$$\mathcal{N}_{BLP} = \max_{\{\rho_1(0), \rho_2(0)\}} \int_{\sigma>0} \sigma(\rho_1(0), \rho_2(0), t')dt'. \tag{6.15}$$

We can see that computing $\mathcal{N}_{BLP}$ implies an optimization all possible pairs of initial states. Wissmann *et al.* showed that the pair of states that maximizes (6.15) should be orthogonal and thus $D(\rho_1(0), \rho_2(0)) = 1$, and also that for a two level system, those states are pure [182].

This proposal for a NM measure possesses a number of inconvenient properties, which have been pointed out and thoroughly studied by Pineda and coworkers in [183]. The main issue is that it overestimates the weight of fluctuations in $D(\rho_1(t), \rho_2(t))$. Note that fluctuations may arise from finite-sized environments, but also from temporal driving and the contribution of counter-rotating terms in the Hamiltonian [184], as we shall see later on. This issue be readily seen from the integral expression in (6.15), which will continuously increase for a fluctuating function as the evolution time increases. As a result, for a given quantum channel $\mathcal{N}_{BLP}$ may easily diverge for increasing evolution time. In [183], the authors propose another method to quantify non-Markovian effects. Applied to the BLP criterion of distinguishability, this new measure is calculated as the largest revival of $D(\rho_1(t), \rho_2(t))$ with respect to its minimum value prior to the revival, i.e.

$$\mathcal{N}_{LR} = \max_{tf, t \leq tf} \left[D(\rho_1(t_f), \rho_2(t_f)) - D(\rho_1(t), \rho_2(t)) \right] \tag{6.16}$$

This quantity clearly avoids the aforementioned pitfalls of the BLP measure. For instance, it is insensitive to fluctuations by construction: once the largest revival has been taken into account, all subsequent features of the evolution do not affect $\mathcal{N}_{LR}$ (unless, of course, a larger revival appears). Also, quantum channels with different evolution times can be compared on firm grounds via the evaluation $\mathcal{N}_{LR}$, and it is guaranteed that the measures will not diverge. Note, as well, that witnessing of non-Markovianity is equivalent in both cases, since naturally $\mathcal{N}_{BLP} = 0$ if and only if $\mathcal{N}_{LR} = 0$. Finally, the physical interpretation is clearer in this case. Take for example two quantum channels A and B, where $\mathcal{N}^A_{LR} > \mathcal{N}^B_{LR}$. This means that channel A shows the biggest revival of distinguishability, and so it shows a higher capacity to reverse the flow of information from the environment back to the system.

6.2 Driven open quantum systems: an exactly solvable model

Up to now in this Chapter we have given an overview about the main features of the theory of open quantum systems and mentioned some relevant results regarding quantum control of Markovian dynamics. We also discussed how to quantify the degree of non-Markovianity of a dynamical map, and from now on we will focus on investigating the relation between control of quantum systems and the degree of NM. Given the lack of a general Lindblad-like formalism for non-Markovian maps, we will concentrate on an exactly solvable model, i.e. a model for which we can derive the equations of motion without resorting to neither the Markov nor Born approximation, consequently describing the (generally non-Markovian) dynamics of the system.

Let us consider a two-level quantum system interacting with a set of N harmonic oscillators. The total Hamiltonian which describes the dynamics is of the form (6.2), i.e.

$$H = H_S + H_E + H_{int} \tag{6.17}$$

where

$$H_S = \omega_0(t)\sigma_+\sigma_- \tag{6.18}$$

$$H_E = \sum_{k=1}^{N} \omega_k b_k b_k^\dagger \tag{6.19}$$

$$H_{int} = \sigma_x \sum_{k=1}^{N} g_k (b_k + b_k^\dagger) \tag{6.20}$$

where $\sigma_\pm = \frac{1}{2}(\sigma_x \pm i\sigma_y)$ and σ_α with $\alpha = x, y, z$ are Pauli matrices, b_k and $b_k^\dagger$ are the usual annihilation and creation operators corresponding to the kth mode of the bath, g_k are the coupling constants and $\omega_0(t)$ is the time dependent energy difference between states $|1\rangle$ and $|0\rangle$ of the two-level system [2], which we will assume to be of the form

$$\omega_0(t) = \Omega_0 + \Delta(t). \tag{6.21}$$

For now we consider $\Delta(t)$ to be an arbitrary driving field, and proceed to derive an equation for the reduced dynamics of the two-level system. To do this, we go to the interaction representation with respect to H_S and H_E by means of an unitary

[2] Note that here we take $\sigma_+ |0\rangle = |1\rangle$ and $\sigma_- |1\rangle = |0\rangle$, such that $\sigma_+\sigma_- = |1\rangle\langle 1|$

transformation U_0 and obtain the transformed interaction Hamiltonian (6.20)

$$\tilde{H}_{int}(t) = U_0^\dagger H U_0 \text{ with } U_0 = \exp\left(-i\int_0^t H_S(t')dt'\right) \otimes \exp\left(-iH_E t\right), \tag{6.22}$$

which gives

$$\tilde{H}_{int}(t) = \tilde{\sigma}_+(t)B(t) + \tilde{\sigma}_-(t)B^\dagger(t) + \tilde{\sigma}_+(t)B^\dagger(t) + \tilde{\sigma}_-(t)B(t) \tag{6.23}$$

where he have defined

$$\tilde{\sigma}_\pm(t) = \sigma_\pm \mathrm{e}^{\pm i\epsilon(t)} \text{ and } B(t) = \sum_k g_k b_k \mathrm{e}^{-i\omega_k t} \tag{6.24}$$

and

$$\epsilon(t) = \int_0^t \omega_0(t')dt'. \tag{6.25}$$

Note that the last two terms of (6.24) are proportional to $\mathrm{e}^{i(\epsilon(t)+\omega_k t)}$ and $\mathrm{e}^{-i(\epsilon(t)+\omega_k t)}$ respectively. We now perform the rotating wave approximation (RWA) and discard those terms from the interaction Hamiltonian. The idea is that these counter rotating contributions oscillate at a frequency $\sim \omega_k + \Omega_0$ plus a correction given by the time-dependent field, and thus average out quickly with respect to the first two terms which have frequency $\sim \omega_k - \Omega_0$. This makes sense if the time-dependent correction is small with respect to Ω_0. Nevertheless, we will later on relax this approximation and derive a set of equations for the reduced dynamics of the system taking account the counter rotating terms.

After performing the RWA, the interaction Hamiltonian yields

$$\tilde{H}_{int}(t) = \tilde{\sigma}_+(t)B(t) + \tilde{\sigma}_-(t)B^\dagger(t)., \tag{6.26}$$

and the full system-environment state in the interaction picture $|\Psi\rangle$ obeys

$$\frac{d}{dt}|\Psi(t)\rangle = -i\tilde{H}_{int}(t)|\Psi(t)\rangle. \tag{6.27}$$

Note that $\tilde{H}_{int}$ commutes with $\hat{N} = \sigma_+\sigma_- + \sum_k b_k^\dagger b_k$, which can be viewed as an extended number operator. This means that the total number of excitations is preserved, and if we take the environment to be initially in vacuum $|0\rangle_E$, i.e. a state with no excitations in the bath, then the dynamics of the total system will take place in the subspace spanned by

$$|\psi_0\rangle = |0\rangle_S \otimes |0\rangle_E \tag{6.28}$$

$$|\psi_1\rangle = |1\rangle_S \otimes |0\rangle_E \tag{6.29}$$

$$|\phi_k\rangle = |0\rangle_S \otimes |k\rangle_E = |0\rangle_S \otimes \left(b_k^\dagger |0\rangle_E\right) \tag{6.30}$$

In this way we can write down an expression for $|\Psi(t)\rangle$

$$|\Psi(t)\rangle = c_0(t)|\psi_0\rangle + c_1(t)|\psi_1\rangle + \sum_k d_k(t)|\phi_k\rangle \tag{6.31}$$

We can now combine eqns. (6.24), (6.26), (6.27) and (6.31) straightforwardly to obtain a set of equations for the time-dependent coefficients in (6.31). First of all we get $\dot{c_0}(t) = 0$, which is obvious for number-preserving dynamics. We then obtain

$$\dot{c_1}(t) = -i \sum_k g_k \mathrm{e}^{i(\epsilon(t)-\omega_k t)} d_k(t) \tag{6.32}$$

$$\dot{d_k}(t) = -i g_k^* \mathrm{e}^{-i(\epsilon(t)-\omega_k t)} c_1(t) \tag{6.33}$$

We can integrate (6.33) using $d_k(0) = 0$ (due to our choice of initial state) and then replace $d_k(t)$ in (6.32) to obtain

$$\dot{c_1}(t) = -\int_0^t dt' \sum_k |g_k|^2 \mathrm{e}^{i[\epsilon(t)-\epsilon(t')-\omega_k(t-t')]} c_1(t') \tag{6.34}$$

$$= -\int_0^t dt' F(t,t') \mathrm{e}^{i[\epsilon(t)-\epsilon(t')]} c_1(t') \tag{6.35}$$

For simplicity we now assume the environment to be composed of a continuum of modes, replace the sum with an integral and introduce the spectral density $J(\omega)$, such that the correlation function $F(t,t')$ of the environment takes the form

$$F(t,t') = \int_0^\infty d\omega J(\omega) \mathrm{e}^{-i\omega(t-t')} \tag{6.36}$$

The correlation function condenses all the information of the environment relevant to the evolution of the reduced density matrix of the two-level system, $\tilde{\rho}(t)$. We can see this by writing the full density matrix in the interaction picture and tracing out the environmental degrees of freedom

$$\tilde{\rho}(t) = \mathrm{tr}_E \left(|\Psi(t)\rangle\langle\Psi(t)| \right) \tag{6.37}$$

$$= |0\rangle\langle 0| \left(|c_0|^2 + \sum_k |d_k(t)|^2 \right) + |0\rangle\langle 1| c_0^* c_1(t) + \tag{6.38}$$

$$+ |1\rangle\langle 0| c_0 c_1^*(t) + |1\rangle\langle 1| |c_1(t)|^2 \tag{6.39}$$

Going back to the Schrödinger picture we then obtain, in the $\{|1\rangle, |0\rangle\}$ basis

$$\rho(t) = \begin{pmatrix} \rho_{11}(0)|G(t)|^2 & \rho_{10}(0) G(t) \mathrm{e}^{-i\epsilon(t)} \\ \rho_{10}^*(0) G^*(t) \mathrm{e}^{i\epsilon(t)} & 1 - \rho_{11}(0)|G(t)|^2 \end{pmatrix}, \tag{6.40}$$

where $c_1(t) = c_1(0)G(t)$ and so $G(0) = 1$. Note also that eqn. (6.32) implies $\dot{G}(0) = 0$.

From now on we will consider the spectral density $J(\omega)$ to be of Lorentzian form, i.e.

$$J(\omega) = \frac{\gamma_0}{2\pi} \frac{\lambda^2}{(\omega - \Omega_0)^2 + \lambda^2}, \tag{6.41}$$

where Ω_0 is a characteristic frequency, λ determines the broadening of the spectral

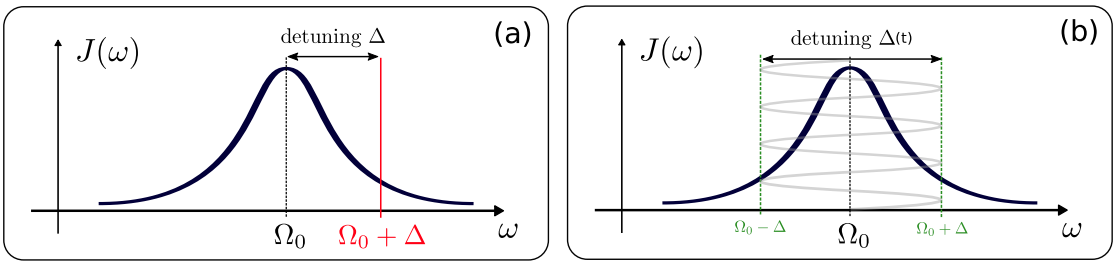

FIGURE 6.1: Plots of the Lorentzian spectral density of eqn. (6.41). (a) In the static case, the characteristic frequency of the two-level system is detuned Δ from the central frequency of the environment Ω_0. (b) In the driven case, the detuning changes between $-\Delta$ and Δ with sinusoidal time dependance and frequency ω_D.

peak, and γ_0 sets the coupling strength between the system and the bath. A plot of $J(\omega)$ is shown in Fig. 6.1. A known example of a physical system which is accurately described by this model is that of an atom coupled to an imperfect cavity [63]. We point out that, by considering this model, we are studying an structured environment which is usually the scenario where non-Markovian effects are more prone to manifest themselves [65]. By inserting expression (6.41) in (6.36) we can evaluate the correlation function which yields, when $\Omega_0 \gg \lambda$,

$$F(t,t') = \frac{\gamma_0 \lambda}{2} \mathrm{e}^{-(\lambda + i\Omega_0)(t-t')}. \tag{6.42}$$

Following a procedure already put forward in the literature [185] for this model, the equation for $G(t)$ can be casted in a time-local form due to the exponential dependence of $F(t-t')$. We show the derivation in Appendix D.1. By defining dimensionless variables and parameters $\lambda t \equiv \tau$ and $x/\lambda \to x$, where x is any parameter with units of energy (Ω_0 or γ_0 for instance), the resulting dynamical equation for $G(t)$ is

$$G''(\tau) + [1 - i\Delta(t)]\, G'(\tau) + \frac{\gamma_0}{2} G(\tau) = 0, \tag{6.43}$$

where we established the notation $f'(\tau) \equiv \frac{df}{d\tau}$. Equation (6.43) is the exact equation of motion for the reduced dynamics of the driven two-level system coupled to a Lorentzian bath at zero temperature, under the RWA. Note that the equation also holds when $\Delta(t)$ is constant, that is, when the system Hamiltonian is time-independent, and an exact solution for $G(t)$ is available [63, 183, 87]. In that case, Δ plays the role of a static detuning between the system and the central frequency of the environment. We will use this eqn. (6.43) extensively in the remainder of this Chapter to investigate the interplay between non-Markovianity and driving in this system.

Since the complex-valued function $G(t)$ determines the complete dynamics of the system, we can also express the non-Markovianity measures $\mathcal{N}$ of eqns. (6.15) and (6.16) in terms of that function rather easily. In order to do that, we need to compute the distance between two states $\rho^A(t)$ and $\rho_B(t)$,

$$\rho^A(t) - \rho^B(t) = \begin{pmatrix} a|G(t)|^2 & b\,G(t)\mathrm{e}^{-i\epsilon(t)} \\ b^*\,G^*(t)\mathrm{e}^{i\epsilon(t)} & -a|G(t)|^2 \end{pmatrix}, \tag{6.44}$$

where $a \equiv \rho^A_{11}(0) - \rho^B_{11}(0)$ and $b \equiv \rho^A_{10}(0) - \rho^B_{10}(0)$. We can now use expression (6.12) to obtain

$$D(\rho^A(t), \rho^B(t)) = |G(t)|\sqrt{|G(t)|^2 a^2 + |b|^2} \tag{6.45}$$

Taking the time derivative gives

$$\sigma(\rho^A, \rho^B, t) = \frac{2|G(t)|^2 a^2 + |b|^2}{\sqrt{|G(t)|^2 a^2 + |b|^2}} \frac{d}{dt}|G(t)| \tag{6.46}$$

Recall from eqn. (6.15) that we need to obtain the maximum of over all pairs of initial states. As mentioned in [186] this happens for $a = 0$ and $|b| = 1$, which correspond for example to initial conditions taken to be the eigenstates of σ_x, $|+\rangle$ and $|-\rangle$. Also interesting is a result shown by Zeng *et al.* that the BLP and RHP measures are equivalent for this system [187].

Before we move on to study the interplay between driving, control and non-Markovianity, we finally point out that it is possible to find an approximate solution for the reduced density matrix $\rho(t)$ without using the rotating wave approximation. We will do this by employing the hierarchy equations of motion method developed by Tanimura et al. [171] and then successfully applied to a variety of interesting problems [188, 86, 189, 190, 191]. This method can be used if (i) the initial state of the system plus bath is separable, (ii) the interaction Hamiltonian is bilinear (i.e. $H_{SE} = X_S \otimes Y_E$), and (iii) if the environmental correlation function can be casted in multi-exponential form. All of these requirements are met in our system, see equations (6.17) and (6.42). We give some details about this method in Appendix D.2. The interest to compare both methods reside on previous studies which show that including counter-rotating terms in the interaction Hamiltonian can affect significantly the value of NM measures [184, 86].

6.3 Non-Markovian effects in periodically driven systems

As already mentioned, the ultimate goal of this Chapter is to study the interplay between non-Markovianity and control in open quantum systems. However, a more general unanswered question arises first: how does the presence of a driving field affect the non-Markovian features of open quantum system dynamics? Addressing this issue is of paramount importance given that non-Markovianity could in some cases be used as a resource for different tasks in quantum information, as already mentioned. Control is needed to harness resources appropriately, so its natural to understand how driving affects NM. We will address this problem in this Section. For that, we will study numerically the dynamics of the reduced two-level system discussed in the previous section.

We begin by proposing a particular choice of driving field, namely

$$\omega_0(\tau) = \Omega_0 + \Delta\cos\left(\omega_D\tau\right). \tag{6.47}$$

Here Δ and ω_D are driving amplitude and frequency, respectively. Recall that we have derived the exact equation of motion under the RWA (6.43) for the function $G(t)$ which completely describes the dynamics, and also we can obtain the reduced density matrix beyond the RWA with the hierarchy equations method of D.2.

First of all, let us consider the static case, i.e. when the driving frequency is set to $\omega_D = 0$, such that Δ represents the static detuning between system and environment, as depicted in Fig. 6.1 (a). Under the RWA, this model admits an exact solution of the equation of motion (6.43) [87, 64]. The behaviour of the NM measure $\mathcal{N}_{BLP}$ has been extensively studied in the literature [179, 181], and it has also been compared with the largest revival measure $\mathcal{N}_{LR}$ [183]. In Fig. 6.2 (a) and (b) we plot both quantities as a function of the dimensionless coupling strength γ_0 and static detuning Δ. In both cases, the NM increases with γ_0 and in general decreases with Δ for fixed γ_0 (except at weak coupling).

An important result arises when comparing the NM measures calculated beyond the RWA. In Fig. 6.2 (c) and (d) we plot $\mathcal{N}_{BLP}$ and $\mathcal{N}_{LR}$ calculated using the hierarchy equation method mentioned in the previous section, which takes into account the effects of the counter-rotating terms in the interaction Hamiltonian. There, it can be seen that the largest revival measure $\mathcal{N}_{LR}$ shows a very similar behavior compared to the RWA case, while the BLP measure $\mathcal{N}_{BLP}$ not only takes

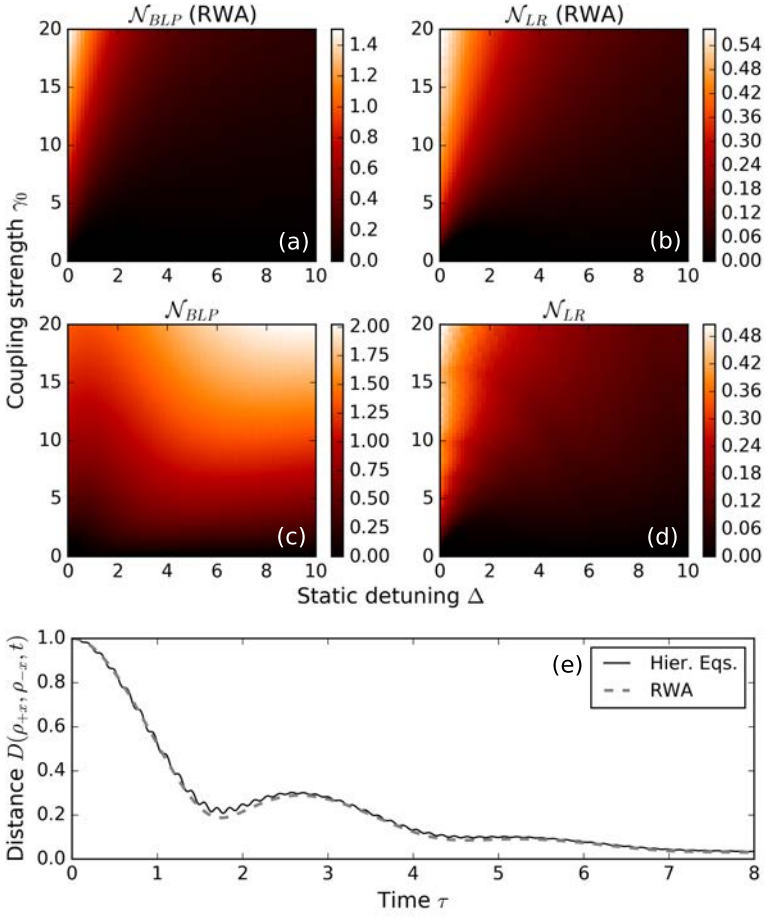

FIGURE 6.2: (a)-(b) Density plots for the non-Markovianity measures $\mathcal{N}_{BLP}$ and $\mathcal{N}_{LR}$ as a function of the dimensionless coupling parameter γ_0 and detuning Δ for the static case ($\omega_D = 0$). Results were obtained under using the equation of motion (6.43), i.e. using the RWA. (c)-(d) Same as (a) and (b), but results obtained using the hierarchy equation method (beyond RWA). Dimensionless parameter values: $\Omega_0 = 20$. (e) An example of the distance between the states evolved from initial conditions ρ_{+x} and ρ_{-x} calculated with and without the RWA.

larger values (as already noted in [184]) but also displays a completely different dependence with the system parameters. Note that, by setting $\Omega_0 >> 1$, we are working in a regime where the RWA and non-RWA evolutions are very similar, apart from fluctuations, as can be seen in Fig. 6.2 (e). This results shows us that the largest revival measure is much more reliable than the BLP measure, which leads to an incorrect quantification of non-Markovian effects in the presence of fluctuations. This robustness is a desired characteristic for a NM quantifier, specially when we consider the system to be driven by a time-dependent field, as we shall do next.

We now turn our attention to the time-dependent case, by tuning the driving frequency ω_D to non-zero values. In order to assess quantitatively how the non-Markovian character of the evolution is affected by the driving, we define a figure of merit called "relative NM value" as

$$\mathcal{N}_x^{rel}(\gamma_0, \Delta, \omega_D) = \frac{\mathcal{N}_x(\gamma_0, \Delta, \omega_D)}{\max_{\Delta'} \mathcal{N}_x(\gamma_0, \Delta', 0)}, \tag{6.48}$$

where x = BLP or LR. This quantity measures the obtained NM value for the driven case in units of the maximum possible degree of NM achieved in the system with no driving ($\omega_D = 0$), at a fixed value of the coupling parameter γ_0. As such, it allows us to assess how the NM is affected by the periodic driving itself and not by, for example, introducing new interactions or injecting energy in the system Hamiltonian (which has been studied, for example, in Refs. [178, 192]). This is because the driven system can be interpreted as the static Hamiltonian

$$H_s = (\Omega_0 + \Delta)\sigma_+\sigma_-, \tag{6.49}$$

but with a time-dependent detuning $\Delta \to \Delta \cos(\omega_D \tau)$, as depicted in Fig. 6.1 (b). In other words, by studying $\mathcal{N}_x^{rel}$ we are analyzing the effects of dynamically changing the detuning in time, and not merely by increasing or diminishing its value.

First of all we wish to asses to what extent the external driving, which acts only on the two-level system, can enhance the non-Markovian character of the evolution. To do this, we compute the maximum of $\mathcal{N}_x^{rel}$ over all values of the driving frequency and amplitude

$$M_x(\gamma_0) = \max_{\Delta,\, \omega_D} \mathcal{N}_x^{rel}(\gamma_0, \Delta, \omega_D), \tag{6.50}$$

where x = BLP or LR. M_x indicates the maximum relative NM value, and so quantifies how much bigger can the NM measure be in the driven case when compared to the static case. Of course, $M_x \geq 1$ since, even in the worst case, the driven case will be equal to the static case for $\omega_D = 0$.

In Fig. 6.3 (a) we show a plot of M_{LR} as a function of the coupling strength γ_0, calculated both with and without the RWA. As was observed in the static regime, the LR measure presents a similar behaviour in both cases. In particular, it can be seen that M_{LR} takes values of the order of 10 for small γ_0, and then decays to its minimum possible value of 1 as the coupling increases. Physically, this tells us that the driving is able to increase the non-Markovianity of the evolution well above the value of the static case, but can only do so in the weak coupling regime.

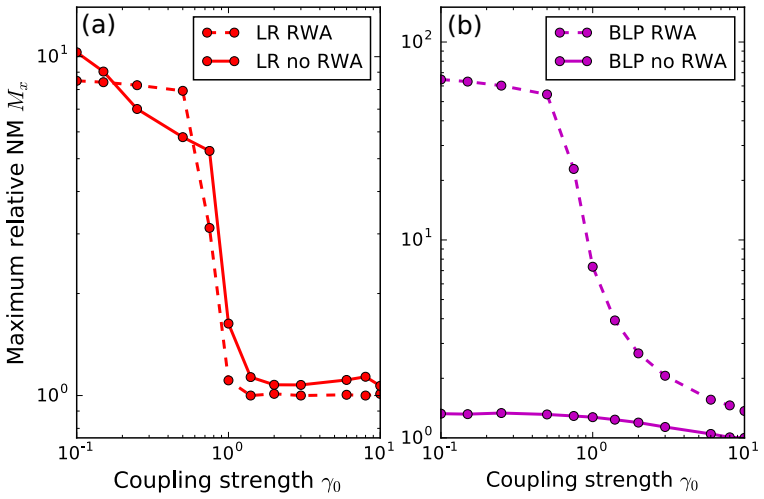

FIGURE 6.3: Maximum relative NM value, as defined in Eq. (6.50), as a function of the coupling parameter γ_0, calculated with (dashed lines) and without (full lines) the rotating wave approximation. Values were obtained for (a) LR measure, (b) BLP measure. Dimensionless parameter values: $\Omega_0 = 20$, Δ, $\omega_D \in [0, 20]$.

For strong coupling, on the other hand, the driving fails to reach values of NM significantly above the static ones. This is the main result of this Section. We stress that the large enhancement of the NM values appear because the revivals of the distinguishability in the static case are small, i.e., when $\gamma_0 \ll 1$ the undriven dynamics is essentially Markovian. Nevertheless, it is surprising that the influence of the driving field is much stronger in the weak-coupling case, which is precisely where non-Markovian effects are usually neglected or discarded by perturbative approaches.

In Fig. 6.3 (b) we show results obtained for M_{BLP}, the maximum NM relative value computed with the BLP measure. There, it can be seen that calculations made using the rotating wave approximation also describe the phenomenon of NM enhancement at weak coupling. However, in the case where the RWA is not applied, $\mathcal{N}_{BLP}$ shows a completely different behaviour, remaining practically constant as the coupling γ_0 varies. These findings are reminiscent of the analysis we performed for the static case. This provides further proof of the reliability of the LR measure as opposed to the BLP measure.

It is interesting to point out that a number of previous works have reported the appearance of non-Markovian effects for small coupling due to driving acting on

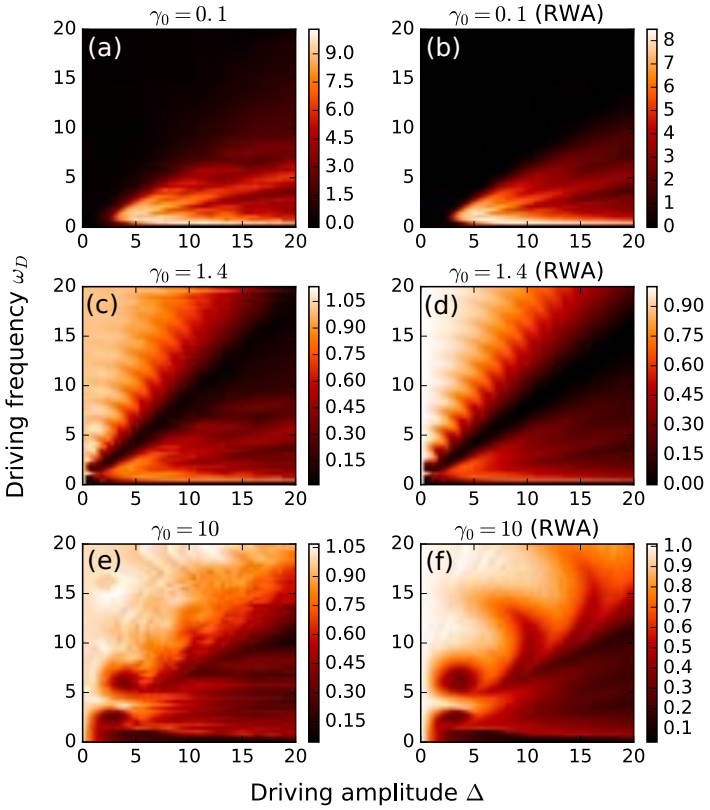

FIGURE 6.4: Density plots for the relative non-Markovianity value $\mathcal{N}_{LR}^{rel}$ computed for the largest revival (LR) measure for different values of the coupling strength γ_0. Results are shown as a function of the dimensionless driving amplitude Δ and frequency ω_D in all cases. (a) and (b) $\gamma_0 = 0.1$. (c) and (d) $\gamma_0 = 1.4$. (e) and (f) $\gamma_0 = 10$. Plots in the right column were obtained under using the equation of motion (6.43), i.e. using the RWA. Plots in the left column were obtained using the hierarchy equation method (beyond RWA). Dimensionless parameter values: $\Omega_0 = 20$.

the system [178, 192, 193, 194]). In those cases, however, the driving was introduced as a new interaction term in the Hamiltonian of the system. Here we show that non-Markovian effects can be generated by just allowing the original system parameters to change in time.

We will now explore in more detail the enhancement of non-Markovian effects induced by the driving field. In Fig. 6.4 we show several density plots of the relative LR measure $\mathcal{N}_{LR}^{rel}$ for different values of the coupling strength, as a function of the driving frequency ω_D and amplitude Δ. From the figure, we can roughly separate the behaviour of the NM values for the regions where $\omega_D/\Delta > 1$ and $\omega_D/\Delta < 1$, which we will refer to as high and low frequency regimes, respectively. In particular, for small coupling (top row in Fig. 6.4), we observe $\mathcal{N}_{LR}^{rel} \simeq 0$ for high frequency

driving, while for $\omega_D/\Delta < 1$ we observe the enhancement of NM discussed earlier. When the system is strongly coupled to the environment (bottom row in Fig. 6.4), the situation is inverted, and the largest values of $\mathcal{N}_{LR}^{rel} \simeq 1$ occur when $\omega_D/\Delta > 1$. For low frequencies, the relative NM is significantly smaller than 1, meaning that the turning on the driving actually causes distinguishability revivals to decrease during the evolution of the system. In the intermediate coupling regimes, we observe a clear transition between both cases. It can also be seen that there is a large region, corresponding to $\omega_D/\Delta \simeq 1$, where NM is suppressed altogether.

We will now look closer to the high frequency case $\omega_D/\Delta > 1$. There, the driving fails to increase the degree of NM with respect to the static case ($\mathcal{N}_{LR}^{rel} \leq 1$), for all coupling strengths. This behaviour can be explained analytically in the following way. First, let us transform the original Hamiltonian (6.17) to a rotating frame via the transformation

$$U_R(t) = \exp\left(-i\left(\int_0^t \Delta\cos(\omega_D s)ds\right)\sigma_+\sigma-\right), \tag{6.51}$$

The complete (system plus bath) state in this frame $|\Psi_R(t)\rangle$ is related to rest frame representation via $|\Psi_R(t)\rangle = U_R(t)\,|\Psi(t)\rangle$. The equation for the evolution of $|\Psi_R(t)\rangle$ can be expressed in the following way

$$\frac{d}{dt}\,|\Psi_R(t)\rangle = i\,H_R(t)\,|\Psi_R(t)\rangle\,, \tag{6.52}$$

where $H_R(t)$ is the transformed Hamiltonian

$$\begin{aligned} H_R(t) &= U_R(t)\,[H(t) - \Delta\cos(\omega_D t)]\,U_R^\dagger(t) && (6.53)\\ &= \Omega_0\sigma_+\sigma_- + \sigma_x^R(t)\sum_k g_k(b_k + b_k^\dagger) + \sum_k \omega_k b_k b_k^\dagger, && (6.54)\end{aligned}$$

where $\sigma_x^R(t) = U_R(t)\sigma_x U_R^\dagger(t)$. By using the following identity

$$\mathrm{e}^{i\gamma\,\sin(\Omega t)} = \sum_{n=-\infty}^{+\infty} J_n(\gamma)\mathrm{e}^{in\Omega t}, \tag{6.55}$$

which we already used in Chap. 3 and in Chap. 4, we can express $\sigma_x^R(t)$ in the following way

$$\sigma_x^R(t) = \cos(\alpha(t))\sigma_x + \sin(\alpha(t))\sigma_y \tag{6.56}$$

where

$$\alpha(t) = \frac{\Delta}{\omega_D}\sin(\omega_D t). \tag{6.57}$$

We can now take the high-frequency limit by assuming that $\omega_D \gg 1$ (recall that all quantities are assumed to be measured in units of λ and thus dimensionless). In such case, we can neglect the fast-oscillating terms in (6.55) and keep only the

constant contribution, such that eqn. (6.56) now takes the form

$$\sigma_x^R(t) \simeq J_0\left(\frac{\Delta}{\omega_D}\right)\sigma_x \equiv \beta\sigma_x, \tag{6.58}$$

and thus the transformed Hamiltonian (6.54) is time-independent to zeroth order in ω_D^{-1}.

It can be easily seen that H_R of eqn. (6.54) has the same form of the original Hamiltonian (6.17) but with no driving, zero detuning and modified coupling constants $g_k \to \beta g_k$. This, in turn, is equivalent to having a modified coupling parameter in the Lorentzian spectral density (6.41)

$$\gamma_0 \to \beta^2\gamma_0 \leq \gamma_0, \tag{6.59}$$

where the inequality arises from the fact that $0 \leq J_0(x) \leq 1$.

In short, when the driving frequency is high (compared to λ), the driven system dynamics is equivalent (up to a unitary transformation) to that of a static system which couples less strongly to the environment. As we showed in Fig. 6.2, the degree of NM in that case increased monotonically with γ_0. Note also that, since the trace distance (6.12) is invariant under unitary transformations, the degree of NM is independent of $U_R(t)$. As a result, the high frequency driving fails to increase the NM measures above the static case, thus proving our numerical finding. We point that that, interestingly, this result is a manifestation of a phenomenon already mentioned in this Chapter: dynamical decoupling [195]. From expression (6.59) it can be seen that by properly choosing the driving parameters we can set the effective coupling between system and environment to zero (to zeroth order in ω_D^{-1}), thus significantly slowing down the relaxation of the system.

We now return to the results in Fig. 6.4. For the weak coupling case we observe the largest values of NM in the low frequency regime, see Fig. 6.4 (a) and (b). We show a detailed plot of the NM relative value for this region in Fig. 6.5. There, it can be seen that maxima for $\mathcal{N}_{LR}^{rel}$ spread along straight lines in the (Δ, ω_D) plane. Interestingly, this lines coincide with the appearance of zeros of $J_0\left(\frac{\Delta}{\omega_D}\right)$ and $J_1\left(\frac{\Delta}{\omega_D}\right)$. In fact, this behavior can be explained from the analytical solution for $G(\tau)$ which can be obtained under the RWA to first order in the dimensionless coupling parameter γ_0, which we show in Appendix D.3. It is interesting to point out that parameter regions determined by the Bessel functions are typical in periodically driven quantum systems [118], as we have already discussed in Chapter 3.

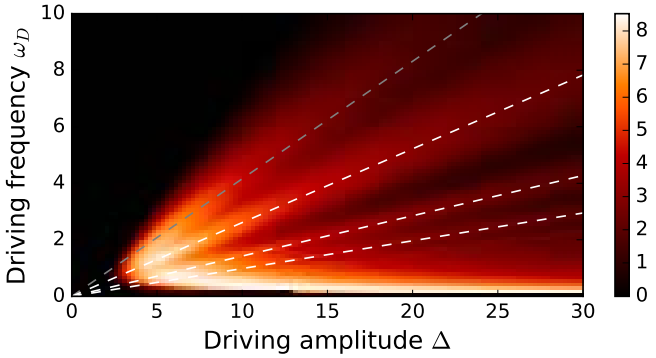

FIGURE 6.5: Density plot for the relative non-Markovianity value $\mathcal{N}_{LR}^{rel}$ computed for the largest revival (LR) measure. Parameters as in Fig. 6.4 (b). Dashed lines represents the values of ω_D/Δ for which $J_0\left(\frac{\Delta}{\omega_D}\right) = 0$ (gray) and $J_1\left(\frac{\Delta}{\omega_D}\right) = 0$ (white).

6.4 Optimal control and non-Markovianity

In the previous section of this Chapter we investigated how the presence of a time-dependent driving field can affect the degree of non-Markovianity in an open two-level quantum system. There we learned that a generic field could change substantially the non-Markovian features of the dynamical map. Now, we set to study a more specific scenario, where we intend to control the system by using these fields. The questions naturally arise: how does the degree of NM relate to the success of the control protocol? can NM be regarded as a resource for controlling open quantum systems?.

To tackle this problem, we will use optimal control methods, which give us a systematic approach to finding successful control fields as already described many times in this Thesis. For convenience, we will restrict ourselves to controlling the dynamics of the system as described under the RWA, c.f. eqn. (6.43). However, we point out that hierarchy equations as described in Appendix D.2 are also suitable for implementation of optimal control techniques, although this is a path currently unexplored as far as our knowledge is concerned. Note that the RWA equation of motion (6.43) is a second order linear differential equation with non-constant coefficients. This can be easily casted as a linear system of the form (2.49), which we introduced when deriving Krotov's method, so it is easy to adapt that formalism to this problem. We do so explicitly here by defining the vector $\vec{x}(\tau) = (x_1(\tau), x_2(\tau))$

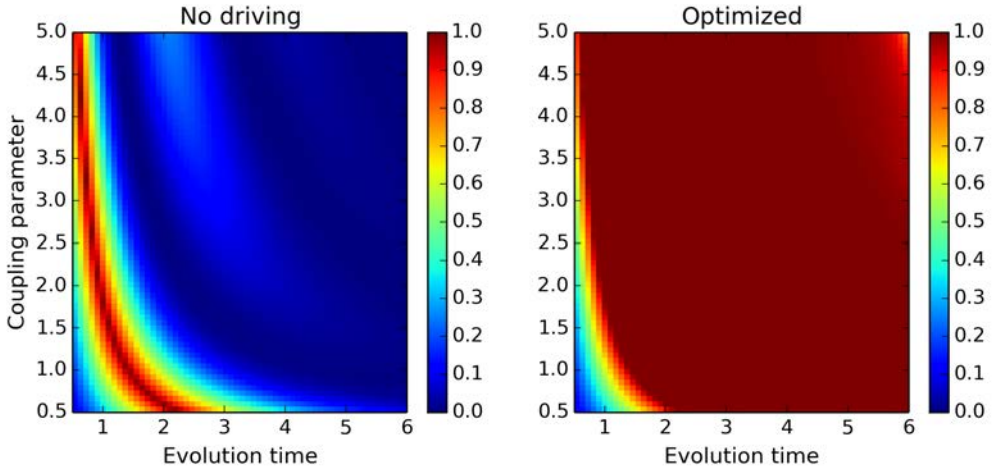

FIGURE 6.6: Density plots of the fidelity of the control process, eqn. (6.73) as a function of the coupling strength γ_0 and evolution time T for undriven dynamics (left) and optimally controlled dynamics (right).

where

$$x_1(\tau) = G(\tau) \tag{6.60}$$

$$x_2(\tau) = G'(\tau), \tag{6.61}$$

such that eqn. (6.43) can be written as the system

$$\begin{cases} \vec{x'}(\tau) = A(\tau)\vec{x}(\tau) \\ \vec{x}(0) = (1,0) \equiv \vec{x}_0 \end{cases} \tag{6.62}$$

where we defined

$$A(\tau) = A_0 + u(\tau)A_c \text{ with } A_0 = \begin{pmatrix} 0 & 1 \\ -\frac{\gamma_0}{2} & -1 \end{pmatrix} \text{ and } A_c = \begin{pmatrix} 0 & 0 \\ 0 & i \end{pmatrix} \tag{6.63}$$

and we changed the notation for the field $u(\tau) \equiv \Delta(\tau)$. We can now proceed to write the Krotov Hamiltonian $h(\tau, \vec{x}, u, \vec{y})$ starting from expression (2.54),

$$h(\tau, \vec{x}, u, \vec{y}) = 2\mathrm{Re}\left(\vec{y}^{\,\dagger} A(\tau)\vec{x}\right) - \lambda f^0(u) \tag{6.64}$$

where $\vec{y}(\tau)$ is the costate of $\vec{x}(\tau)$ (in complete analogy with $|\chi\rangle$ and $|\psi\rangle$ for Schrödinger's equation) and f^0 is as in eqn. (2.61). We then write down the equation of motion for the costate from eqn. (2.55),

$$\begin{cases} \vec{y'}(\tau) = -A^\dagger(\tau)\vec{y}(\tau) \\ \vec{y}(T) = -\frac{\partial \mathcal{J}}{\partial \vec{x}_T} \end{cases} \tag{6.65}$$

The field update rule we obtain is analogous to (2.63),

$$u(t) \to u(t) + \frac{1}{\lambda}\mathrm{Re}\left(\vec{y}^{\,\dagger}(\tau) A_c\, \vec{x}(\tau)\right) \tag{6.66}$$

We now need to define our control objective, which is of the form $\mathcal{J}(\vec{x}(T))$. We will consider the following protocol. For some initial value $\rho_{11}(0)$ of the population

of state $|1\rangle$, we intend to steer the system into a final state at time $\tau = T$ in which population has halved. Looking at $\rho(t)$ in eqn. (6.40), we can see that this is achieved if

$$|G(T)|^2 \equiv g_T = 0.5\,. \tag{6.67}$$

In order to do this, we recall that $G(\tau) \equiv x_1(\tau)$ and propose a functional of the form

$$\mathcal{J}(\vec{x}(T)) = (|x_1(T)|^2 - g_T)^2 \tag{6.68}$$

for which we seek to obtain a minimum. We can rewrite this in a more familiar way for the control theory notation

$$\mathcal{J}(\vec{x}(T)) = \left(\vec{x}^{\,\dagger}(T) P \vec{x}(T) - g_T\right)^2, \text{ where } P = \begin{pmatrix} 1 & 0 \\ 0 & 0 \end{pmatrix}. \tag{6.69}$$

This allows us to write down an explicit boundary condition for the costate equation (6.65)

$$\vec{y}(T) = -\left(\frac{\partial \mathcal{J}}{\partial \vec{x}(T)}\right)_{\vec{x}(T)} \tag{6.70}$$

$$= = -2(|x_1(T)|^2 - g_T) \begin{pmatrix} x_1(T) \\ 0 \end{pmatrix} \tag{6.71}$$

Putting together expressions (6.62), (6.65), (6.66) and (6.71) we have the necessary tools to tackle the optimization problem numerically.

Before we continue, let us point out that this choice of control problem relies on the presence of the environment, since the isolated evolution of the system given by

$$H_S = \omega_0(t)\sigma_+\sigma_- \tag{6.72}$$

would give invariant populations for any choice of the driving field. In this way, we are investigating how to manipulate the way the system relaxes because of the presence of the environment, by using a time-dependent field which couples to the two-level system alone. We point out that we used the same value of target (relative) population (6.67) for all results shown in this section. We have checked that other choices of g_T give similar results.

We proceed as follows. We fix the coupling parameter γ_0 and the final evolution time T and run the optimization algorithm to find the control field required to minimize the functional (6.68), which is equivalent to maximizing the fidelity

$$\mathcal{F} = 1 - 2\mathcal{J}, \text{ with } 0 \leq \mathcal{F} \leq 1 \tag{6.73}$$

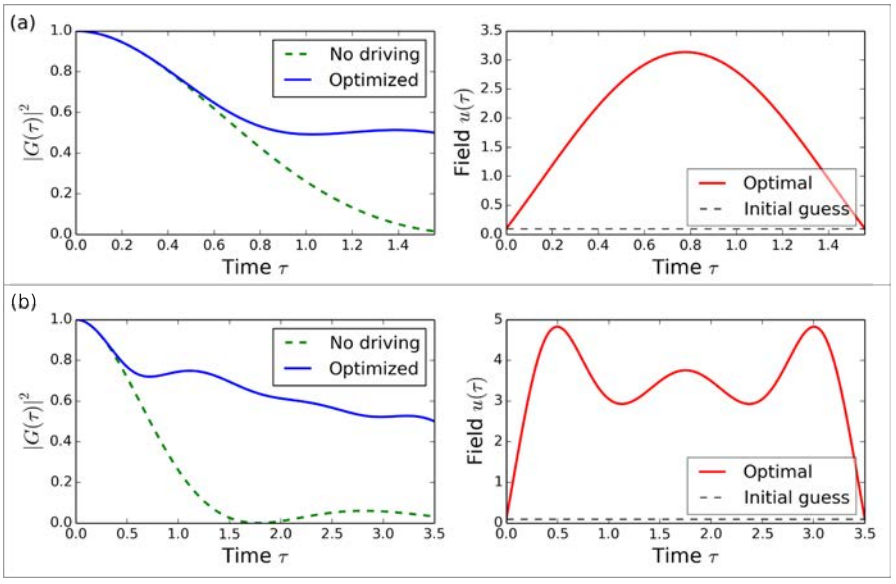

FIGURE 6.7: Evolution of function $|G(\tau)|^2$ which determines the reduced dynamics of the two-level system, for the cases of no driving (dashed line) and optimal driving (full line), together with the control field that generates the optimal evolution. (a) Results for $T = 1.5$ and $\gamma_0 = 3$. (b) Results for $T = 3.5$ and $\gamma_0 = 3$.

No additional constraints are placed to the problem, and the initial guess for the field is chosen to be $u^0(\tau) = 0.1$. We have checked that other choices of initial seed give similar results. In Fig. 6.6 we show density plots of the best achieved fidelity as a function of γ_0 and T. For comparison, we show the same results when we perform no driving, i.e. $u(t) = 0$. It is important to point out the we cannot guarantee that the system is completely controllable, since the tools of dynamical Lie algebras discussed in Chap. 2 do not apply to this case, and general controllability analysis for open quantum system dynamics remains an open subject [66]. Nevertheless we can see from the figure that the we are able to reach the desired target with near perfect fidelity for a vast region of parameter space. One clear exception arises: for small couplings and small evolution times, fidelities are far from ideal, and is arguable that in that case we are trying to control the system below the quantum speed limit time. Note that, although there have been generalizations of the QSL bounds for open systems [83, 84, 82], the connection between these bounds and quantum control has not been studied thoroughly up to now. From our results we can observe that there is a clear minimum evolution time for control which depends on γ_0, but we leave a more thorough study of this for future investigation.

We now turn to the question of whether the non-Markovianity of a dynamical map

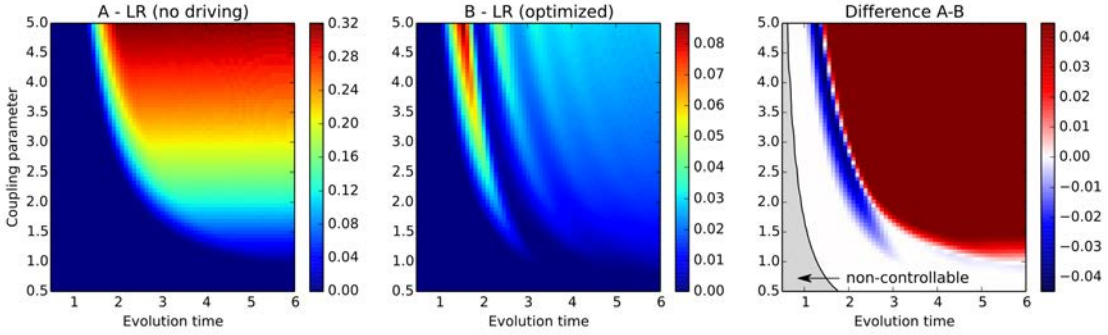

FIGURE 6.8: Non-Markovianity measure for the undriven (A) and controlled (B) evolution for the two-level model discussed in this Chapter. Results were obtained using the largest revival (LR) measure (6.16). Gray area shows a contour plot of the fidelity of the control process as shown in Fig. 6.6, indicating the region of parameter space where the system is not controllable.

can be regarded as a resource for quantum control. To analyze this, we calculated for each optimization run the largest revival measure of NM (6.16) already studied in this Chapter. We point out that we also calculated the BLP measure for all cases, rendering very similar results which are not shown here. We plot the LR measure as a function of the evolution parameters in Fig. 6.8 for the controlled dynamics and again for the undriven case for comparison. By comparing these plots with Fig. 6.6, we can observe that the degree of NM does not present a clear correlation with the success of the control: there is a large region of parameter space where optimization renders a much larger degree of NM as compared to the undriven case, but also there is a regime where the undriven dynamics of the system is Markovian and turns non-Markovian upon optimization of the control. This can be seen directly from the last plot of Fig. 6.8, where we show the sign of the difference between the NM measure in both cases. The red zone indicates parameter values where the control turns the evolution less Markovian, while the opposite happens in the blue zone. The large white region indicates that in both cases the level of NM is very similar, and this includes the (grayed-colored) non-controllable region where $T \lesssim T_{QSL}$.

The results shown here represent a compelling argument against regarding non-Markovianity as a resource for control. The basic reason for this is at the core of our main result from last section: driving fields (used for control or not) can greatly change the values of NM with respect to the static case. From the results in this section, we confirm that the level of NM which the system "possesses" in the static case does not influence the success of the optimization (since good fidelities are found even when the undriven dynamics is Markovian). Moreover, the

controlled dynamics may or may not increase the degree of NM. These results tell us that NM cannot be viewed as something that can be stored and/or expended in order to successfully perform a control process.

It is, however, interesting to note that the control field does actively manipulate the appearance of revivals (irrespectively of their magnitude) to drive the system to the desired target. This can be appreciated from the evolutions in Fig. 6.7 and from the fact that most of the optimized evolutions are non-Markovian, in spite of the very small values shown by of NM measures. This also in agreement with our result from the previous section, which shows that the driving can easily turn on the degree of non-Markovianity, even for small couplings. So we can conjecture that, albeit the *degree* of NM does not play the role of a resource per se, the fact that our model *admits* non-Markovian effects affects controllability of the system significantly. This is in agreement with previous results on the subject: in Ref. [69] Reich *et al.* showed that coupling a multilevel system to a structured environment (which, in turn, generated non-Markovian effects) increased the dimension of the set of possible unitaries that could be generated by optimal control. It would be interesting to study a driven quantum system whose reduced dynamics could be described by a Lindblad-like equation for arbitrary field, and study the degree of controllability displayed there. We leave this matter for future research.

Control en sistemas abiertos y efectos no Markovianos

En este capítulo centramos nuestra atención en el control de la dinámica de sistemas cuánticos abiertos. Aunque ya hemos estudiado algunos problemas de control en sistemas disipativos en el Cap. 2, allí nos enfocamos en cómo acelerar la evolución con el fin de reducir el impacto de los efectos ambientales, que no podían ser manipulados. Aquí tomamos un enfoque más general, y analizamos hasta qué punto podemos controlar los sistemas cuánticos abiertos dependiendo de las características de sus entornos. Después de presentar una visión general sobre los sistemas cuánticos abiertos y el control bajo evoluciones Markovianas, nos enfocamos completamente en mapas cuánticos no-Markovianos, que muestran un terreno más fértil (y también menos explorado) para el control cuántico.

Para sistemas Markovianos se considera generalmente que hay dos escenarios básicos que engloban problemas del control; aquellos en los que los efectos ambientales son perjudiciales para el objetivo, y aquellos en los que son favorables al objetivo. En el primer caso, en el que, por ejemplo, podemos intentar conducir al sistema entre estados puros o generar compuertas unitarias, el enfoque habitual consiste en combinar el protocolo de control unitario usual y otros esquemas adicionales, como desacople dinámico o el estudio de espacios libres de decoherencia. Por otro lado, puede haber casos donde el entorno puede tener un efecto favorable o incluso vital en el control de un sistema. Este es el caso, por ejemplo, cuando queremos llevar un estado inicial mixto a un estado puro, dado que la pureza es invariante bajo la evolución unitaria. Cirac y Verstraete [67] estudiaron un escenario más general, y demostraron que es posible preparar de manera robusta estados fuertemente correlacionados mediante el acoplamiento de subsistemas a entornos disipativos, cuya dinámica está descrita por las ecuaciones de Lindblad. Aunque el estado asintótico a veces puede ser térmico o incluso de entropía máxima, una ingeniería cuidadosa del entorno a través de sus operadores de Lindblad puede conducir el sistema a cualquier configuración deseada. Por

supuesto, este esquema involucra la habilidad de controlar la estructura propia del entorno (lo que, de alguna manera, contradice la definición misma de entorno) y aunque parece demasiado difícil de realizar en experimentos de materia condensada, se ha demostrado en óptica cuántica.

Las evoluciones no Markovianas describen un tipo más general de evoluciones para sistemas abiertos, en donde pueden producirse efectos interesantes como la aparición de estados asintóticos no estacionarios o un flujo de información desde el entorno de vuelta hacia el sistema. Actualmente se debate la utilidad de estos efectos no Markovianos en el contexto de las tecnologías cuánticas, y surge entonces una pregunta natural: ¿cómo se ven modificados estos efectos ante la presencia de un campo externo variable que, por ejemplo, controle el sistema?. En la Sección 6.2 presentamos un modelo simple pero paradigmático para estudiar la evolución de un sistema abierto de dos niveles con la inclusión de driving. Luego, atacamos de lleno el interrogante planteado estudiando cuantitativamente las distintas medidas de no-Markovianidad en un sistema forzado periódicamente. Mostramos un resultado llamativo: la presencia del campo dependiente del tiempo puede cambiar aumentar significativamente el grado de no-Markovianidad de un mapa (con respecto al caso estático), pero solo cuando el acoplamiento entre el sistema y el entorno es débil. En el régimen de acoplamiento fuerte, este efecto se pierde y el efecto del driving pasa a ser el de disminuir la intensidad de dichos efectos.

Finalmente, en la sección 6.4 estudiamos el rol de la no-Markovianidad en problemas de control. Para ello, adaptamos el algoritmo de control óptimo descripto en el Cap. 2 a nuestro problema y lo utilizamos para realiazar distintos protocolos de control. Encontramos que el grado de no-Markovianidad de un mapa no guarda correlación con el éxito de un proceso de control, y que por lo tanto no puede ser visto como un recurso en este contexto. Sin embargo, notamos que la evolución controlada en general se ve beneficiada por la descripción no-Markoviana de la dinámica, la cual permite por ejemplo manipular revivals de coherencia y distinguibilidad en el sistema.

Chapter 7

Conclusions

In this Thesis we have studied the problem of controlling quantum systems from a wide perspective, with the goal of determining which aspects of the system, the driving field and the environment are relevant to achieving successful control strategies in different scenarios. We have approached this problem by studying various models and using several methods. As a result, we have obtained novel and interesting results about the design of control strategies, both based on physical intuition about the system (coherent control) and using optimization methods (optimal control). We have thoroughly analyzed the important issue about the minimum time needed to control a system, where we proposed a new framework for constructing bounds on the evolution time for a quantum system undergoing unitary dynamics, which is specially suitable for control problems. We have also investigated the interplay between the complexity of a system and its controllability, and used the power of optimal control to systematically assess the relation between the features of a many-body quantum system and the shape of the control field. Finally, we studied the role of non-Markovian effects on the control of open quantum systems, and showed that time-dependent control fields can substantially change the degree of non-Markovianity while controlling the system.

The problems tackled throughout this work are of current relevance in the area of quantum control and our results represent a step forward in the body of knowledge on that subject. This Thesis is thus meant to serve as a basis for future research on topics which are becoming of increasing relevance for a wider scope of investigations, including the development of quantum information processing and measurement devices. For instance, we expect the development of faster processing capabilities to rely on methods to correctly assess the fundamental limitations about the speed of quantum evolution. Also, as devices operating on the quantum regime expand to interacting many-body systems, it is necessary to understand

how complex the manipulation of those systems tends to become. Finally, from a fundamental point of view, we expect our study about driven open quantum systems to trigger a definitive discussion about what can and what cannot be accomplished by actively manipulating non-Markovian effects in such systems.

Here we proceed to give a brief overview of the results obtained in this Thesis, and point out some relevant open questions derived from them. In Chap. 3 we presented the Landau-Zener (LZ) model for a two-level quantum system, based on which we proposed and implemented an efficient method to control the state of a multilevel system. The method is founded on the navigation of the energy spectrum using fast variations of a control parameter, and is successful in overcoming the adverse influence of decoherence, a feature wich relies in the speed with which the transitions are performed. We also studied the dynamics of the LZ model under the effects of time-periodical driving fields, where we derive analytical results showing the possibility of complete population transfer in the intermediate driving frequency regime. This allowed us also to show the feasibility of such protocols in a realistic multilevel system.

In Chap. 4 we studied optimal control of systems with many avoided crossings in their energy spectrum. For the two-level case, we confirmed that the control method presented previously is time-optimal at each avoided crossing. We also used this model to explore the results obtained from the usual Quantum Speed Limit (QSL) formulation for the case of time-dependent Hamiltonians. We show that a number of bounds on the evolution time can be obtained, which can be in general different for the same physical process. In our analysis, we discuss the specific meaning of the QSL time, which can be described as the minimum time required by a quantum system to traverse a certain distance in state space, under the action of a fully determined Hamiltonian. Following the analysis proposed in Sect. 2.2.3.1 we connect the QSL problem with quantum control, and prove that in some cases no meaningful bound for the total evolution time of a control protocol (i.e., only $T \geq 0$) can be drawn from this expressions, a feature that is only possible in the time-dependent regime (in non-trivial cases). We also point out that for time-dependent Hamiltonians, the QSL formulation in general requires knowledge about the state of the system at all times.

In the multilevel setup, where the energy spectrum of the system show several avoided crossings (ACs), we use standard numerical optimal control tools to assess the time-performance of the navigation method. We found that the procedure

introduced in Ref. [54] allows to correctly estimate the minimum evolution time for N-level systems with multiple ACs, and we show the minimum time required to cross two ACs is smaller than the sum of the optimal times at each crossing. We then generalized this result to N-level systems, showing that the derived speed-up still holds but reaches a saturation points as N increases.

It is worth pointing out that using optimal control to obtain the actual quantum speed limit time can be troublesome, specially for complex quantum systems, as pointed out in Ref. [55]. There, the authors show that different initial guesses could lead to different estimations of the QSL time, a behavior that can be explained from the fact that the control landscape becomes increasingly complex when the evolution time is constrained. It is argued that in those cases the landscape may lose partially or completely its bening topological features [31]. It is currently of great practical interest to design more robust optimization methods that could overcome these limitations, for example using global optimization methods [196]. Related to this, and from a more fundamental point of view, it is becoming increasingly important to devise methods to probe the landscape in order to comprehensively analyze the relation between the structure of the landscape and the complexity of the system under control.

For the control problems analyzed in Chap. 4 we were able to test a new approach for bounding evolution times for quantum control problems proposed by us in Chap. 2. The main idea of our approach is to derive bounds which are independent on the actual shape of the control field, and that can be derived without solving the full time-evolution of the state. We show that this new method successes in deriving meaningful bounds for the evolution time which are comparable with the ones obtained from the usual QSL formulation, albeit using much less information about the dynamics. However, we also show that applications to more complex system lead to weaker bounds due to unfavorable scaling with the system space dimension. Nevertheless, the main concept of our approach remains valid, and there is room for obtaining improved bounds, for example using information about nested commutators between free and controlled Hamiltonians as pointed out in [74], or geometrical tools as discussed in [197].

As an interesting byproduct of our analysis of the multilevel model, we found that the control fields derived by optimal control are easily described by means of a few well-defined parameters. Thanks to that, we found that the physical mechanism that cause the QSL enhancement is based on the collective effects between the

states which interact at each AC and others, which are dynamically coupled by the control fields. Based on these results, we were able to construct a model for the control problem which we solved analytically. We also studied how the outcome and performance of the optimization were modified when varying the initial guess for the control protocol. We found that using different initial guesses can lead to very different shapes of the optimized control field. We point out that, in light of the novel results about the complexity of the landscape mentioned previously, it is of paramount practical importance to be able to engineer robust choices for the initial guess in optimal control. Our results indicate that a preliminary analysis of the system spectrum, as done here, can act as pre-optimization method as it lead us to a good choice of such initial field.

In Chap. 5 we investigated how the complexity of the physical system affects its controllability, based on studying the complexity of the control field used to drive it. For that we studied control processes in a chain of spin-1/2 particles which allowed us to consider separately different space dimensions by adding excitations to the system. By allowing next-to-nearest neighbour interactions, we were also able to parametrically tune the system from regular to chaotic. We found the time-dependent control fields required to drive different processes using optimal control theory and defined two measures of complexity based on the Fourier spectra of those fields. By doing so, we could identify which aspects of the system complexity affect the control fields. For instance, we found that the spectral bandwidth, which measures the maximum frequency present in the field, is quite generally independent of the system space dimension. However, we showed that exceptions to this rule occur if we choose highly non-local control fields. Also, we investigated how many frequencies are present inside the signal bandwidth, by defining a measure of localization: the spectral inverse participation ratio (sIPR). We found that this measure of field complexity does increase when excitations are added to system. Finally, we assessed the role of quantum chaos in the control of the system by studying the fields as a function of the chaos parameter. We found no evidence of the regular - chaotic transition in the field spectral measures, allowing us to assert that the fields required to control chaotic and integrable systems display the same complexity.

We believe that these results shed light in the relation between quantum control and complexity in many-body systems. When considering a more realistic scenario, a number of important issues are raised, such as the role of disorder in the inter-particle couplings and the bandwidth limitations of the control source. It would be interesting to study the robustness of our results in such scenarios.

Concerning the role of quantum chaos in the dynamics of many-body systems, it is interesting to point out that a previous work [198] studied relaxation processes in such systems. Although working in an opposite scenario to coherent control, the authors there also found no trace of the chaoticity of the system in the relaxation dynamics. In our case, we present further evidence about the irrelevance of quantum chaos in the coherent dynamics of many-body system.

In Chap. 6 we explored the interplay between driving and non-Markovianity (NM) on the dynamics of an open quantum system. We derived the exact equation of motion for the reduced dynamics of a two-level system coupled to an structured environment, and found a remarkable result: the driving can produce a large enhancement non-Markovian effects, but only when the coupling between system and environment is small. In the strong-coupling regime, on the other hand, the driving is unable to increase the degree of NM. We performed extensive numerical calculations which prove that this effect is present also beyond the rotating wave approximation. We also provide analytical arguments which allows us to explain the effects of the driving in the high-frequency regime, and also in the weak coupling regime.

Finally, we set out to study the role of NM in the controllability of the system. By adapting the Krotov scheme used in previous chapters to a general linear system of differential equations, we derived the optimal fields required to control the reduced dynamics of the system in various situations. By comparing the non-Markovianity values displayed by the controlled evolution as opposed to the undriven case, we observe that there are cases where the system may require to show a higher or a lower degree of NM to efficiently be controlled. This simple yet novel result tells us that NM cannot be regarded as a proper resource for this type of tasks, since it cannot be expended or stored in order to achieve a better control. However, we also conjecture that potentially non-Markovian models (regardless of the magnitude of the NM measures) allow for better controllability. It would be interesting to show this by studying a model described by a Lindblad-like equation which allowed for arbitrary control field shapes, and compare it to the model studied here. Another interesting direction for future research would be adapting the hierarchy equations of motion method for optimal control, which seems feasible. This would allow for a systematic approach for tackling control problems in more complicated open systems, which is currently lacking. Having this tool will, in turn, allow for a broader range of studies about the specific features of non-Markovian dynamics that can affect controllability [66].

Conclusiones

En esta Tesis hemos estudiado el problema de control en sistemas cuánticos desde una perspectiva amplia, con el objetivo de determinar qué aspectos del sistema, los campos y el entorno son relevantes para lograr estrategias de control exitosas en diferentes escenarios. Hemos abordado este problema estudiando varios modelos y usando diversos métodos. Como resultado, hemos obtenido resultados novedosos e interesantes sobre el diseño de estrategias de control, basadas tanto en la intuición física sobre el sistema (control coherente) como en el uso de métodos de optimización (control óptimo). Hemos discutido extensamente la existencia de tiempos mínimos de evolución al controlar un sistema, en cuyo contexto propusimos un nuevo marco para construir cotas para dichos tiempos en sistemas cuánticos cerrados. Este marco es especialmente adecuado para problemas de control. También hemos investigado la relación entre la complejidad de un sistema y su controlabilidad y hemos utilizado herramientas de control óptimo para evaluar sistemáticamente la relación entre las características de un sistema cuántico de muchos cuerpos y la forma del campo de control. Finalmente, se estudió el papel de los efectos no-Markovianos en el control de los sistemas cuánticos abiertos y se demostró que los campos de control dependientes del tiempo pueden cambiar sustancialmente el grado de no-Markovianidad mientras se controla el sistema.

Los problemas abordados a lo largo de este trabajo son de relevancia actual en el área de control cuántico y nuestros resultados representan un paso adelante en el conjunto de conocimientos sobre el tema. Por lo tanto, esta Tesis sirve como base para futuras investigaciones sobre temas que están adquiriendo una relevancia creciente en una clase mas amplia de investigaciones, incluyendo el desarrollo de dispositivos de medición y procesamiento de información cuántica. Por ejemplo, esperamos que el desarrollo de capacidades de procesamiento más rápido se basen en métodos para evaluar correctamente las limitaciones fundamentales sobre la velocidad de la evolución cuántica. Además, a medida que los dispositivos que operan en el régimen cuántico se vuelvan mas sofisticados e involucran dinámica de muchos cuerpos interactuantes, será necesario evaluar la complejidad de manipular

estos sistemas. Por último, desde un punto de vista fundamental, esperamos que nuestro estudio sobre sistemas cuánticos abiertos forzados genere una discusión definitiva sobre qué puede y qué no puede lograrse manipulando activamente efectos no-Markovianos en estos sistemas.

Procedemos a elaborar una breve reseña de los resultados obtenidos en esta Tesis. En el cap. 3 presentamos el modelo de Landau-Zener (LZ) para un sistema cuántico de dos niveles, basado en el cual propusimos e implementamos un método eficiente para controlar el estado de un sistema de muchos niveles. El método se basa en la navegación del espectro de energía utilizando variaciones rápidas de un parámetro de control y tiene éxito en superar la influencia adversa de la decoherencia. También se estudió la dinámica del modelo LZ bajo los efectos de los campos de conducción periódica, donde se obtienen resultados analíticos que muestran la posibilidad de transferencia de población completa en el régimen de frecuencia de conducción intermedia. En el cap. 4 estudiamos el control óptimo de sistemas con muchos cruces evitados en su espectro energético. Para el caso de dos niveles, hemos confirmado que el método de control presentado previamente es óptimo en su duración en cada cruce evitado. También utilizamos este modelo para explorar los resultados obtenidos de la formulación habitual del Límite de Velocidad Cuántica (QSL) para el caso de hamiltonianos dependientes del tiempo. Siguiendo el análisis propuesto en la sec. 2.2.3.1 conectamos el problema QSL con el control cuántico y probamos que en algunos casos no se puede extraer ningún límite significativo para el tiempo de evolución total de un protocolo de control a partir de este formalismo.

En dicho capítulo tambien utilizamos herramientas numéricas de control óptimo para evaluar el tiempo de funcionamiento del método de navegación. Se encontró que el procedimiento introducido en la Ref. [54] permite estimar correctamente el tiempo de evolución mínimo para sistemas varios niveles con múltiples ACs, y mostramos que el tiempo mínimo requerido para cruzar varios ACs es menor que la suma de los tiempos óptimos en cada cruce. Asimismo, para estos sistemas aplicamos un nuevo enfoque para establecer cotas para los tiempos de evolución en problemas de control cuántico, el cual proponemos en el Cap. 2. La idea principal de nuestro enfoque es derivar límites que son independientes de la forma explícita del campo de control, y que se pueden derivar sin resolver la evolución a tiempo completo del estado. Mostramos que este nuevo método logra derivar límites significativos para el tiempo de evolución que son comparables con los obtenidos a partir de la formulación QSL usual, aunque utilizando mucha menos información

sobre la dinámica.

En el cap. 5 investigamos cómo la complejidad de un sistema físico afecta su controlabilidad, a partir del estudio de la complejidad del campo de control utilizado para controlarlo. Para ello estudiamos diversos procesos en una cadena de partículas de spin-1/2, que nos permitió estudiar por separado diferentes dimensiones del espacio mediante la adición de excitaciones al sistema. Al permitir interacciones más allá del régimen de primeros vecinos, también pudimos modificar paramétricamente el espectro de energía del sistema de regular a caótico. Encontramos los campos de control dependientes del tiempo necesarios para conducir diferentes procesos usando la teoría de control óptimo y definimos dos medidas de complejidad basadas en los espectros de Fourier de esos campos. A partir de ello, identificamos qué aspectos de la complejidad del sistema afectan a los campos de control. Por ejemplo, encontramos que el ancho de banda espectral, que mide la frecuencia máxima presente en el campo, es en general independiente de la dimensión del sistema. Además, investigamos cuántas frecuencias se encuentran presentes dentro del ancho de banda de la señal, mediante la definición de una medida de localización: la relación de participación inversa espectral (sIPR). Encontramos que esta medida de la complejidad de campo aumenta cuando se agregan las excitaciones al sistema. Por último, se evaluó el papel del caos cuántico en el control del sistema mediante el estudio de los campos en función del parámetro caos. No encontramos evidencia de la transición caótica-regular en las medidas espectrales de campo, lo que nos permite afirmar que los campos requeridos para controlar sistemas caóticos e integrables muestran la misma complejidad.

En el cap. 6 exploramos la relación entre campos dependientes del tiempo y efectos no-Markovianos en la dinámica de un sistema cuántico abierto. Derivamos la ecuación exacta de movimiento para la dinámica reducida de un sistema de dos niveles acoplado a un entorno estructurado, y encontramos un resultado notable: el forzado puede producir un gran aumento de la no-Markovianidad (NM), pero sólo cuando el acoplamiento entre el sistema y el entorno es pequeño. En el régimen de acoplamiento fuerte, por otro lado, el forzado es incapaz de aumentar el grado de NM. Realizamos cálculos numéricos exhaustivos que demuestran que este efecto está presente también más allá de la aproximación de la onda rotante. También estudiamos la relación entre NM y control, mostrando que herramientas de control óptimo permiten encontrar protocolos de control cuyo éxito no guarda correlación con las medidas de NM de la evolución.

Appendix A

Quantum speed limit calculations

A.1 Derivation of Pfeifer's theorem

Here we derive eqn. (2.32). Consider a quantum system described by a state $\rho(t) = |\psi(t)\rangle\langle\psi(t)|$ which evolves according to a time-dependent Hamiltonian $H(t)$, together with some reference state $|\varphi\rangle$. The evolution operator $U(t,s)$ satisfies

$$i\hbar\frac{\partial U_{t,s}}{\partial t} = H_t U_{t,s} \text{ and } U_{s,s} = \mathbb{I}, \tag{A.1}$$

where we use subscripts to denote time-dependence so as to lighten the notation. By noting that $U_{t,s} = U_{s,t}^\dagger$ we can also write

$$i\hbar\frac{\partial U_{t,s}}{\partial s} = -U_{t,s} H_s \text{ and } U_{t,t} = \mathbb{I}. \tag{A.2}$$

We now define

$$\rho_{t,s} = U_{t,s}\rho_0 U_{t,s}^\dagger, \tag{A.3}$$

where $\rho_0 \equiv \rho(0)$ and also

$$p_{t,s} = \mathrm{tr}\left(P\rho_{t,s}\right) \text{ where } P = |\varphi\rangle\langle\varphi|. \tag{A.4}$$

Deriving eqn. (A.3) and its adjoint with respect to t and s and using eqns. (A.1) and (A.2) we obtain

$$i\hbar\frac{\partial \rho_{t,s}}{\partial t} = [H_t, \rho_{t,s}] \tag{A.5}$$

$$i\hbar\frac{\partial \rho_{t,s}}{\partial s} = -U_{t,s}\left[H_s, \rho_0\right] U_{t,s}^\dagger. \tag{A.6}$$

We can now express the derivatives of $p_{t,s}$ by combining eqns. (A.4) and (A.5). Looking at its absolute value we get

$$\hbar\left|\frac{\partial p_{t,s}}{\partial t}\right| = \left|\mathrm{tr}\left(P\left[H_t, \rho_{t,s}\right]\right)\right| \leq 2 f(P, H_t) f(P, \rho_{t,s}), \tag{A.7}$$

where we defined

$$f(|\phi\rangle\langle\phi|, A) = \sqrt{\langle\phi| (A - \langle A\rangle)^2 |\phi\rangle} \equiv \Delta A|_\phi \tag{A.8}$$

and also used Theorem 1 from Ref. [92]. Combining eqns. (A.4) and (A.6) now yields

$$\hbar \left| \frac{\partial p_{t,s}}{\partial s} \right| = \left| \mathrm{tr} \left(P U_{t,s} \left[H_s, \rho_0 \right] U_{t,s}^\dagger \right) \right| \leq 2 f(\rho_0, H_s) f(\rho_{t,s}, P) \tag{A.9}$$

The last factors in eqns. (A.7) and (A.9) are simply evaluated to give $\sqrt{p_{t,s} - p_{t,s}^2}$ and so we are left with two intermediate results

$$\pm \frac{\partial p_{\tau,s}}{\partial \tau} \leq \frac{2}{\hbar} f(P, H_\tau) \sqrt{p_{\tau,s} - p_{\tau,s}^2} \tag{A.10}$$

$$\pm \frac{\partial p_{t,\sigma}}{\partial \sigma} \leq \frac{2}{\hbar} f(\rho_0, H_\sigma) \sqrt{p_{t,\sigma} - p_{t,\sigma}^2}. \tag{A.11}$$

Noting that $p_{t,t} = p_{s,s} \equiv p_0 = |\langle\psi(0)|\varphi\rangle|^2$, we can see that both inequalities compete in the sense that they can be casted as

$$\pm \int_{p_0}^{p_{t,s}} \frac{dp}{\sqrt{p - p^2}} \leq \frac{2}{\hbar} \min \left\{ \int_s^t \Delta E_\varphi(\tau)\, d\tau, \int_s^t \Delta E_{\psi_0}(\sigma)\, d\sigma \right\} \tag{A.12}$$

Calculating the integral on the l.h.s. of the expression above, setting $s = 0$ and identifying $h(t)$ as in eqn. (2.34) we get

$$\pm \left(\arcsin(\sqrt{p_0}) - \arcsin(\sqrt{p_{t,0}}) \right) \leq h(t). \tag{A.13}$$

Finally, we can work out $p_{t,0}$ and get

$$\arcsin\left(\sqrt{p_{t,0}}\right) \lesseqgtr \delta \pm h(t) \tag{A.14}$$

where we introduced $\delta = \arcsin(\sqrt{p_0})$ as in the main text. We finally apply the function $\sin_*$ which is monotonic increasing to both sides of the inequality and obtain

$$\sqrt{p_{t,0}} = |\langle\varphi|\psi(t)\rangle| \lesseqgtr \sin_* \left(\delta \pm h(t) \right). \tag{A.15}$$

A.2 QSL for a constrained two-level problem

Here we derive the QSL bounds T_{Q1} and T_{Q2} for the constrained optimal control solutions of Sect. 4.1. We begin by the bang-off-bang protocol, and we first compute T_{Q2} by using expression (4.21). To do so we calculate the distance of the evolution path as

$$2 \int_0^{T_{min}} \Delta E(t')\, dt' = d_I + d_{II} + d_{III}, \tag{A.16}$$

where we consider explicitly the three steps of the protocol. For simmetry we have that $d_I = d_{II}$, and also we can see that in each step ΔE is time-independent. We

can then calculate d_I simply by evaluating the variance (4.15) in the initial state

$$d_I = 2\int_0^{T_\Lambda} \left(\Lambda \sin(\theta) + \frac{\Delta}{2}\cos(\theta)\right) dt' = 2\left(\Lambda \sin(\theta) + \frac{\Delta}{2}\cos(\theta)\right) T_\Lambda \tag{A.17}$$

We can proceed in a similar way to calculate d_{II}. There it is easier to evaluate the variance in intermediate state where $\chi = \varphi = \frac{\pi}{2}$. Note that in this second step we have $\lambda = 0$, so we end up with $\Delta E = \Delta/2$ and then

$$d_{II} = 2\Delta E\, T_{off} = T_{off}\Delta \tag{A.18}$$

We now put the results together and obtain

$$T_{Q2} = \frac{s(\theta)}{s_{\text{path}}} T_{min} = \frac{s(\theta)}{4\left(\Lambda \sin(\theta) + \frac{\Delta}{2}\cos(\theta)\right) T_\Lambda + T_{off}\Delta} T_{min} \tag{A.19}$$

For obtaining T_{Q1} we have to solve

$$s(\theta) = 2\int_0^{T_{Q1}} \Delta E(t')\, dt' \tag{A.20}$$

Given the piecewise dependence of ΔE with time, is clear that T_{Q1} will have different results whether $s(\theta) \leq d_I$, in which case the above expression translates to

$$s(\theta) = 2\left(\Lambda \sin(\theta) + \frac{\Delta}{2}\cos(\theta)\right) T_{Q1}, \tag{A.21}$$

or whether $s(\theta) > d_I$, in which case we get

$$s(\theta) = d_I + \Delta\,(T_{Q1} - T_\Lambda) \tag{A.22}$$

So, working out T_{Q1} from this expressions we obtain

$$T_{Q1} = \begin{cases} \frac{s(\theta)}{2\left(\Lambda \sin(\theta) + \frac{\Delta}{2}\cos(\theta)\right)} & \text{if} \quad s(\theta) \leq d_I(\theta) \\ T_\Lambda + \frac{s(\theta) - d_I}{\Delta} & \text{if} \quad s(\theta) > d_I(\theta) \end{cases} \tag{A.23}$$

For the bang-bang protocol, it is straightforward to evaluate the energy variance (4.15) to see that it is constant for this protocol,

$$\Delta E = \left(\Lambda \sin(\theta) + \frac{\Delta}{2}\cos(\theta)\right). \tag{A.24}$$

As a result, T_{Q1} and T_{Q2} coincide,

$$T_{Q1} = T_{Q2} = \frac{s(\theta)}{4\left(\Lambda \sin(\theta) + \frac{\Delta}{2}\cos(\theta)\right) T_\Lambda} T_{min} = \frac{s(\theta)}{2\left(\Lambda \sin(\theta) + \frac{\Delta}{2}\cos(\theta)\right)}. \tag{A.25}$$

A.3 Minimum time bounds for the many-level problem

Here we calculate t^P_{min} and t^{R1}_{min} for the N level Hamiltonian of eqn. (4.33). For the first one we need to evaluate the variance of H_N in the initial and target states

$|0\rangle$ and $|K\rangle$, which yield

$$\Delta H_N|_{|0\rangle} = \frac{\Delta_0}{2} \tag{A.26}$$

$$\Delta H_N|_{|K\rangle} = \frac{\Delta_{K-1}}{2} \tag{A.27}$$

Since both states are ortogonal, $s(0, K) = \pi$ and we finally get

$$t^P_{min} = \frac{\pi}{\min(\Delta_0, \Delta_{K-1})} \tag{A.28}$$

For t^{R1}_{min}, we need to write down $H_N(\lambda) = H^{(0)}_N + \lambda H^{(C)}_N$. Although we do not write its full expression here, is easy to see that $H^{(C)}_N$ is diagonal in the diabatic basis, and thus we can calculate the denominator of (2.47) in a straightforward way

$$\sum_{j=0}^{N-1} |\langle\psi_g|j\rangle \langle j|\psi_0\rangle| = \sum_j |\langle K|j\rangle \langle j|0\rangle| = 0. \tag{A.29}$$

We then have

$$t^{R1}_{min} = \frac{1}{\|H^{(0)}_N\|}, \tag{A.30}$$

where $\|\|H^{(0)}_N\|$ is computed numerically, but is independent of $\lambda(t)$.

Appendix B

The LiCN/LiNC isomerizing system

The LiNC/LiCN isomerizing system presents two stable isomers at the linear configurations: Li–N–C and Li–C–N, which are separated by a relatively modest energy barrier of only 0.0157376 a.u. The C and N atoms are strongly bounded by a triple covalent bond, while the Li is attached to the CN moiety by mostly ionic forces, due to the large charge separation existing between them. For these reasons, the CN vibrational mode effectively decouples from the other degrees of freedom of the molecule, and it can be considered frozen at its equilibrium value, $r_e = 2.186$. On the other hand, the relative position of Li with respect to the center of mass of the CN is much more flexible. In particular the bending along the angular coordinate is very floppy, and the corresponding vibration performs very large amplitude motions even at moderate values of the excitation energy. Accordingly, the vibrations of the whole system can be adequately described by the following 2 degrees of freedom. Using scattering or Jacobi coordinates (R, r, θ), where R is the distance from the Li atom to the center of mass of the CN fragment, r the C–N distance, and θ the angle formed by these two vectors, the corresponding classical $(J = 0)$ Hamiltonian is given by

$$H = \frac{P_R^2}{2\mu_{\mathrm{Li-CN}}} + \frac{1}{2}\left(\frac{1}{\mu_{\mathrm{Li-CN}}R^2} + \frac{1}{\mu_{\mathrm{CN}}r_e^2}\right)P_\theta^2 + V(R,\theta), \tag{B.1}$$

where P_R and P_θ are the associate conjugate momenta, and the corresponding reduced masses are given by $\mu_{\mathrm{Li-CN}} = m_{\mathrm{Li}}m_{\mathrm{CN}}/(m_{\mathrm{Li}} + m_{\mathrm{CN}}) = 10072$ and $\mu_{\mathrm{CN}} = m_{\mathrm{C}}m_{\mathrm{N}}/m_{\mathrm{CN}} = 11780$.

Note that we assume that the isomerization process is fast compared with the

rotation of the molecule. The potential interaction, $V(R,\theta)$, is given by a 10–terms expansion in Legendre polynomials,

$$V(R,\theta) = \sum_{\lambda=0}^{9} v_\lambda(R) P_\lambda(\cos\theta), \tag{B.2}$$

where the coefficients, $v_\lambda(R)$, are combinations of long and short–term interactions whose actual expressions have been taken from the literature [199]. This potential has a global minimum at $(R,\theta) = (4.349,\pi)$, a relative minimum at $(R,\theta) = (4.795,0)$, and a saddle point at $(R,\theta) = (4.221, 0.292\pi)$. The two minima correspond to the stable isomers at the linear configurations, LiNC and LiCN, respectively. The LiNC configuration, $\theta = \pi$, is more stable than that for LiCN, $\theta = 0$. The LiCN molecule is a polar molecule, i.e., it has a permanent dipole moment, so that in the presence of an electric field, $\vec{\mathcal{E}}$, an additional potential energy term appears, this leading to the following effective Hamiltonian function

$$H = H_{\mathrm{LiCN}} - \vec{d}(R,\theta)\cdot\vec{\mathcal{E}}, \tag{B.3}$$

where $\vec{d}(R,\theta)$ is the dipole moment of the LiNC/LiCN molecular system. For the dipole moment, we have taken from the literature the *ab initio* calculations fitted to an analytic expansion in associated Legendre functions of Brocks *et al.* [200]. The energy spectrum of the full Hamiltonian (B.3) is plotted in Chapter 3.

Appendix C

Spin chain model

C.1 Symmetries

Here we show that the total magnetization $S_z = \frac{1}{2}\sum_{i=1}^{L}\sigma_i^z$ is a constant of motion of Hamiltonian (5.6). We do this by computing the commutator

$$[H_{01}, S_z] = [H_0, S_z] + \Gamma\,[H_1, S_z] \tag{C.1}$$

We calculate the first term in the last expression

$$\begin{aligned}
[H_0, S_z] &= \frac{J}{8}\sum_{i=1}^{L-1}\sum_{j=1}^{L}\left(\left[\sigma_i^x\sigma_{i+1}^x, \sigma_j^z\right] + \left[\sigma_i^y\sigma_{i+1}^y, \sigma_j^z\right] + \alpha_z\left[\sigma_i^z\sigma_{i+1}^z, \sigma_j^z\right]\right) \\
&= \frac{J}{8}\sum_{i=1}^{L-1}\sum_{j=1}^{L}\left(\sigma_i^x\left[\sigma_{i+1}^x, \sigma_j^z\right] + \left[\sigma_i^x, \sigma_j^z\right]\sigma_{i+1}^x + \sigma_i^y\left[\sigma_{i+1}^y, \sigma_j^z\right] + \left[\sigma_i^y, \sigma_j^z\right]\sigma_{i+1}^y\right) \\
&= \frac{J}{8}\sum_{i=1}^{L-1}\sum_{j=1}^{L}\left(\sigma_i^x(-i\delta_{j,i+1}\sigma_{i+1}^y) + (-i\delta_{j,i}\sigma_i^y)\sigma_{i+1}^x + \sigma_i^y(i\delta_{j,i+1}\sigma_{i+1}^x) + (i\delta_{j,i}\sigma_i^x)\sigma_{i+1}^y\right) \\
&= i\frac{J}{8}\sum_{i=1}^{L-1}\left(-\sigma_i^x\sigma_{i+1}^y - \sigma_i^y\sigma_{i+1}^x + \sigma_i^y\sigma_{i+1}^x + \sigma_i^x\sigma_{i+1}^y\right) = 0
\end{aligned} \tag{C.2}$$

The procedure is analogous for the second commutator $[H_1, S_z]$.

The conservation of the total spin S^2 in the free Hamiltonian H_{01} was avoided by setting the interparticle couplings in the z direction to be different than 1. Although that derivation is a bit tedious, we can easily see that just by using an non-homogeneous control field such as $H_c = \frac{J}{2}\epsilon(t)(\sigma_1^z + \sigma_L^z)$ we already achieve our goal. For that purpose we can calculate the commutator between S^2 and a general

sum of local fields in the z-direction,

$$\begin{aligned}\left[\frac{1}{2}\sum_{n=1}^{L}\epsilon_n\sigma_n^z, S^2\right] &= \frac{1}{8}\sum_{n,i,j=1}^{L}\sum_{k=x,y,z}\epsilon_n\left[\sigma_n^z, \sigma_i^k\sigma_j^k\right] \\ &= \frac{1}{8}\sum_{n,i,j}\sum_{k}\epsilon_n\left(\sigma_i^k\left[\sigma_n^z,\sigma_j^k\right]+\left[\sigma_n^z,\sigma_i^k\right]\sigma_j^k\right) \\ &= \frac{1}{8}\sum_{n,i}\sum_{k}\epsilon_n\left(\sigma_i^k\left[\sigma_n^z,\sigma_n^k\right]+\left[\sigma_n^z,\sigma_n^k\right]\sigma_i^k\right) \\ &= \frac{i}{8}\sum_{n,i}\epsilon_n\left(\sigma_i^x\sigma_n^y+\sigma_n^y\sigma_i^x-\sigma_i^y\sigma_n^x-\sigma_n^x\sigma_i^y\right) \\ &= \frac{i}{4}\left(\left\{S_x,\sum_n\epsilon_n\sigma_n^y\right\}-\left\{S_y,\sum_n\epsilon_n\sigma_n^x\right\}\right), \end{aligned} \tag{C.3}$$

where we define $S_k = \frac{1}{2}\sum_{i=1}^{L}\sigma_i^k$ in the last line. The above expression clearly shows that S^2 is conserved only if $\epsilon_n = \epsilon$ for all n. This is not the case for the proposed control Hamiltonian H_c.

Finally we prove that our choice for the control Hamiltonian also commutes with the parity operator, c.f. eqn. (5.18). For that we again calculate the commutator between Π and a general sum of local fields,

$$\left[\frac{1}{2}\sum_{n=1}^{L}\varepsilon_n\sigma_n^z, \Pi\right] = \frac{1}{2}\sum_{n=1}^{L}\epsilon_n\left[\sigma_n^z,\Pi\right], \tag{C.4}$$

and we use that, by definition, Π is unitary and that

$$\Pi\sigma_n^z\Pi = \sigma_{\bar{n}}^z \;\Rightarrow\; \Pi\sigma_n^z = \sigma_{\bar{n}}^z\Pi \;\Rightarrow\; \left[\sigma_n^z,\Pi\right] = \left(\sigma_{\bar{n}}^z-\sigma_n^z\right)\Pi \tag{C.5}$$

where $\bar{n} = L - n + 1$ is the mirrored position of n. So, for the commutator we obtain

$$\begin{aligned}\left[\frac{1}{2}\sum_{n=1}^{L}\varepsilon_n\sigma_n^z, \Pi\right] &= \frac{1}{2}\left(\sum_{n=1}^{L}\epsilon_n\sigma_{\bar{n}}^z\Pi-\sum_{n=1}^{L}\epsilon_n\sigma_n^z\Pi\right) \\ &= \frac{1}{2}\sum_{n=1}^{L}\left(\epsilon_{\bar{n}}-\epsilon_n\right)\sigma_n^z\Pi. \end{aligned} \tag{C.6}$$

In light of this expression, we can see that any choice that ensures $\epsilon_{\bar{n}} = \epsilon_n$ will preserve the parity of the system.

C.2 Split-operator technique

For a bilineal control Hamiltonian of the form

$$H(t) = H_0 + \lambda(t)H_c \tag{C.7}$$

we can approximate the time evolution operator as

$$U(t+\Delta t,t) \simeq \exp\left(-i(H_0+\lambda(t)H_c)\Delta t\right) \tag{C.8}$$

which is a good approximation for small enough Δt. Even in this case, this implementation would require to diagonalize the full Hamiltonian $H(t)$ at each time step. We can work around this issue by approximating (C.8) by the expression

$$\begin{aligned} U(t+\Delta t,t) &\simeq \exp\left(-iH_0\frac{\Delta t}{2}\right)\exp\left(-i\lambda(t)H_c\Delta t\right)\exp\left(-iH_0\frac{\Delta t}{2}\right) && \text{(C.9)} \\ &\simeq U_0\left(\frac{\Delta t}{2}\right)U_c(\Delta t,\lambda(t))U_0\left(\frac{\Delta t}{2}\right) && \text{(C.10)} \end{aligned}$$

By using this method, called the split-operator technique [201], we can compute and store U_0 in the basis of eigenstates of H_c, and then use it at each time step to approximate the full evolution operator (C.8).

Appendix D

Driven open two-level system

D.1 Time-local equation of motion under the RWA

In this section we derive the (time-local) differential equation for $G(t)$, eqn. (6.43) from the integrodifferential equation (6.35). We start from this last expression and divide it by $c_1(t)$ to obtain

$$\frac{\dot{c_1}(t)}{c_1(t)} \equiv g(t) = -\int_0^t dt' F(t,t') \mathrm{e}^{i[\epsilon(t)-\epsilon(t')]} \frac{c_1(t')}{c_1(t)}. \tag{D.1}$$

We introduce the function $h(t,t')$ such that the above equation has the form

$$g(t) = -\int_0^t dt' F(t,t') h(t,t') \tag{D.2}$$

Now, we use that $F(t,t')$ has actually an exponential dependance on $t-t'$, see eqn. (6.36). For convenience we write it as

$$F(t,t') = p_0 \mathrm{e}^{q0(t-t')} \tag{D.3}$$

and we compute the time derivative of $g(t)$ from eqn. (D.2)

$$\frac{d}{dt}g(t) = -\frac{d}{dt}\left(\int_0^t dt' F(t,t') h(t,t')\right) \tag{D.4}$$

$$= -F(0)h(t,t) - \int_0^t dt' \left(\frac{\partial}{\partial t}\left[F(t,t')h(t,t')\right]\right) \tag{D.5}$$

where we have used that

$$\frac{d}{dx}\int_0^x f(x,y)dy = f(x,x) + \int_0^x \frac{\partial f}{\partial x}(x,y)dy. \tag{D.6}$$

We can then evaluate (D.5) rather easily to obtain

$$\frac{d}{dt}g(t) = -p_0 + g(t)\left(q_0 + i\omega_0(t) - g(t)\right) \tag{D.7}$$

In this case, $p_0 = \gamma_0\lambda/2$ and $q_0 = -\lambda - i\Omega_0$ so we finally get, remembering that $\omega_0(t) = \Omega_0 + \Delta(t)$,

$$\frac{d}{dt}g(t) = -\frac{\gamma_0\lambda}{2} - g(t)\left(\lambda + g(t) - i\Delta(t)\right) \tag{D.8}$$

This equation is indeed time-local, but for $g(t)$. But, we can further use that

$$g = \frac{\dot{c_1}}{c_1} \Rightarrow \dot{g} = \frac{\ddot{c_1}c_1 - \dot{c_1}^2}{c_1^2} \tag{D.9}$$

to finally express

$$\dot{c_1}(t) = -\frac{\gamma_0\lambda}{2}c_1(t) - (\lambda - i\Delta(t))\dot{c_1}(t). \tag{D.10}$$

Note that, although this equation is independent of Ω_0, it relies on the assumption $\Omega_0 \gg \lambda$.

D.2 Hierarchy equations of motion

Consider the total system Hamiltonian which describes the dynamics of the two-level system and the environment

$$H = \omega_0(t)\sigma_+\sigma_- + \sigma_x\sum_k g_k(b_k + b_k^\dagger) + \sum_k \omega_k b_k b_k^\dagger. \tag{D.11}$$

From Eq. (D.11), it is straightforward to write down a formal solution for the reduced density matrix of the two-level system in the interaction picture

$$\tilde{\rho}(t) = \mathcal{T}\exp\Bigg\{ -\int_0^t dt_2 \int_0^{t_2} dt_1\, \tilde{\sigma}_x(t_2)^\times \Big[F_R(t_2 - t_1)\tilde{\sigma}_x(t_1)^\times \tag{D.12}$$

$$+ \; i\,F_I(t_2 - t_1)\tilde{\sigma}_x(t_1)^\circ\Big]\Bigg\}\tilde{\rho}(0), \tag{D.13}$$

where $\tilde{O}$ denotes an operator in the interaction picture and $\mathcal{T}$ is the usual time-ordering operator. Functions $C_R(t)$ and $C_I(t)$ are the real and imaginary parts of the environmental correlation function, which is defined as

$$F(t - t') = \mathrm{tr}\left[\rho_E Y_E(t)Y_E(t')\right] = \int_0^\infty d\omega\; J(\omega)\mathrm{e}^{-i\omega(t-t')}. \tag{D.14}$$

In (D.13) we have also used a short-hand notation for the commutator and anticommutator operations: $A^\circ B = \{A, B\}$ and $A^\times B = [A, B]$. The hierarchy equation method casts the expression (D.13) into a set of ordinary differential

equations

$$\frac{d\varrho_{\vec{n}}}{d\tau} = -\left[iH_s(\tau)^{\times} + \vec{n}.\vec{\nu}\right]\varrho_{\vec{n}} - i\sum_{k=1}^{2}\Big\{\sigma_x^{\times}\varrho_{\vec{n}+\vec{e}_k} \tag{D.15}$$

$$+ \frac{\gamma_0}{2}n_k\left[\sigma_x^{\times} + (-1)^k\sigma_x^{\circ}\right]\varrho_{\vec{n}-\vec{e}_k}\Big\}, \tag{D.16}$$

where we have defined $\vec{\nu} = (1 - i\Omega_0, 1 + i\Omega_0)$ and $\vec{n} = (n_x, n_y)$, where $n_x, n_y \geq 0$. Note that equations (D.16) have been expressed in dimensionless units as explained in the main text. This system can be solved for the operator $\varrho_{\vec{n}}(\tau)$, with initial conditions

$$\varrho_{\vec{n}}(0) = \begin{cases} \rho(0) & \text{for } \vec{n} = (0,0) \\ 0 & \text{otherwise} \end{cases} \tag{D.17}$$

Of course, the hierarchy equations (D.16) must be truncated for large enough $\vec{n}$ for numerical purposes. In this work we take $n_x, n_y \leq N$. Using N of the order of 10 gives a converged, positive density matrix $\rho(\tau)$.

D.3 Weak coupling solution

Consider the equation of motion for $G(\tau)$ under the rotating wave approximation (RWA) as introduced in the main text

$$G''(\tau) + \left[1 - i\Delta\cos\left(\omega_D\tau\right)\right]G'(\tau) + \frac{\gamma_0}{2}G(\tau) = 0, \tag{D.18}$$

where $G(0) = 1$ and $G'(0) = 0$. We now treat the term $\frac{\gamma_0}{2}G(\tau)$ as a perturbation and expand the solution in powers of γ_0

$$G(\tau) = \sum_n \gamma_0^n g_n(\tau). \tag{D.19}$$

By inserting (D.19) in (D.18) we obtain

$$\sum_n \gamma_0^n g_n''(\tau) + \left[1 - i\Delta(\tau)\right]\sum_n \gamma_0^n g_n'(\tau) + \frac{1}{2}\sum_n \gamma_0^{n+1} g_n(\tau) = 0, \tag{D.20}$$

where we have used the short-hand notation $\Delta(\tau) \equiv \Delta\cos(\omega_D\tau)$. By arranging powers of γ_0 we obtain the equation for the zeroth-order term $g_0(\tau)$,

$$\begin{cases} g_0'' + [1 - i\Delta(\tau)]g_0' = 0 \\ g_0(0) = 1 \\ g_0'(0) = 0 \end{cases}, \tag{D.21}$$

which has the trivial solution $g_0(\tau) = 1$. For the following order, we obtain

$$\begin{cases} g_1'' + [1 - i\Delta(\tau)]g_1' + \frac{1}{2}g_0 &= 0 \\ g_1(0) &= 0 \\ g_1'(0) &= 0 \end{cases}, \tag{D.22}$$

This system can be integrated in a straightforward fashion to obtain

$$g_1'(\tau) = -\frac{1}{2}\sum_n \sum_m \frac{J_n\left(\frac{\Delta}{\omega_D}\right) J_m\left(\frac{\Delta}{\omega_D}\right)}{1 - in\omega_D} \left(\mathrm{e}^{-i(n-m)\omega_D\tau} - \mathrm{e}^{-\tau}\mathrm{e}^{im\omega_D\tau}\right) \tag{D.23}$$

We can obtain $g_1(\tau)$ by integrating expression (D.23). The full approximated solution is then given by

$$G(\tau) \simeq g_0(\tau) + \gamma_0 g_1(\tau) = 1 + \gamma_0 g_1(\tau). \tag{D.24}$$

The dependence of $G(\tau)$ with the Bessel functions evaluated in Δ/ω_D is evident from expression (D.23).

Bibliography

[1] T. Tan, J. Gaebler, Y. Lin, Y. Wan, R. Bowler, D. Leibfried, and D. Wineland, "Multi-element logic gates for trapped-ion qubits," *Nature*, vol. 528, no. 7582, pp. 380–383, 2015.

[2] T. Monz, D. Nigg, E. A. Martinez, M. F. Brandl, P. Schindler, R. Rines, S. X. Wang, I. L. Chuang, and R. Blatt, "Realization of a scalable shor algorithm," *Science*, vol. 351, no. 6277, pp. 1068–1070, 2016.

[3] X. Mi, J. Cady, D. Zajac, P. Deelman, and J. Petta, "Strong coupling of a single electron in silicon to a microwave photon," *Science*, p. 2469, 2016.

[4] N. Ofek, A. Petrenko, R. Heeres, P. Reinhold, Z. Leghtas, B. Vlastakis, Y. Liu, L. Frunzio, S. Girvin, L. Jiang, *et al.*, "Extending the lifetime of a quantum bit with error correction in superconducting circuits," *Nature*, vol. 536, pp. 441–445, 2016.

[5] J. L. O'brien, A. Furusawa, and J. Vučković, "Photonic quantum technologies," *Nature Photonics*, vol. 3, no. 12, pp. 687–695, 2009.

[6] T. D. Ladd, F. Jelezko, R. Laflamme, Y. Nakamura, C. Monroe, and J. L. O'Brien, "Quantum computers," *Nature*, vol. 464, no. 7285, pp. 45–53, 2010.

[7] M. A. Nielsen and I. Chuang, "Quantum computation and quantum information," 2002.

[8] D. Deutsch and R. Jozsa, "Rapid solution of problems by quantum computation," in *Proceedings of the Royal Society of London A: Mathematical, Physical and Engineering Sciences*, vol. 439, pp. 553–558, The Royal Society, 1992.

[9] I. Walmsley and E. Rabitz, "Quantum physics under control," *Physics Today*, vol. 56, no. 8, pp. 43–49, 2003.

[10] D. Dong and I. R. Petersen, "Quantum control theory and applications: a survey," *IET Control Theory & Applications*, vol. 4, no. 12, pp. 2651–2671, 2010.

[11] D. J. Tannor, *Introduction to quantum mechanics: a time-dependent perspective*. University Science Books, 2007.

[12] M. Shapiro and P. Brumer, *Quantum control of molecular processes*. John Wiley & Sons, 2012.

[13] W. S. Warren, H. Rabitz, and M. Dahleh, "Coherent control of quantum dynamics: the dream is alive," *Science*, vol. 259, no. 5101, pp. 1581–1589, 1993.

[14] D. J. Tannor and S. A. Rice, "Control of selectivity of chemical reaction via control of wave packet evolution," *The Journal of chemical physics*, vol. 83, no. 10, pp. 5013–5018, 1985.

[15] D. J. Tannor, R. Kosloff, and S. A. Rice, "Coherent pulse sequence induced control of selectivity of reactions: Exact quantum mechanical calculations," *The Journal of chemical physics*, vol. 85, no. 10, pp. 5805–5820, 1986.

[16] P. Brumer and M. Shapiro, "Control of unimolecular reactions using coherent light," *Chemical physics letters*, vol. 126, no. 6, pp. 541–546, 1986.

[17] T. Baumert, V. Engel, C. Meier, and G. Gerber, "High laser field effects in multiphoton ionization of na2. experiment and quantum calculations," *Chemical physics letters*, vol. 200, no. 5, pp. 488–494, 1992.

[18] L. Zhu, V. Kleiman, X. Li, S. P. Lu, K. Trentelman, R. J. Gordon, *et al.*, "Coherent laser control of the product distribution obtained in the photoexcitation of hi," *Science-*, pp. 77–77, 1995.

[19] J. Meditch, "On the problem of optimal thrust programming for a lunar soft landing," *IEEE Transactions on Automatic Control*, vol. 9, no. 4, pp. 477–484, 1964.

[20] L. S. Pontryagin, *Mathematical theory of optimal processes*. CRC Press, 1987.

[21] A. P. Peirce, M. A. Dahleh, and H. Rabitz, "Optimal control of quantum-mechanical systems: Existence, numerical approximation, and applications," *Physical Review A*, vol. 37, no. 12, p. 4950, 1988.

[22] S. Shi, A. Woody, and H. Rabitz, "Optimal control of selective vibrational excitation in harmonic linear chain molecules," *The Journal of chemical physics*, vol. 88, no. 11, pp. 6870–6883, 1988.

[23] J. Somlói, V. A. Kazakov, and D. J. Tannor, "Controlled dissociation of i2 via optical transitions between the x and b electronic states," *Chemical physics*, vol. 172, no. 1, pp. 85–98, 1993.

[24] A. Konnov and V. F. Krotov, "On global methods for the successive improvement of control processes," *Automation and Remote Control*, vol. 60, no. 10, pp. 77–88, 1999.

[25] S. J. Glaser, U. Boscain, T. Calarco, C. P. Koch, W. Köckenberger, R. Kosloff, I. Kuprov, B. Luy, S. Schirmer, T. Schulte-Herbrüggen, *et al.*, "Training schrödinger's cat: quantum optimal control," *The European Physical Journal D*, vol. 69, no. 12, p. 279, 2015.

[26] N. Khaneja, T. Reiss, C. Kehlet, T. Schulte-Herbrüggen, and S. J. Glaser, "Optimal control of coupled spin dynamics: design of nmr pulse sequences by gradient ascent algorithms," *Journal of magnetic resonance*, vol. 172, no. 2, pp. 296–305, 2005.

[27] S. Machnes, U. Sander, S. Glaser, P. de Fouquieres, A. Gruslys, S. Schirmer, and T. Schulte-Herbrüggen, "Comparing, optimizing, and benchmarking quantum-control algorithms in a unifying programming framework," *Physical Review A*, vol. 84, no. 2, p. 022305, 2011.

[28] S. Kallush and R. Kosloff, "Quantum governor: Automatic quantum control and reduction of the influence of noise without measuring," *Physical Review A*, vol. 73, no. 3, p. 032324, 2006.

[29] T. Schulte-Herbrüggen, A. Spörl, N. Khaneja, and S. Glaser, "Optimal control for generating quantum gates in open dissipative systems," *Journal of Physics B: Atomic, Molecular and Optical Physics*, vol. 44, no. 15, p. 154013, 2011.

[30] M. H. Goerz, D. M. Reich, and C. P. Koch, "Optimal control theory for a unitary operation under dissipative evolution," *New Journal of Physics*, vol. 16, no. 5, p. 055012, 2014.

[31] H. A. Rabitz, M. M. Hsieh, and C. M. Rosenthal, "Quantum optimally controlled transition landscapes," *Science*, vol. 303, no. 5666, pp. 1998–2001, 2004.

[32] Z. Shen, M. Hsieh, and H. Rabitz, "Quantum optimal control: Hessian analysis of the control landscape," *The Journal of chemical physics*, vol. 124, no. 20, p. 204106, 2006.

[33] M. Hsieh, R. Wu, and H. Rabitz, "Topology of the quantum control landscape for observables," *The Journal of chemical physics*, vol. 130, no. 10, p. 104109, 2009.

[34] K. Moore, M. Hsieh, and H. Rabitz, "On the relationship between quantum control landscape structure and optimization complexity," *The Journal of chemical physics*, vol. 128, no. 15, p. 154117, 2008.

[35] V. Beltrani, J. Dominy, T.-S. Ho, and H. Rabitz, "Exploring the top and bottom of the quantum control landscape," *The Journal of chemical physics*, vol. 134, no. 19, p. 194106, 2011.

[36] K. W. Moore and H. Rabitz, "Exploring constrained quantum control landscapes," *The Journal of chemical physics*, vol. 137, no. 13, p. 134113, 2012.

[37] A. N. Pechen and D. J. Tannor, "Are there traps in quantum control landscapes?," *Physical review letters*, vol. 106, no. 12, p. 120402, 2011.

[38] J. Grond, J. Schmiedmayer, and U. Hohenester, "Optimizing number squeezing when splitting a mesoscopic condensate," *Physical Review A*, vol. 79, no. 2, p. 021603, 2009.

[39] K. Rojan, D. M. Reich, I. Dotsenko, J.-M. Raimond, C. P. Koch, and G. Morigi, "Arbitrary-quantum-state preparation of a harmonic oscillator via optimal control," *Physical Review A*, vol. 90, no. 2, p. 023824, 2014.

[40] G. De Chiara, T. Calarco, M. Anderlini, S. Montangero, P. Lee, B. Brown, W. Phillips, and J. Porto, "Optimal control of atom transport for quantum gates in optical lattices," *Physical Review A*, vol. 77, no. 5, p. 052333, 2008.

[41] U. V. Poulsen, S. Sklarz, D. Tannor, and T. Calarco, "Correcting errors in a quantum gate with pushed ions via optimal control," *Physical Review A*, vol. 82, no. 1, p. 012339, 2010.

[42] M. H. Goerz, T. Calarco, and C. P. Koch, "The quantum speed limit of optimal controlled phasegates for trapped neutral atoms," *Journal of Physics B: Atomic, Molecular and Optical Physics*, vol. 44, no. 15, p. 154011, 2011.

[43] G. Waldherr, Y. Wang, S. Zaiser, M. Jamali, T. Schulte-Herbrüggen, H. Abe, T. Ohshima, J. Isoya, P. Neumann, and J. Wrachtrup, "Quantum error correction in a solid-state hybrid spin register," *Nature*, vol. 506, pp. 204–207, 2014.

[44] D. J. Egger and F. K. Wilhelm, "Optimized controlled-z gates for two superconducting qubits coupled through a resonator," *Superconductor Science and Technology*, vol. 27, no. 1, p. 014001, 2013.

[45] H. Fürst, M. Goerz, U. Poschinger, M. Murphy, S. Montangero, T. Calarco, F. Schmidt-Kaler, K. Singer, and C. Koch, "Controlling the transport of an ion: classical and quantum mechanical solutions," *New Journal of Physics*, vol. 16, no. 7, p. 075007, 2014.

[46] T. Häberle, D. Schmid-Lorch, K. Karrai, F. Reinhard, and J. Wrachtrup, "High-dynamic-range imaging of nanoscale magnetic fields using optimal control of a single qubit," *Physical review letters*, vol. 111, no. 17, p. 170801, 2013.

[47] C. Weidner, H. Yu, R. Kosloff, and D. Z. Anderson, "Atom interferometry using a shaken optical lattice," *Physical Review A*, vol. 95, no. 4, p. 043624, 2017.

[48] A. W. Cross and J. M. Gambetta, "Optimized pulse shapes for a resonator-induced phase gate," *Physical Review A*, vol. 91, no. 3, p. 032325, 2015.

[49] V. Giovannetti, S. Lloyd, and L. Maccone, "Quantum limits to dynamical evolution," *Physical Review A*, vol. 67, no. 5, p. 052109, 2003.

[50] L. Mandelstam and I. Tamm, "The uncertainty relation between energy and time in non-relativistic quantum mechanics," *Journal of Physics USSR*, vol. 9, no. 249, 1945.

[51] K. Bhattacharyya, "Quantum decay and the mandelstam-tamm-energy inequality," *Journal of Physics A: Mathematical and General*, vol. 16, no. 13, p. 2993, 1983.

[52] M. R. Frey, "Quantum speed limits—primer, perspectives, and potential future directions," *Quantum Information Processing*, vol. 15, no. 10, pp. 3919–3950, 2016.

[53] S. Deffner and S. Campbell, "Quantum speed limits: from heisenberg's uncertainty principle to optimal quantum control," *arXiv preprint arXiv:1705.08023*, 2017.

[54] T. Caneva, M. Murphy, T. Calarco, R. Fazio, S. Montangero, V. Giovannetti, and G. E. Santoro, "Optimal control at the quantum speed limit," *Physical review letters*, vol. 103, no. 24, p. 240501, 2009.

[55] J. J. W. Sørensen, M. K. Pedersen, M. Munch, P. Haikka, J. H. Jensen, T. Planke, M. G. Andreasen, M. Gajdacz, K. Mølmer, A. Lieberoth, *et al.*, "Exploring the quantum speed limit with computer games," *Nature*, vol. 532, no. 7598, pp. 210–213, 2016.

[56] I. Brouzos, A. I. Streltsov, A. Negretti, R. S. Said, T. Caneva, S. Montangero, and T. Calarco, "Quantum speed limit and optimal control of many-boson dynamics," *Physical Review A*, vol. 92, no. 6, p. 062110, 2015.

[57] T. Caneva, T. Calarco, R. Fazio, G. E. Santoro, and S. Montangero, "Speeding up critical system dynamics through optimized evolution," *Physical Review A*, vol. 84, no. 1, p. 012312, 2011.

[58] B. Anderson, H. Sosa-Martinez, C. Riofrío, I. H. Deutsch, and P. S. Jessen, "Accurate and robust unitary transformations of a high-dimensional quantum system," *Physical review letters*, vol. 114, no. 24, p. 240401, 2015.

[59] T. Caneva, T. Calarco, and S. Montangero, "Chopped random-basis quantum optimization," *Physical Review A*, vol. 84, no. 2, p. 022326, 2011.

[60] T. Caneva, A. Silva, R. Fazio, S. Lloyd, T. Calarco, and S. Montangero, "Complexity of controlling quantum many-body dynamics," *Physical Review A*, vol. 89, no. 4, p. 042322, 2014.

[61] S. Lloyd and S. Montangero, "Information theoretical analysis of quantum optimal control," *Physical review letters*, vol. 113, no. 1, p. 010502, 2014.

[62] M. A. Schlosshauer, *Decoherence: and the quantum-to-classical transition*. Springer Science & Business Media, 2007.

[63] H.-P. Breuer and F. Petruccione, *The theory of open quantum systems*. Oxford University Press on Demand, 2002.

[64] H.-P. Breuer, E.-M. Laine, J. Piilo, and B. Vacchini, "Colloquium: Non-markovian dynamics in open quantum systems," *Reviews of Modern Physics*, vol. 88, no. 2, p. 021002, 2016.

[65] I. de Vega and D. Alonso, "Dynamics of non-markovian open quantum systems," *Rev. Mod. Phys.*, vol. 89, p. 015001, 2017.

[66] C. P. Koch, "Controlling open quantum systems: tools, achievements, and limitations," *Journal of Physics: Condensed Matter*, vol. 28, no. 21, p. 213001, 2016.

[67] F. Verstraete, M. M. Wolf, and J. Ignacio Cirac, "Quantum computation and quantum-state engineering driven by dissipation," *Nature Physics*, vol. 5, pp. 633–636, 2009.

[68] R. Schmidt, A. Negretti, J. Ankerhold, T. Calarco, and J. T. Stockburger, "Optimal control of open quantum systems: cooperative effects of driving and dissipation," *Physical review letters*, vol. 107, no. 13, p. 130404, 2011.

[69] D. M. Reich, N. Katz, and C. P. Koch, "Exploiting non-markovianity for quantum control," *Scientific reports*, vol. 5, 2015.

[70] L. Landau, "Zur theorie der energieübertragung," *Physics of the Soviet Union*, vol. 2, no. 46, 1932.

[71] C. Zener, "Non-adiabatic crossing of energy levels," in *Proceedings of the Royal Society of London A: Mathematical, Physical and Engineering Sciences*, vol. 137, pp. 696–702, The Royal Society, 1932.

[72] G. Murgida, D. Wisniacki, and P. Tamborenea, "Coherent control of interacting electrons in quantum dots via navigation in the energy spectrum," *Physical review letters*, vol. 99, no. 3, p. 036806, 2007.

[73] D. d'Alessandro, *Introduction to quantum control and dynamics*. New York: CRC press, 2007.

[74] C. Arenz, G. Gualdi, and D. Burgarth, "Control of open quantum systems: case study of the central spin model," *New Journal of Physics*, vol. 16, no. 6, p. 065023, 2014.

[75] S. Schirmer, A. Solomon, and J. Leahy, "Criteria for reachability of quantum states," *Journal of Physics A: Mathematical and General*, vol. 35, no. 40, p. 8551, 2002.

[76] H. Robertson, "A general formulation of the uncertainty principle and its classical interpretation," *Phys. Rev*, vol. 35, no. 5, pp. 667–667, 1930.

[77] G. N. Fleming, "A unitarity bound on the evolution of nonstationary states," *Nuovo Cimento A (1965-1970)*, vol. 16, no. 2, pp. 232–240, 1973.

[78] N. Margolus and L. B. Levitin, "The maximum speed of dynamical evolution," *Physica D: Nonlinear Phenomena*, vol. 120, no. 1, pp. 188–195, 1998.

[79] L. B. Levitin and T. Toffoli, "Fundamental limit on the rate of quantum dynamics: the unified bound is tight," *Physical review letters*, vol. 103, no. 16, p. 160502, 2009.

[80] J. Anandan and Y. Aharonov, "Geometry of quantum evolution," *Physical review letters*, vol. 65, no. 14, p. 1697, 1990.

[81] M. Gajdacz, K. K. Das, J. Arlt, J. F. Sherson, and T. Opatrnỳ, "Time-limited optimal dynamics beyond the quantum speed limit," *Physical Review A*, vol. 92, no. 6, p. 062106, 2015.

[82] S. Deffner and E. Lutz, "Quantum speed limit for non-markovian dynamics," *Physical review letters*, vol. 111, no. 1, p. 010402, 2013.

[83] A. Del Campo, I. Egusquiza, M. Plenio, and S. Huelga, "Quantum speed limits in open system dynamics," *Physical review letters*, vol. 110, no. 5, p. 050403, 2013.

[84] M. M. Taddei, B. M. Escher, L. Davidovich, and R. L. de Matos Filho, "Quantum speed limit for physical processes," *Physical review letters*, vol. 110, no. 5, p. 050402, 2013.

[85] A. Cimmarusti, Z. Yan, B. Patterson, L. Corcos, L. Orozco, and S. Deffner, "Environment-assisted speed-up of the field evolution in cavity quantum electrodynamics," *Physical review letters*, vol. 114, no. 23, p. 233602, 2015.

[86] Z. Sun, J. Liu, J. Ma, and X. Wang, "Quantum speed limits in open systems: Non-markovian dynamics without rotating-wave approximation," *Scientific reports*, vol. 5, 2015.

[87] N. Mirkin, F. Toscano, and D. A. Wisniacki, "Quantum-speed-limit bounds in an open quantum evolution," *Physical Review A*, vol. 94, no. 5, p. 052125, 2016.

[88] M. Cianciaruso, S. Maniscalco, and G. Adesso, "Role of non-markovianity and backflow of information in the speed of quantum evolution," *arXiv preprint arXiv:1704.08061*, 2017.

[89] S. Deffner and E. Lutz, "Energy–time uncertainty relation for driven quantum systems," *Journal of Physics A: Mathematical and Theoretical*, vol. 46, no. 33, p. 335302, 2013.

[90] D. C. Brody, G. W. Gibbons, and D. M. Meier, "Time-optimal navigation through quantum wind," *New Journal of Physics*, vol. 17, no. 3, p. 033048, 2015.

[91] P. Pfeifer, "How fast can a quantum state change with time?," *Physical review letters*, vol. 70, no. 22, p. 3365, 1993.

[92] P. Pfeifer and J. Fröhlich, "Generalized time-energy uncertainty relations and bounds on lifetimes of resonances," *Reviews of Modern Physics*, vol. 67, no. 4, p. 759, 1995.

[93] C. Arenz, B. Russell, D. Burgarth, and H. Rabitz, "The roles of drift and control field constraints upon quantum control speed limits," *arXiv preprint arXiv:1704.06289*, 2017.

[94] S. E. Sklarz and D. J. Tannor, "Loading a bose-einstein condensate onto an optical lattice: An application of optimal control theory to the nonlinear schrödinger equation," *Physical Review A*, vol. 66, no. 5, p. 053619, 2002.

[95] S. Montangero, T. Calarco, and R. Fazio, "Robust optimal quantum gates for josephson charge qubits," *Physical review letters*, vol. 99, no. 17, p. 170501, 2007.

[96] W. Zhu, J. Botina, and H. Rabitz, "Rapidly convergent iteration methods for quantum optimal control of population," *The Journal of Chemical Physics*, vol. 108, no. 5, pp. 1953–1963, 1998.

[97] W. Zhu and H. Rabitz, "A rapid monotonically convergent iteration algorithm for quantum optimal control over the expectation value of a positive definite operator," *The Journal of Chemical Physics*, vol. 109, no. 2, pp. 385–391, 1998.

[98] K. Sundermann and R. de Vivie-Riedle, "Extensions to quantum optimal control algorithms and applications to special problems in state selective molecular dynamics," *The Journal of chemical physics*, vol. 110, no. 4, pp. 1896–1904, 1999.

[99] R. Bartels, S. Backus, E. Zeek, L. Misoguti, *et al.*, "Shaped-pulse optimization of coherent emission of high-harmonic soft x-rays," *Nature*, vol. 406, no. 6792, p. 164, 2000.

[100] R. J. Levis, G. M. Menkir, and H. Rabitz, "Selective bond dissociation and rearrangement with optimally tailored, strong-field laser pulses," *Science*, vol. 292, no. 5517, pp. 709–713, 2001.

[101] T. Weinacht, R. Bartels, S. Backus, P. Bucksbaum, B. Pearson, J. Geremia, H. Rabitz, H. Kapteyn, and M. Murnane, "Coherent learning control of vibrational motion in room temperature molecular gases," *Chemical Physics Letters*, vol. 344, no. 3, pp. 333–338, 2001.

[102] A. Nanduri, A. Donovan, T.-S. Ho, and H. Rabitz, "Exploring quantum control landscape structure," *Physical Review A*, vol. 88, no. 3, p. 033425, 2013.

[103] P. Poggi, F. Lombardo, and D. Wisniacki, "Enhancement of quantum speed limit time due to cooperative effects in multilevel systems," *Journal of Physics A: Mathematical and Theoretical*, vol. 48, no. 35, p. 35FT02, 2015.

[104] M. Sánchez, E. Vergini, and D. Wisniacki, "Characterization of landau-zener transitions in systems with complex spectra," *Physical Review E*, vol. 54, no. 5, p. 4812, 1996.

[105] G. Murgida, D. Wisniacki, and P. Tamborenea, "Coherent control of localization, entanglement, and state superpositions in a double quantum dot with two electrons," *Physical Review B*, vol. 79, no. 3, p. 035326, 2009.

[106] G. Murgida, D. Wisniacki, and P. Tamborenea, "Landau–zener transitions in a semiconductor quantum dot," *Journal of Modern Optics*, vol. 56, no. 6, pp. 799–804, 2009.

[107] G. Murgida, D. Wisniacki, P. Tamborenea, and F. Borondo, "Control of chemical reactions using external electric fields: The case of the linc-licn isomerization," *Chemical Physics Letters*, vol. 496, no. 4, pp. 356–361, 2010.

[108] P. Ao *et al.*, "Quantum dynamics of a two-state system in a dissipative environment," *Physical Review B*, vol. 43, no. 7, p. 5397, 1991.

[109] Y. Kayanuma and H. Nakayama, "Nonadiabatic transition at a level crossing with dissipation," *Physical Review B*, vol. 57, no. 20, p. 13099, 1998.

[110] P. Tamborenea and H. Metiu, "Interacting two-electron model of a coherent quantum-dot single-electron turnstile," *Physical review letters*, vol. 83, no. 19, p. 3912, 1999.

[111] B. W. Shore and P. L. Knight, "The jaynes-cummings model," *Journal of Modern Optics*, vol. 40, no. 7, pp. 1195–1238, 1993.

[112] L. DiCarlo, J. Chow, J. Gambetta, L. S. Bishop, B. Johnson, D. Schuster, J. Majer, A. Blais, L. Frunzio, S. Girvin, *et al.*, "Demonstration of two-qubit algorithms with a superconducting quantum processor," *arXiv preprint arXiv:0903.2030*, 2009.

[113] M. H. Devoret and R. J. Schoelkopf, "Superconducting circuits for quantum information: an outlook," *Science*, vol. 339, no. 6124, pp. 1169–1174, 2013.

[114] D. Zueco, P. Hänggi, and S. Kohler, "Landau–zener tunnelling in dissipative circuit qed," *New Journal of Physics*, vol. 10, no. 11, p. 115012, 2008.

[115] S. Shevchenko, S. Ashhab, and F. Nori, "Landau–zener–stückelberg interferometry," *Physics Reports*, vol. 492, no. 1, pp. 1–30, 2010.

[116] D. V. Else, B. Bauer, and C. Nayak, "Floquet time crystals," *Physical review letters*, vol. 117, no. 9, p. 090402, 2016.

[117] L. F. Torres, P. Perez-Piskunow, C. Balseiro, and G. Usaj, "Multiterminal conductance of a floquet topological insulator," *Physical review letters*, vol. 113, no. 26, p. 266801, 2014.

[118] F. Grossmann, T. Dittrich, P. Jung, and P. Hänggi, "Coherent destruction of tunneling," *Physical review letters*, vol. 67, no. 4, p. 516, 1991.

[119] E. Kierig, U. Schnorrberger, A. Schietinger, J. Tomkovic, and M. Oberthaler, "Single-particle tunneling in strongly driven double-well potentials," *Physical review letters*, vol. 100, no. 19, p. 190405, 2008.

[120] J. H. Shirley, "Solution of the schrödinger equation with a hamiltonian periodic in time," *Physical Review*, vol. 138, no. 4B, p. B979, 1965.

[121] S.-I. Chu and D. A. Telnov, "Beyond the floquet theorem: generalized floquet formalisms and quasienergy methods for atomic and molecular multiphoton processes in intense laser fields," *Physics reports*, vol. 390, no. 1, pp. 1–131, 2004.

[122] S. Ashhab, J. Johansson, A. Zagoskin, and F. Nori, "Two-level systems driven by large-amplitude fields," *Physical Review A*, vol. 75, no. 6, p. 063414, 2007.

[123] C. Creffield, "Location of crossings in the floquet spectrum of a driven two-level system," *Physical Review B*, vol. 67, no. 16, p. 165301, 2003.

[124] K. Hijii and S. Miyashita, "Symmetry for the nonadiabatic transition in floquet states," *Physical Review A*, vol. 81, no. 1, p. 013403, 2010.

[125] G. C. Hegerfeldt, "Driving at the quantum speed limit: optimal control of a two-level system," *Physical review letters*, vol. 111, no. 26, p. 260501, 2013.

[126] M. G. Bason, M. Viteau, N. Malossi, P. Huillery, E. Arimondo, D. Ciampini, R. Fazio, V. Giovannetti, R. Mannella, and O. Morsch, "High-fidelity quantum driving," *Nature Physics*, vol. 8, no. 2, pp. 147–152, 2012.

[127] I. Lizuain, J. Echanobe, A. Ruschhaupt, J. Muga, and D. Steck, "Structural and dynamical aspects of avoided-crossing resonances in a three-level λ system," *Physical Review A*, vol. 82, no. 6, p. 065602, 2010.

[128] I. R. Solá, V. S. Malinovsky, B. Y. Chang, J. Santamaria, and K. Bergmann, "Coherent population transfer in three-level λ systems by chirped laser pulses: Minimization of the intermediate-level population," *Physical Review A*, vol. 59, no. 6, p. 4494, 1999.

[129] S. Guérin and H. Jauslin, "Control of quantum dynamics by laser pulses: Adiabatic floquet theory," *Advances in Chemical Physics*, vol. 125, pp. 147–268, 2003.

[130] M. C. Tichy, M. K. Pedersen, K. Mølmer, and J. F. Sherson, "Nonadiabatic quantum state control of many bosons in few wells," *Physical Review A*, vol. 87, no. 6, p. 063422, 2013.

[131] M. V. Berry and M. Tabor, "Level clustering in the regular spectrum," in *Proceedings of the Royal Society of London A: Mathematical, Physical and Engineering Sciences*, vol. 356, pp. 375–394, The Royal Society, 1977.

[132] O. Bohigas and M. Giannoni, "Chaos and quantum physics, proceedings of the les houches summer school, session lii," 1991.

[133] H.-J. Stöckmann, "Quantum chaos: an introduction," 2000.

[134] L. Santos, F. Borgonovi, and F. Izrailev, "Onset of chaos and relaxation in isolated systems of interacting spins: Energy shell approach," *Physical Review E*, vol. 85, no. 3, p. 036209, 2012.

[135] G. Casati, B. Chirikov, and I. Guarneri, "Energy-level statistics of integrable quantum systems," *Physical review letters*, vol. 54, no. 13, p. 1350, 1985.

[136] O. Bohigas, M.-J. Giannoni, and C. Schmit, "Characterization of chaotic quantum spectra and universality of level fluctuation laws," *Physical Review Letters*, vol. 52, no. 1, p. 1, 1984.

[137] E. P. Wigner, "On the statistical distribution of the widths and spacings of nuclear resonance levels," in *Mathematical Proceedings of the Cambridge Philosophical Society*, vol. 47, pp. 790–798, Cambridge University Press, 1951.

[138] D. Ullmo, "Bohigas-Giannoni-Schmit conjecture," *Scholarpedia*, vol. 11, no. 9, p. 31721, 2016. revision #169195.

[139] I. Percival, "Regular and irregular spectra," *Journal of Physics B: Atomic and Molecular Physics*, vol. 6, no. 9, p. L229, 1973.

[140] E. Haller, H. Köppel, and L. Cederbaum, "On the statistical behaviour of molecular vibronic energy levels," *Chemical physics letters*, vol. 101, no. 3, pp. 215–220, 1983.

[141] H. Bethe, "Zur theorie der metalle," *Zeitschrift für Physik*, vol. 71, no. 3-4, pp. 205–226, 1931.

[142] M. Arnesen, S. Bose, and V. Vedral, "Natural thermal and magnetic entanglement in the 1d heisenberg model," *Physical Review Letters*, vol. 87, no. 1, p. 017901, 2001.

[143] A. Osterloh, L. Amico, G. Falci, and R. Fazio, "Scaling of entanglement close to a quantum phase transition," *Nature*, vol. 416, no. 6881, pp. 608–610, 2002.

[144] S. Bose, "Quantum communication through spin chain dynamics: an introductory overview," *Contemporary Physics*, vol. 48, no. 1, pp. 13–30, 2007.

[145] M. Murphy, S. Montangero, V. Giovannetti, and T. Calarco, "Communication at the quantum speed limit along a spin chain," *Physical Review A*, vol. 82, no. 2, p. 022318, 2010.

[146] X. Wang, A. Bayat, S. G. Schirmer, and S. Bose, "Robust entanglement in antiferromagnetic heisenberg chains by single-spin optimal control," *Physical Review A*, vol. 81, no. 3, p. 032312, 2010.

[147] D. Burgarth, K. Maruyama, M. Murphy, S. Montangero, T. Calarco, F. Nori, and M. B. Plenio, "Scalable quantum computation via local control of only two qubits," *Physical Review A*, vol. 81, no. 4, p. 040303, 2010.

[148] K. Korzekwa, P. Machnikowski, and P. Horodecki, "Quantum-state transfer in spin chains via isolated resonance of terminal spins," *Physical Review A*, vol. 89, no. 6, p. 062301, 2014.

[149] S. Ashhab, "Quantum state transfer in a disordered one-dimensional lattice," *Physical Review A*, vol. 92, no. 6, p. 062305, 2015.

[150] S. C. Srivastava, S. Tomsovic, A. Lakshminarayan, R. Ketzmerick, and A. Bäcker, "Universal scaling of spectral fluctuation transitions for interacting chaotic systems," *Physical review letters*, vol. 116, no. 5, p. 054101, 2016.

[151] T. Takami and H. Fujisaki, "Analytic approach for controlling quantum states in complex systems," *Physical Review E*, vol. 75, no. 3, p. 036219, 2007.

[152] S. Kallush and R. Kosloff, "Mutual influence of locality and chaotic dynamics on quantum controllability," *Physical Review A*, vol. 86, no. 1, p. 013420, 2012.

[153] C. M. Tesch and R. de Vivie-Riedle, "Quantum computation with vibrationally excited molecules," *Physical review letters*, vol. 89, no. 15, p. 157901, 2002.

[154] F. Evers and A. Mirlin, "Fluctuations of the inverse participation ratio at the anderson transition," *Physical review letters*, vol. 84, no. 16, p. 3690, 2000.

[155] E. Canovi, D. Rossini, R. Fazio, G. E. Santoro, and A. Silva, "Quantum quenches, thermalization, and many-body localization," *Physical Review B*, vol. 83, no. 9, p. 094431, 2011.

[156] H.-P. Breuer, "Foundations and measures of quantum non-markovianity," *Journal of Physics B: Atomic, Molecular and Optical Physics*, vol. 45, no. 15, p. 154001, 2012.

[157] B. Vacchini, A. Smirne, E.-M. Laine, J. Piilo, and H.-P. Breuer, "Markovianity and non-markovianity in quantum and classical systems," *New Journal of Physics*, vol. 13, no. 9, p. 093004, 2011.

[158] V. Gorini, A. Kossakowski, and E. C. G. Sudarshan, "Completely positive dynamical semigroups of n-level systems," *Journal of Mathematical Physics*, vol. 17, no. 5, pp. 821–825, 1976.

[159] G. Lindblad, "On the generators of quantum dynamical semigroups," *Communications in Mathematical Physics*, vol. 48, no. 2, pp. 119–130, 1976.

[160] S. Lloyd and L. Viola, "Engineering quantum dynamics," *Physical Review A*, vol. 65, no. 1, p. 010101, 2001.

[161] C. Altafini, "Controllability properties for finite dimensional quantum markovian master equations," *Journal of Mathematical Physics*, vol. 44, no. 6, pp. 2357–2372, 2003.

[162] C. Altafini and F. Ticozzi, "Modeling and control of quantum systems: an introduction," *IEEE Transactions on Automatic Control*, vol. 57, no. 8, pp. 1898–1917, 2012.

[163] D. A. Lidar, I. L. Chuang, and K. B. Whaley, "Decoherence-free subspaces for quantum computation," *Physical Review Letters*, vol. 81, no. 12, p. 2594, 1998.

[164] L.-M. Duan and G.-C. Guo, "Preserving coherence in quantum computation by pairing quantum bits," *Physical Review Letters*, vol. 79, no. 10, p. 1953, 1997.

[165] L. Viola, E. Knill, and S. Lloyd, "Dynamical decoupling of open quantum systems," *Physical Review Letters*, vol. 82, no. 12, p. 2417, 1999.

[166] L. Viola, "Advances in decoherence control," *Journal of Modern Optics*, vol. 51, no. 16-18, pp. 2357–2367, 2004.

[167] X. Yi, X. Huang, C. Wu, and C. Oh, "Driving quantum systems into decoherence-free subspaces by lyapunov control," *Physical Review A*, vol. 80, no. 5, p. 052316, 2009.

[168] D. J. Gorman, K. C. Young, and K. B. Whaley, "Overcoming dephasing noise with robust optimal control," *Physical Review A*, vol. 86, no. 1, p. 012317, 2012.

[169] A. Bartana, R. Kosloff, and D. J. Tannor, "Laser cooling of internal degrees of freedom. ii," *The Journal of chemical physics*, vol. 106, no. 4, pp. 1435–1448, 1997.

[170] D. Chruściński, A. Kossakowski, and S. Pascazio, "Long-time memory in non-markovian evolutions," *Physical Review A*, vol. 81, no. 3, p. 032101, 2010.

[171] Y. Tanimura, "Stochastic liouville, langevin, fokker–planck, and master equation approaches to quantum dissipative systems," *Journal of the Physical Society of Japan*, vol. 75, no. 8, p. 082001, 2006.

[172] B. Bylicka, D. Chruściński, and S. Maniscalco, "Non-markovianity and reservoir memory of quantum channels: a quantum information theory perspective," *Sci. Rep.*, vol. 4, p. 5720, 2014.

[173] S. F. Huelga, Á. Rivas, and M. B. Plenio, "Non-markovianity-assisted steady state entanglement," *Phys. Rev. Lett.*, vol. 108, no. 16, p. 160402, 2012.

[174] C. Cormick, A. Bermudez, S. F. Huelga, and M. B. Plenio, "Dissipative ground-state preparation of a spin chain by a structured environment," *New J. Phys.*, vol. 15, no. 7, p. 073027, 2013.

[175] X. Meng, C. Wu, and H. Guo, "Minimal evolution time and quantum speed limit of non-markovian open systems," *Sci. Rep.*, vol. 5, 2015.

[176] D. M. Reich, N. Katz, and C. P. Koch, "Exploiting non-markovianity for quantum control," *Sci. Rep.*, vol. 5, p. 2430, 2015.

[177] J. F. Triana, A. F. Estrada, and L. A. Pachón, "Ultrafast optimal sideband cooling under non-markovian evolution," *Phys. Rev. Lett.*, vol. 116, no. 18, p. 183602, 2016.

[178] C. Addis, F. Ciccarello, M. Cascio, G. M. Palma, and S. Maniscalco, "Dynamical decoupling efficiency versus quantum non-markovianity," *New J. Phys.*, vol. 17, no. 12, p. 123004, 2015.

[179] A. Rivas, S. F. Huelga, and M. B. Plenio, "Quantum non-markovianity: characterization, quantification and detection," *Reports on Progress in Physics*, vol. 77, no. 9, p. 094001, 2014.

[180] Á. Rivas, S. F. Huelga, and M. B. Plenio, "Entanglement and non-markovianity of quantum evolutions," *Phys. Rev. Lett.*, vol. 105, no. 5, p. 050403, 2010.

[181] H.-P. Breuer, E.-M. Laine, and J. Piilo, "Measure for the degree of non-markovian behavior of quantum processes in open systems," *Phys. Rev. Lett.*, vol. 103, no. 21, p. 210401, 2009.

[182] S. Wißmann, A. Karlsson, E.-M. Laine, J. Piilo, and H.-P. Breuer, "Optimal state pairs for non-markovian quantum dynamics," *Phys. Rev. A*, vol. 86, no. 6, p. 062108, 2012.

[183] C. Pineda, T. Gorin, D. Davalos, D. A. Wisniacki, and I. García-Mata, "Measuring and using non-markovianity," *Phys. Rev. A*, vol. 93, no. 2, p. 022117, 2016.

[184] H. Mäkelä and M. Möttönen, "Effects of the rotating-wave and secular approximations on non-markovianity," *Phys. Rev. A*, vol. 88, no. 5, p. 052111, 2013.

[185] J.-S. Tai, K.-T. Lin, and H.-S. Goan, "Optimal control of quantum gates in an exactly solvable non-markovian open quantum bit system," *Phys. Rev. A*, vol. 89, no. 6, p. 062310, 2014.

[186] C. Addis, B. Bylicka, D. Chruściński, and S. Maniscalco, "Comparative study of non-markovianity measures in exactly solvable one-and two-qubit models," *Physical Review A*, vol. 90, no. 5, p. 052103, 2014.

[187] H.-S. Zeng, N. Tang, Y.-P. Zheng, and G.-Y. Wang, "Equivalence of the measures of non-markovianity for open two-level systems," *Phys. Rev. A*, vol. 84, no. 3, p. 032118, 2011.

[188] J. Ma, Z. Sun, X. Wang, and F. Nori, "Entanglement dynamics of two qubits in a common bath," *Phys. Rev. A*, vol. 85, no. 6, p. 062323, 2012.

[189] H.-B. Chen, N. Lambert, Y.-C. Cheng, Y.-N. Chen, and F. Nori, "Using non-markovian measures to evaluate quantum master equations for photosynthesis," *Sci. Rep.*, vol. 5, p. 12753, 2015.

[190] W. Guo, J. Ma, X. Yin, W. Zhong, and X. Wang, "Non-markovian dynamics of the mixed-state geometric phase of dissipative qubits," *Phys. Rev. A*, vol. 90, no. 6, p. 062133, 2014.

[191] Z. Sun, L. Zhou, G. Xiao, D. Poletti, and J. Gong, "Finite-time landau-zener processes and counterdiabatic driving in open systems: Beyond born, markov, and rotating-wave approximations," *Phys. Rev. A*, vol. 93, no. 1, p. 012121, 2016.

[192] P. Haikka, J. D. Cresser, and S. Maniscalco, "Comparing different non-markovianity measures in a driven qubit system," *Phys. Rev. A*, vol. 83, no. 1, p. 012112, 2011.

[193] Y.-J. Zhang, W. Han, Y.-J. Xia, J.-P. Cao, and H. Fan, "Classical-driving-assisted quantum speed-up," *Phys. Rev. A*, vol. 91, no. 3, p. 032112, 2015.

[194] J. Costa-Filho, R. Lima, R. Paiva, P. Soares, W. Morgado, R. L. Franco, and D. Soares-Pinto, "Enabling quantum non-markovian dynamics by injection of classical colored noise," *Physical Review A*, vol. 95, no. 5, p. 052126, 2017.

[195] K. M. Fonseca-Romero, S. Kohler, and P. Hänggi, "Coherence control for qubits," *Chem. Phys.*, vol. 296, no. 2, pp. 307–314, 2004.

[196] R. Heck, O. Vuculescu, J. J. Sørensen, J. Zoller, M. G. Andreasen, M. G. Bason, P. Ejlertsen, O. Elíasson, P. Haikka, J. S. Laustsen, *et al.*, "Do physicists stop searches too early? a remote-science, optimization landscape investigation," *arXiv preprint arXiv:1709.02230*, 2017.

[197] B. Russell and S. Stepney, "The geometry of speed limiting resources in physical models of computation," *arXiv preprint arXiv:1611.09220*, 2016.

[198] I. García-Mata, A. J. Roncaglia, and D. A. Wisniacki, "Relaxation of isolated quantum systems beyond chaos," *Physical Review E*, vol. 91, no. 1, p. 010902, 2015.

[199] R. Essers, J. Tennyson, and P. Wormer, "An scf potential energy surface for lithium cyanide," *Chemical Physics Letters*, vol. 89, no. 3, pp. 223–227, 1982.

[200] G. Brocks, J. Tennyson, and A. van der Avoird, "A binitio dipole surfaces, vibrationally averaged dipole moments, and infrared transition intensities for kcn and licn," *The Journal of chemical physics*, vol. 80, no. 7, pp. 3223–3233, 1984.

[201] A. D. Bandrauk and H. Shen, "Improved exponential split operator method for solving the time-dependent schrödinger equation," *Chemical physics letters*, vol. 176, no. 5, pp. 428–432, 1991.